

May 2018

# Solvent Extraction and Extraction Chromatography of Homologs and Pseudohomologs of Rutherfordium Using TEHA and TEHP

Jeffrey Rolfes  
jeffrolfes@gmail.com

Follow this and additional works at: <https://digitalscholarship.unlv.edu/thesesdissertations>

 Part of the [Chemistry Commons](#)

---

## Repository Citation

Rolfes, Jeffrey, "Solvent Extraction and Extraction Chromatography of Homologs and Pseudohomologs of Rutherfordium Using TEHA and TEHP" (2018). *UNLV Theses, Dissertations, Professional Papers, and Capstones*. 3322.  
<https://digitalscholarship.unlv.edu/thesesdissertations/3322>

This Dissertation is brought to you for free and open access by Digital Scholarship@UNLV. It has been accepted for inclusion in UNLV Theses, Dissertations, Professional Papers, and Capstones by an authorized administrator of Digital Scholarship@UNLV. For more information, please contact [digitalscholarship@unlv.edu](mailto:digitalscholarship@unlv.edu).

SOLVENT EXTRACTION AND EXTRACTION CHROMATOGRAPHY OF HOMOLOGS  
AND PSEUDOHOMOLOGS OF RUTHERFORDIUM USING TEHA AND TEHP

By

Jeffrey Neal Rolfes

Bachelor of Science in Chemistry  
Newman University  
2010

A dissertation submitted in partial  
fulfillment of the requirements for the

Doctor of Philosophy – Radiochemistry

Department of Chemistry and Biochemistry  
College of Sciences  
The Graduate College

University of Nevada, Las Vegas  
May 2018

Copyright by Jeffrey Neal Rolfes

All rights reserved

**Dissertation Approval**

The Graduate College  
The University of Nevada, Las Vegas

September 29, 2017

This dissertation prepared by

Jeffrey Neal Rolfes

entitled

Solvent Extraction and Extraction Chromatography of Homologs and Pseudohomologs of Rutherfordium Using TEHA and TEHP

is approved in partial fulfillment of the requirements for the degree of

Doctor of Philosophy – Radiochemistry  
Department of Chemistry and Biochemistry

Ralf Sudowe, Ph.D.  
*Examination Committee Chair*

Kathryn Hausbeck Korgan, Ph.D.  
*Graduate College Interim Dean*

Ken Czerwinski, Ph.D.  
*Examination Committee Member*

Roger Henderson, Ph.D.  
*Examination Committee Member*

Steen Madsen, Ph.D.  
*Graduate College Faculty Representative*

## ABSTRACT

Studies of the chemical properties of the heaviest elements have always been difficult due to the short half-lives and low cross sections involved. To solve this problem, atom-at-a-time methods are necessary to determine the properties of these short-lived isotopes. Extremely fast kinetics for the chemical reactions studied (on the same order as the nuclide's half-life) are required, and the system should have the potential for automation. Solvent extraction, with its selectivity and quick kinetics, has historically been used for these investigations into characteristics of super heavy elements. Another technique, extraction chromatography, offers potentially a way of investigating rutherfordium's properties, without the solvent waste generated in liquid-liquid extractions. A rapid method involving the use of a ligand with high intragroup selectivity is necessary to discover more about rutherfordium. Studies with the homologs of rutherfordium, zirconium and hafnium, can be performed using liquid-liquid extractions as well as extraction chromatography. These investigations can then be used as a basis for comparison with future studies involving the transactinide element. Based on literature reviews, tertiary amines and phosphates show promise in extracting group 4 elements. In particular, tris(2-ethylhexyl)amine (TEHA) and tris(2-ethylhexyl)phosphate (TEHP) can be used to selectively extract zirconium, hafnium, neptunium, and plutonium from a chloride matrix. The results of a detailed study investigating the solvent extraction of Zr, Hf, and Pu from various mineral acids by these two ligands will be presented together with the use of extraction chromatography to separate these elements. The development of a suitable system for rutherfordium based on these extractants can help to further elucidate its properties.

## ACKNOWLEDGEMENTS

This work was only possible with the encouragement and assistance of many people. First, I would like Ralf Sudowe, my advisor, for his counsel and patience. Next, I would like to thank Roger Henderson for being my lab mentor, LLNL supervisor, and for taking his time as a committee member. Many thanks goes to Ken Czerwinski for his support as a professor and committee member and to Gary Cerefice, who always had time for a long talk in the afternoon. I would like to thank the lab staff, Mary Turner, Julie Bertoia, and Trevor Low at UNLV for day-to-day support, especially in my last days of finishing my lab work in Las Vegas. Many thanks to John Despotupolus who helped me get started in my extractions at UNLV and at LLNL. Also, I would like to thank all my fellow graduate students and office mates, in particular: Derek McClain, Bill Kerlin, and Bradley Childs and the rest of the radiochemistry program.

Lastly, and most importantly, I would like to commend and thank my wife Christine and Ambrose for coming along with me on my journey through graduate school. I can't possibly repay the love and support you have given me in the past 6 years.

I would also like to thank the CAMS facility staff and Narek Gharibyan for preparing the  $^{175}\text{Hf}$  tracer over the course of this experiment.

Lastly, and most importantly, I would like to commend and thank my wife Christine and Ambrose for coming along with me on my journey through graduate school. I can't possibly repay the love and support you have given me in the past 6 years.

### **Department of Homeland Security Disclaimer**

This material is based upon work supported by the U.S. Department of Homeland Security under Grand Award Number 2012-DN-130-NF0001. The views and conclusions contained in this document are those of the author and should not be interpreted as representing the official policies, either expressed or implied, of the U.S. Department of Homeland Security.

## TABLE OF CONTENTS

ABSTRACT.....	iii
ACKNOWLEDGEMENTS.....	iv
1. INTRODUCTION.....	1
1.1 Project Goals .....	1
1.2 Background .....	1
1.2.1 Historical Perspective .....	1
1.2.2 Transactinide Production .....	6
1.2.3 Solvent Extraction.....	12
1.2.4 Extraction Chromatography.....	14
1.2.5 Atom-at-a-Time Chemistry.....	17
1.2.6 Zirconium and Hafnium Aqueous Chemistry.....	21
1.2.7 Group IV Liquid Phase Online Chemistry.....	23
2. MATERIALS AND INSTRUMENTatION.....	26
2.1 Offline Studies.....	26
2.1.1 Tris(2-ethylhexyl)amine and tris(2-ethylhexyl)phosphate .....	26
2.1.2 Radionuclide tracers.....	27
2.1.3 Other reagents used.....	30
2.2 Instrumentation.....	31
2.2.1 Sodium Iodide Detector .....	31
2.2.2 Germanium detectors .....	33
2.2.3 Liquid Scintillation Counting .....	34
3 METHODS.....	37
3.1 Solvent Extraction .....	37
3.2 Batch Studies.....	38
3.2.1 Batch Study Corrections .....	38
3.3 Column Studies .....	39
4 SOLVENT EXTRACTIONS .....	41
4.1 Exploratory Extractions.....	41

4.2	Solvent Extraction from Hydrochloric Acid .....	41
4.2.1	Solvent Selection .....	41
4.2.2	Solvent Extractions with <sup>89</sup> Zr, <sup>175</sup> Hf, <sup>239</sup> Pu .....	50
4.2.3	<sup>89</sup> Zr, <sup>175</sup> Hf, <sup>239</sup> Pu speciation .....	54
4.2.4	Kinetics of <sup>89</sup> Zr, <sup>175</sup> Hf, and <sup>239</sup> Pu Extraction.....	59
4.2.5	Discussion.....	63
5	BATCH STUDIES .....	66
5.1	Exploratory Batch Studies with Resin Backbones and Ligand Loading .....	66
5.1.1	TEHA .....	66
5.1.2	TEHP.....	74
5.2	Kinetic Studies .....	81
5.2.1	TEHA .....	81
5.2.2	TEHP.....	83
5.2.3	Discussion.....	86
6	COLUMN STUDIES .....	87
6.1	Column Elution with 11 M HCl, 7 M HCl, and 6 M HCl.....	87
6.2	Column Elution with 11M HCl and 6M HCl.....	90
6.3	Discussion .....	92
7	CONCLUSIONS .....	94
7.1	Solvent Extraction .....	94
7.2	Batch Studies and Column Studies .....	95
7.3	Future Work .....	96
	REFERENCES .....	98
	Curriculum vitae .....	<b>Error! Bookmark not defined.</b>



## LIST OF FIGURES

<b>Figure 1.1:</b> The current periodic table of the elements. <sup>21</sup> .....	5
<b>Figure 1.2:</b> A visual comparison of hot and cold fusion reactions. <sup>16</sup> .....	8
<b>Figure 1.3</b> List of hot fusion reactions with a stable beam and a radionuclide beam (RNB) their cross sections ( $\sigma$ ) in picobarns and associated ion beam strength $\varphi$ (ions/sec). <sup>39</sup> .....	9
<b>Figure 1.4:</b> The relativistic (solid line) and non-relativistic (dashed lines) distribution of Db's 7s electrons. <sup>40</sup> .....	11
<b>Figure 1.5</b> Diagram of the components of an extraction chromatographic system. <sup>46</sup> .....	15
<b>Figure 1.6</b> Schematic of the Dubna Gas-filled Recoil Separator (DGFRS). <sup>53</sup> .....	20
<b>Figure 2.1</b> Structure of Tris(2-ethylhexyl)amine .....	26
<b>Figure 2.2</b> and tris(2-ethylhexyl)phosphate .....	27
<b>Figure 2.3</b> Wizard 2480 automated gamma counter .....	33
<b>Figure 4.1</b> Percent Extraction of <sup>89</sup> Zr with 0.05 M TEHA in kerosene. ....	43
<b>Figure 4.2</b> Percent Extraction of <sup>89</sup> Zr with 0.05 M TEHA in DCM .....	44
<b>Figure 4.3</b> Percent Extraction of <sup>89</sup> Zr with 0.05 M TEHP in DCM. ....	45
<b>Figure 4.4</b> Percent Extraction of <sup>89</sup> Zr with 0.05 M TEHA in hexanes. ....	46
<b>Figure 4.5</b> Percent Extraction of <sup>89</sup> Zr with 0.05 M TEHP in hexanes. ....	47
<b>Figure 4.6</b> Percent Extraction of <sup>89</sup> Zr with 0.05 M TEHA in toluene.....	48
<b>Figure 4.7</b> Percent Extraction of <sup>89</sup> Zr with 0.05 M TEHP in toluene .....	49
<b>Figure 4.8</b> Percent Extraction of <sup>89</sup> Zr, <sup>175</sup> Hf, and <sup>239</sup> Pu with 0.05 M TEHA .....	51
<b>Figure 4.9</b> Separation factors of <sup>89</sup> Zr, <sup>175</sup> Hf, and <sup>239</sup> Pu with 0.05 M TEHA .....	52
<b>Figure 4.10</b> Percent Extraction of <sup>89</sup> Zr, <sup>175</sup> Hf, and <sup>239</sup> Pu with 0.05 M TEHP .....	53
<b>Figure 4.11</b> Separation factors of <sup>89</sup> Zr, <sup>175</sup> Hf, and <sup>239</sup> Pu with 0.05M TEHP.....	54

<b>Figure 4.12</b> The natural log of the distribution ratios for $^{89}\text{Zr}$ as a function of the natural log of the concentration of TEHA in toluene at 8 M HCl.....	56
<b>Figure 4.13</b> The natural log of the distribution ratios for $^{175}\text{Hf}$ as a function of the natural log of the concentration of TEHA in toluene at 8 M HCl.....	56
<b>Figure 4.14</b> The natural log of the distribution ratios for $^{89}\text{Zr}$ as a function of the natural log of the concentration of TEHP in toluene at 8 M HCl.....	57
<b>Figure 4.15</b> The natural log of the distribution ratios for $^{175}\text{Hf}$ as a function of the natural log of the concentration of TEHP in toluene at 8 M HCl.....	58
<b>Figure 4.16</b> The natural log of the distribution ratios for $^{239}\text{Pu}$ as a function of the natural log of the concentration of TEHP in toluene at 8 M HCl.....	58
<b>Figure 4.17</b> Kinetics of $^{89}\text{Zr}$ in 0.05 M TEHA/12 M HCl .....	60
<b>Figure 4.18</b> Kinetics of $^{175}\text{Hf}$ in 0.05 M TEHA/12 M HCl.....	60
<b>Figure 4.19</b> Kinetics of $^{239}\text{Pu}$ in 0.05 M TEHA/12 M HCl.....	61
<b>Figure 4.20</b> Kinetics of $^{89}\text{Zr}$ in 0.05 M TEHP/12 M HCl .....	62
<b>Figure 4.21</b> Kinetics of $^{175}\text{Hf}$ in 0.05 M TEHP/12M HCl .....	62
<b>Figure 4.22</b> Kinetics of $^{239}\text{Pu}$ in 0.05 M TEHP/12M HCl .....	63
<b>Figure 5.1</b> Batch study of $^{89}\text{Zr}$ on different percent loadings TEHA loaded Amberchrome backbone .....	67
<b>Figure 5.2</b> Batch study of $^{89}\text{Zr}$ on different percent loadings TEHA loaded XAD7HP backbone .....	68
<b>Figure 5.3</b> Batch study of $^{89}\text{Zr}$ on different percent loadings TEHA loaded XAD4 backbone ...	68
<b>Figure 5.4</b> Batch study of $^{175}\text{Hf}$ on TEHA loaded Amberchrome, XAD7HP, and XAD4 backbone .....	70

**Figure 5.5** Batch study of  $^{239}\text{Pu}$  on different percent loadings TEHA loaded Amberchrome backbone ..... 71

**Figure 5.6** Batch study of  $^{239}\text{Pu}$  on different percent loadings TEHA loaded XAD7HP backbone ..... 72

**Figure 5.7** Batch study of  $^{239}\text{Pu}$  on different percent loadings TEHA loaded XAD4 backbone . 72

**Figure 5.8:** Separation factors of  $^{89}\text{Zr}$ ,  $^{175}\text{Hf}$ , and  $^{239}\text{Pu}$  on TEHA 40% Amberchrome resin ..... 74

**Figure 5.9** Batch study of  $^{89}\text{Zr}$  on different percent loadings TEHP loaded Amberchrome backbone ..... 75

**Figure 5.10** Batch study of  $^{89}\text{Zr}$  on different percent loadings TEHP loaded XAD7HP backbone ..... 76

**Figure 5.11** Batch study of  $^{89}\text{Zr}$  on different percent loadings TEHP loaded XAD4 backbone.. 76

**Figure 5.12** Batch study of  $^{175}\text{Hf}$  on a TEHP loaded Amberchrome, XAD7HP, and XAD4 backbone ..... 77

**Figure 5.13** Batch study of  $^{239}\text{Pu}$  on different percent loadings TEHP loaded Amberchrome backbone ..... 78

**Figure 5.14** Batch study of  $^{239}\text{Pu}$  on different percent loadings TEHP loaded XAD7HP backbone ..... 79

**Figure 5.15** Batch study of  $^{239}\text{Pu}$  on different percent loadings TEHP loaded XAD4 backbone 79

**Figure 5.16** Separation factors of  $^{89}\text{Zr}$ ,  $^{175}\text{Hf}$ , and  $^{239}\text{Pu}$  on TEHP 40% Amberchrome resin ..... 81

**Figure 5.17** Kinetics of  $^{89}\text{Zr}$  on TEHA Amberchrome in 12 M HCl ..... 82

**Figure 5.18** Kinetics of  $^{175}\text{Hf}$  on TEHA Amberchrome in 12 M HCl ..... 83

**Figure 5.19** Kinetics of  $^{239}\text{Pu}$  on TEHA Amberchrome in 12 M HCl ..... 83

**Figure 5.20** Kinetics of  $^{89}\text{Zr}$  on TEHP Amberchrome in 12 M HCl..... 84

<b>Figure 5.21</b> Kinetics of $^{175}\text{Hf}$ on TEHP Amberchrome in 12 M HCl.....	85
<b>Figure 5.22</b> Kinetics of $^{239}\text{Pu}$ on TEHP Amberchrome in 12M HCl.....	85
<b>Figure 6.1</b> Column elution of $^{89}\text{Zr}$ , $^{175}\text{Hf}$ , and $^{239}\text{Pu}$ on a 40% TEHA Amberchrome resin, eluting by 2 mL of 11 M HCl, followed by 2 ml of 7 M HCl, and then by 2 mL of 6 M HCl. ...	89
<b>Figure 6.2</b> Column elution of $^{89}\text{Zr}$ , $^{175}\text{Hf}$ , and $^{239}\text{Pu}$ on a 40% TEHP Amberchrome resin, eluting by 2 mL of 11 M HCl, followed by 2 ml of 7 M HCl, and then by 2 mL of 6 M HCl.....	89
<b>Figure 6.3</b> Column elution of $^{89}\text{Zr}$ , $^{175}\text{Hf}$ , and $^{239}\text{Pu}$ on a 40% TEHA Amberchrome resin, eluting by 2 mL of 11 M HCl and then by 2 mL of 6 M HCl. ....	91
<b>Figure 6.4</b> Column elution of and $^{239}\text{Pu}$ on a 40% TEHP Amberchrome resin, eluting by 2 mL of 11 M HCl and then by 2 mL of 6 M HCl.....	91

# 1. INTRODUCTION

## 1.1 Project Goals

The ultimate goal of this work is to find and investigate and find ligands suitable to explore the chemistry of rutherfordium. Both solvent extraction and extraction chromatography can be used in tandem with available automated chemistry setups that have been developed and utilized at accelerators. By first using offline studies, the chemistry of the selected ligands can be fully understood to prepare the experiments for online use with accelerator-produced homologs and rutherfordium. These offline separations analyzing the kinetics, chemistry, and efficiency can determine whether a ligand can be used in an actual online chemistry setup with rutherfordium.

A secondary goal can be the exploration and development of new extraction chromatographic resins. Both ligands presented in this research have not been developed or characterized in the literature as resins. New resins can possibly provide a unique separation method of different elements as each will give different  $k'$  values. Both TEHA and TEHP may offer another unique resin and lead to novel separation method for radionuclides in fuel cycle and environmental procedures.

## 1.2 Background

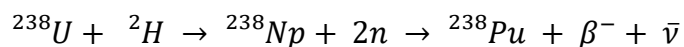
### 1.2.1 Historical Perspective

The creation of transuranic elements began in the 1940s. Previously, only naturally occurring elements up to uranium ( $Z=92$ ) had been discovered. The first nuclear reaction that had successfully achieved artificial transmutation was Rutherford's reaction of alpha particles on nitrogen, creating oxygen-17 in 1919.<sup>1</sup> However, in the 1930s, developments in the understanding of the structure of the nucleus provided the groundwork for techniques and methods in artificial nuclide synthesis. In 1930, W. Bothe and H. Becker ran an experiment where lithium, beryllium, and boron were bombarded by alpha particles.<sup>2</sup> Their results found that some of the radiation emitted was nonionizing, uncharged, and highly penetrating. Later, Irene

Curie and Frederic Joliot found that protons were produced when this radiation hit hydrogen containing materials.<sup>3</sup> Repeating the same experiments from Curie and Joliot, James Chadwick interpreted the phenomena as caused by an undiscovered particle, the neutron, with the same mass of a proton but uncharged.<sup>4</sup>

The first artificially created radioactive nuclide,  $^{30}\text{P}$ , was created by Curie and Joliot in 1932, using aluminum to absorb alpha particles and in the process being transmuted to phosphorus with the emission of a neutron.<sup>5</sup> This discovery, along with the development of particle accelerators and cyclotrons and the discovery of  $\beta$ -decay, paved the way for using nuclear reactions as a synthesis method for more new unstable elements. Later, in 1937, Carlo Perrier, when visiting Lawrence Berkeley National Laboratory, asked Lawrence for some old cyclotron parts, including a deflector molybdenum foil. Using this foil, Perrier was able chemically isolate technetium, an element in the middle of the periodic table without any stable isotopes.<sup>6</sup>

The transuranic element discoveries started shortly after the discovery of technetium with a few false claims along the way. In 1934, Fermi claimed to have made a new element by bombarding uranium with slow moving neutrons.<sup>7</sup> However, in reality, he unwittingly had discovered fission. Otto Hahn and Fritz Strassmann repeated the experiment and relayed the results to Lise Meitner and her nephew, Otto Frisch.<sup>8</sup> They then provided the theoretical foundation for fission and concluded that the uranium nucleus was separating.<sup>9</sup> Nonetheless, Fermi is believed to have produced neptunium, though he did not provide the correct evidence for its discovery. In 1940, Edwin McMillian and Philip H Abelson first discovered neptunium by the following reaction:



Glenn T. Seaborg and McMillian synthesized plutonium later that year by bombarding uranium with deuterons using the 60 inch cyclotron.<sup>10</sup> At a later time during the Manhattan Project, Glenn Seaborg et. al. also discovered americium and curium.<sup>11</sup> Seaborg then introduced the actinoid concept, placing the elements from thorium to lawrencium (undiscovered at the time) underneath the lanthanoid series. Although the chemistry of the early actinides somewhat mimicked the transition metals, the later actinides (starting with curium) began to exhibit chemical properties similar to the lanthanides. In 1949 and 1950, Berkelium and californium were later discovered after deuteron bombardment of actinide targets.<sup>12-13</sup> An analysis of the debris found in the aftermath of the Ivy Mike test's rubble led to the discovery of fermium and einsteinium in 1952.<sup>14</sup> While using the method of successive neutron captures with  $\beta^-$  decay allowed for to successful discoveries of new elements leading up to Es, the elements beyond mendelevium would have to be produced an atom-at-a-time. These heavier nuclides, starting with mendelevium (Md), have low production rates, extremely short half-lives, and large probabilities for spontaneous fission. Because of these factors, the production rates and half-lives of these elements are too low to create quantities large enough for target preparation. Thus, the previously described sequential neutron capture and  $\beta^-$  decay process ceases to be a viable method of element production.

The instability of the transfermium elements can be explained through the liquid drop and nuclear shell model. A number of factors influence the stability of the nucleus, which include the binding energy and size. By using the idea of a liquid drop, the liquid drop model states that the binding energy is governed by the semi empirical mass formula<sup>15</sup>:

$$E_B(\text{MeV}) = a_v A - a_s A^{2/3} - a_c \frac{Z(Z-1)}{A^{1/3}} - a_{\text{sym}} \frac{(A-2Z)^2}{A} \pm \delta(A, Z)$$

The  $a_v A$  term is defined as the volume term that accounts for the interaction of each nucleon in relation to its nearest neighbor. The  $a_s A^{2/3}$  term is the surface term; for the nucleons on the edge of the nucleus, they have fewer nucleons to interact with. The  $a_c \frac{Z(Z-1)}{A^{1/3}}$  term represents the Coulomb repulsion between protons. The  $a_{\text{sym}} \frac{(A-2Z)^2}{A}$  is the symmetry term; for low  $A$  nuclei, stability is greater when  $N=Z$ . However, at higher  $A$ , more stable nuclei begin to favor more  $N$  within the nucleus. This term accounts for this shift of conditions. Lastly, the pairing term  $\delta(A, Z)$  considers the effect of odd-even pairing of nucleons. For odd proton-odd neutron (odd-odd) nuclei, the term is negative; for even proton-even neutron (even-even) nuclei, the term is positive; and for odd  $A$  nuclei, the term is zero. The total value of the binding energy indicates how much energy would be required to separate the nucleus into its basic components of protons and neutrons. A higher binding energy signifies a higher nuclear stability. A general trend that the semi empirical mass equation shows is that as  $Z$  increases, the symmetry term and Coulombic term increase and thereby decreases the stability of the nucleus. This instability increases the chance that the nucleus will spontaneously fission and decreases production rates and half-lives of these higher  $Z$  elements. The liquid drop model predicts that elements beyond  $Z=100$  are too unstable to produce. However, since elements with a  $Z>100$  have been produced, the liquid drop is insufficient to explain all factors that increase nuclear stability affecting the transfermium elements.

The nuclear shell model further expands on the stability of nuclei beyond fermium by arranging protons and neutrons into separate shells, similar to electron orbitals. When a shell becomes full with protons or neutrons, it gains a higher binding energy and greater stability. The number of nucleons at which a shell becomes full is called a “magic number”; these occur at 2, 8, 20, 28, 50, and 82. When a nucleus has a closed shell of both protons and neutrons, it becomes



doubly magic and gains even more stability. At a higher  $A$ , the magic numbers for protons are predicted to be 114, 164, and 182; for neutrons, they are 126, 184, and 196.<sup>16</sup> According to William Myers and Wladyslaw Swiatecki, an island of nuclear stability should occur at the intersection of the proton number 114 and 184 due to the increase stability of a spherically doubly magic nucleus. This island of nuclei would be separated from the known more stable elements by a sea of instability.<sup>17</sup> Initial calculations based on this island of stability predicted half-lives up to a billion years for some nuclei. These predictions encouraged experimental attempts to create and investigate the transactinides' nuclear and chemical properties. Although experiments have yet to explore the inland portion of island of stability, the believed shore of the island has been reached.<sup>18-20</sup>

The historical method of discovery heavy element based on the neutron capture and successive  $\beta^-$  decays becomes less reliable as  $Z$  increases. Figure 1.1 shows the current periodic table.

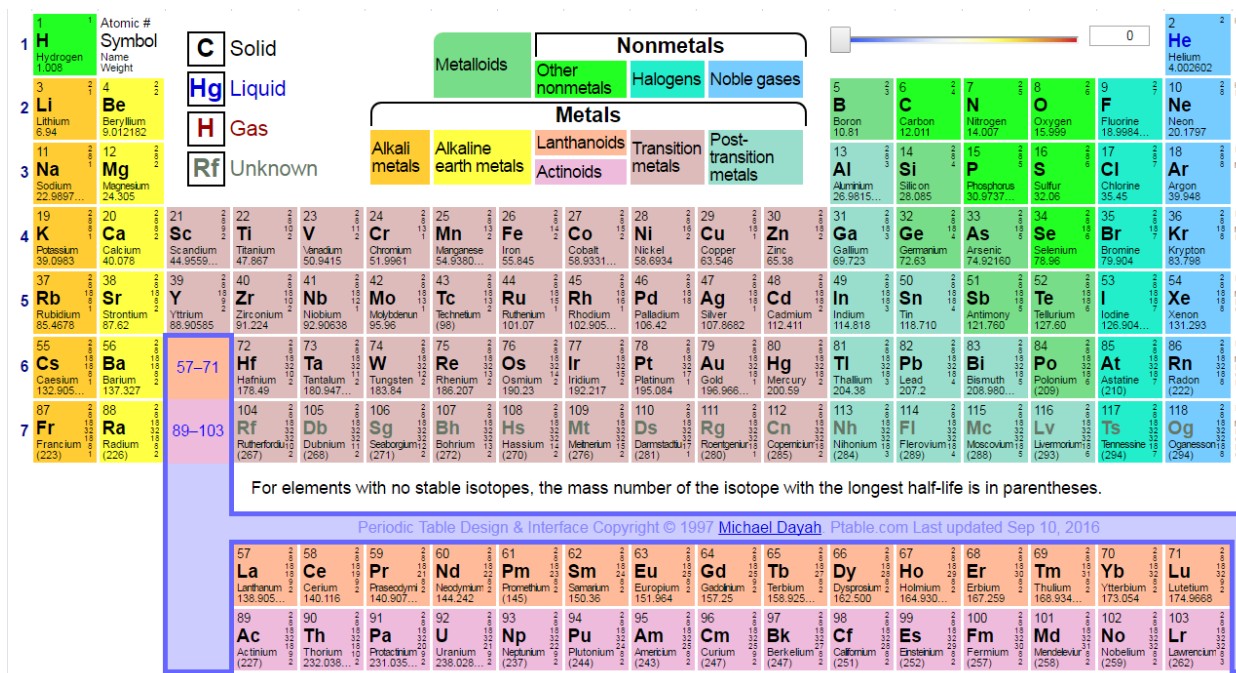
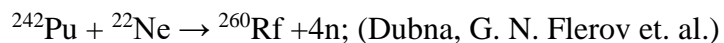
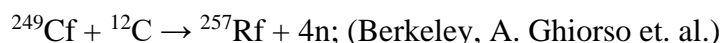


Figure 1.1: The current periodic table of the elements.<sup>21</sup>

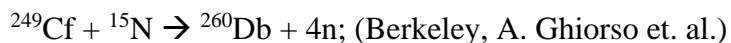
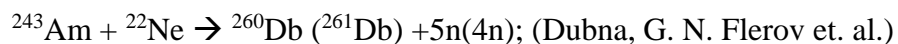
Rutherfordium (Rf) starts the beginning of a new metal transition series, known as the transactinides. In 1964, the Joint Institute for Nuclear Research (JINR) in Dubna claimed discovery for this element with the following reaction:<sup>22</sup>



In 1969, scientists at the Berkeley Heavy Ion Linear Collider (HILAC) in Berkeley, California also claimed to have discovered the element as well:<sup>23</sup>



These same groups claimed discovery of element 105 with JINR in 1968 and HILAC in 1970:<sup>24-25</sup>



The International Union of Pure and Applied Chemistry (IUPAC) decided to award credit for these elements to both of the teams. In the years that followed the beginning of the transactinide discovery, the atom-at-a-time techniques were used to find elements all the way up to element 118. IUPAC has recognized discovery of elements 106-118 to JINR, HILAC, RIKEN and Gesellschaft für Schwerionenforschung (GSI) and they have been designated as: seaborgium (Sg), bohrium (Bh), hassium (Hs), meitnerium (Mt), darmstadtium (Ds), roentgenium (Rn), copernicium (Cn), nihonium (Nh), flerovium (Fl), Moscovium (Mc), livermorium (Lv), Tennessine (Ts), and Oganesson (Og).<sup>19, 26-34</sup>

### 1.2.2 Transactinide Production

Since transfermium elements have a high instability, they are all made artificially and are not found in nature. Cyclotrons and accelerators are the only instruments that can create these elements, using heavy ion nuclear reactions to achieve this goal.<sup>35</sup> A target plated with up to

~0.8mg/cm<sup>2</sup> of material is hit with beams containing approximately  $3 \times 10^{12}$  ions per second and then the reaction products recoil out of the foil and into a detection system. With this setup, transactinide production rates can vary from a few atoms per minute for Rf and Db to as low as a few atoms per year for the heavier super heavy elements.<sup>34, 36</sup>

Transactinides can be synthesized in two ways: through *cold* and *hot* fusion reactions. A successful creation of a transactinide needs the projectile and target atom to fuse together and to cook off neutrons to fully de-excite the compound nucleus that forms. The Coulomb barrier is an obstacle that prevents effective fusion from occurring.<sup>34</sup> Unstable compound nuclei, transfer reactions (partial fusion) or no reaction at all are the results that occur if this barrier is not overcome.

Cold fusion is a nuclear reaction that has an excitation energy of 10-15 MeV. These reactions rely on spherical target nuclei and projectiles, such as <sup>208</sup>Pb or <sup>62,64</sup>Ni, to enhance the stability of the reaction and to lower the chances of a spontaneous fission while fusing. They typically evaporate 1-2 neutrons. GSI focused on using these reactions to discover elements 107-112.<sup>37</sup> However, cold fusion reactions have a serious drawback. Because these nuclides are more neutron deficient, they have very short half-lives; since at a heavier A, they need more neutrons to be stable. Chemical studies of these elements have not been performed because the short half-lives do not provide the time, which is needed to perform automated experiments.<sup>16</sup>

Hot fusion is a nuclear reaction that has an excitation energy of 40-50 MeV. These reactions rely on neutron rich actinide targets and a lighter projectile, such as <sup>22</sup>Ne and <sup>18</sup>O. Hot fusions de-excite by evaporating 4 to 5 neutrons from the compound nucleus. While it is more prone to spontaneous fission, the compound nuclei formed have much longer half-lives than those formed through cold fusion. Their cross-sections are also typically higher than cold fusion

since the weight between the target and the projectile is greater.<sup>16</sup> Figure 1.2.1 shows the comparison between hot and cold fusion of Hs.

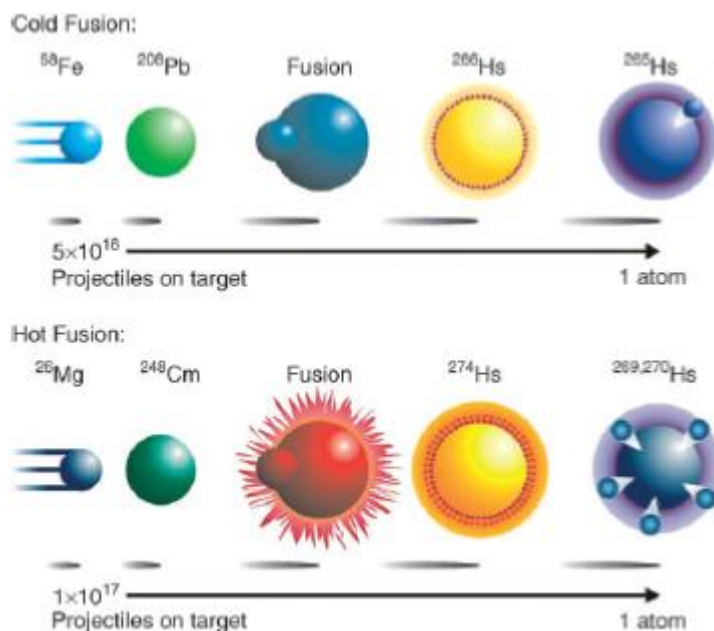


**Figure 1.2:** A visual comparison of hot and cold fusion reactions.<sup>16</sup>

For the heavier transactinides, experiments have used the projectile  $^{48}\text{Ca}$  on an actinide target. These experiments have resulted in much higher cross sections, on the order of picobarns, which would correspond to about an atom per day.<sup>18, 38</sup> The doubly magic nature of  $^{48}\text{Ca}$  is thought to provide additional stabilization to the compound nucleus; while the  $^{48}\text{Ca}$  nuclei has a smaller chance of a spontaneous fission event, the hot fusion reaction asymmetry bolsters the chances of a successful fusion. These factors have helped produce superheavy nuclides (from element 112-118) along with their decay daughters with longer half-lives relative to elements 107-112.<sup>16</sup>

Cross sections ( $\sigma$ ) are the probabilities that state how likely a nuclear reaction will occur. They are measured in barns: 1barn (b) =  $10^{-24}$  cm<sup>2</sup>. Since the average nucleus has about a radius of  $6 \times 10^{-13}$ , a geometric cross section would be on the order of  $10^{-24}$  cm<sup>2</sup>. Cross sections for the

super heavy elements can range from 10 nb to 1 fb. The production rate of the transactinides can be represented by the following equation:<sup>16</sup>

$$R = (\sigma \text{ (cm}^2\text{)})(\text{Target Nuclei per cm}^2\text{)}(\text{Projectile flux (s}^{-1}\text{)})$$

Many of the common transactinide production reactions together with their cross sections are listed in Figure 1.3. The cross sections generally decrease as the mass of the product increases.

Z	Best stable beam reaction	$\sigma$ (pb)	$\phi$	Best RNB reaction	$\sigma$ (pb)	$\phi$
102	$^{243}\text{Am}(^{14}\text{N},3\text{n})$	2900000	$6 \times 10^{12}$	$^{248}\text{Cm}(^{16}\text{C},4\text{n})$	8100000	$4 \times 10^9$
103	$^{248}\text{Cm}(^{14}\text{N},5\text{n})$	2200000	$6 \times 10^{12}$	$^{238}\text{U}(^{24}\text{Na},5\text{n})$	16200	$2 \times 10^{13}$
104	$^{249}\text{Bk}(^{14}\text{N},5\text{n})$	2700000	$6 \times 10^{12}$	$^{237}\text{Np}(^{24}\text{Na},5\text{n})$	1550	$2 \times 10^{13}$
105	$^{252}\text{Cf}(^{14}\text{N},3\text{n})$	340000	$6 \times 10^{12}$	$^{244}\text{Pu}(^{24}\text{Na},5\text{n})$	3630	$2 \times 10^{13}$
106	$^{249}\text{Bk}(^{19}\text{F},5\text{n})$	715	$6 \times 10^{12}$	$^{252}\text{Cf}(^{21}\text{O},5\text{n})$	2500000	$2 \times 10^{10}$
107	$^{253}\text{Es}(^{18}\text{O},4\text{n})$	40800	$6 \times 10^{12}$	$^{248}\text{Cm}(^{24}\text{Na},5\text{n})$	3200	$2 \times 10^{13}$
108	$^{252}\text{Cf}(^{22}\text{Ne},4\text{n})$	4940	$6 \times 10^{12}$	$^{249}\text{Bk}(^{24}\text{Na},5\text{n})$	1220	$2 \times 10^{13}$
109	$^{253}\text{Es}(^{22}\text{Ne},4\text{n})$	3030	$6 \times 10^{12}$	$^{252}\text{Cf}(^{24}\text{Na},5\text{n})$	2000	$2 \times 10^{13}$
110	$^{246}\text{Cm}(^{30}\text{Si},4\text{n})$	224	$6 \times 10^{12}$	$^{253}\text{Es}(^{24}\text{Na},5\text{n})$	275	$2 \times 10^{13}$
111	$^{249}\text{Bk}(^{30}\text{Si},4\text{n})$	96	$6 \times 10^{12}$	$^{238}\text{U}(^{42}\text{K},5\text{n})$	5.2	$4 \times 10^{12}$
112	$^{250}\text{Cf}(^{30}\text{Si},4\text{n})$	17	$6 \times 10^{12}$	$^{237}\text{Np}(^{43}\text{K},4\text{n})$	0.6	$3 \times 10^{12}$
113	$^{249}\text{Bk}(^{36}\text{S},4\text{n})$	11	$6 \times 10^{12}$	$^{244}\text{Pu}(^{42}\text{K},5\text{n})$	1.7	$4 \times 10^{12}$
114	$^{244}\text{Pu}(^{48}\text{Ca},4\text{n})$	120	$6 \times 10^{12}$	$^{248}\text{Cm}(^{46}\text{Ar},4\text{n})$	740	$4 \times 10^9$
115	$^{253}\text{Es}(^{36}\text{S},4\text{n})$	2.3	$6 \times 10^{12}$	$^{248}\text{Cm}(^{46}\text{K},5\text{n})$	91	$4 \times 10^{11}$
116	$^{248}\text{Cm}(^{48}\text{Ca},4\text{n})$	60	$6 \times 10^{12}$	$^{249}\text{Bk}(^{43}\text{K},4\text{n})$	1.9	$3 \times 10^{12}$
117	$^{249}\text{Bk}(^{48}\text{Ca},4\text{n})$	17	$6 \times 10^{12}$	$^{252}\text{Cf}(^{46}\text{K},5\text{n})$	22	$4 \times 10^{11}$
118	$^{252}\text{Cf}(^{48}\text{Ca},4\text{n})$	7.8	$6 \times 10^{12}$	$^{253}\text{Es}(^{46}\text{K},5\text{n})$	2	$4 \times 10^{11}$
119	$^{253}\text{Es}(^{48}\text{Ca},4\text{n})$	1.6	$6 \times 10^{12}$	$^{209}\text{Bi}(^{92}\text{Kr},4\text{n})$	0.01	$4 \times 10^{11}$
120	$^{252}\text{Cf}(^{50}\text{Ti},4\text{n})$	0.03	$6 \times 10^{12}$			

**Figure 1.3** List of hot fusion reactions with a stable beam and a radionuclide beam (RNB) their cross sections ( $\sigma$ ) in picobarns and associated ion beam strength  $\phi$  (ions/sec).<sup>39</sup>

### 1.2.2.1 Relativistic Effects

The transactinides offer a unique chance to gain better of understanding of the principles governing the periodic table. The elements are arranged and grouped together based on

similarities in chemical properties. These groupings allow for the extrapolation of chemical behavior; therefore, the correct position of a transactinide can be determined by comparing its chemical properties with its homologs and pseudo-homolog. A homolog of an element is located in the same vertical group in the periodic table, whereas a pseudo-homolog is an element that possesses the same oxidation state and similar ionic radii, but is not in the same group as the transactinides. For example, rutherfordium's homologs are zirconium and hafnium (Zr and Hf), and its pseudo-homologs are thorium and plutonium (Th and Pu). One of the primary reasons to investigate the chemical properties of the transactinide elements is due to relativistic effects that may or may not change the chemical behavior of these elements in relation with its homologs and/or pseudo-homologs.

Relativistic effects occur when the nucleus becomes populated with more protons. As more protons are accumulated, the Coulombic attraction increases between the protons and electrons. Specifically, the inner s and p orbital electrons' velocities can come close to the speed of light and these electrons' radii begin to contract. This is shown by Einstein's theory of relativity; it reasons that as an object gains velocity near the speed of light, it increasingly gains mass:

$$m = \frac{m_o}{\sqrt{\left(1 - \left(\frac{v}{c}\right)^2\right)}}$$

If  $m_o$  is the rest mass of an electron and  $v$  is the speed of an electron, the Bohr radius can be calculated as:

$$a_o = \frac{(4\pi\epsilon_o)}{\left(\frac{\hbar^2}{me^2}\right)}$$

So as the electrons' speed increases, the Bohr radius decreases. Figure 1.3.1 shows the comparison between the relativistic and the theoretical nonrelativistic distribution of the 7s electrons.

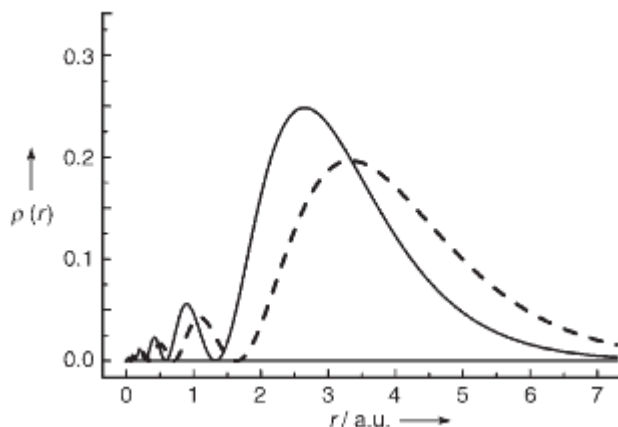


**Figure 1.4:** The relativistic (solid line) and non-relativistic (dashed lines) distribution of Db's 7s electrons.<sup>40</sup>

The s electrons are particularly vulnerable to this effect as they have no angular momentum. The p electrons, having angular momentum, are still susceptible to the mass-velocity effect but not with the same magnitude. They do, however, experience a spin-orbit split that separates the three p orbitals into one  $p_{1/2}$  and two  $p_{3/2}$  orbitals. The  $p_{1/2}$  orbital undergoes the same magnitude of contraction as the s electrons; but for the  $p_{3/2}$  electrons, these effects negate each other. The contraction of the s and  $p_{1/2}$  orbital are considered the “direct relativistic effect.” Because of the contraction of these orbitals, they shield the effective nuclear charge and cause the d and f orbitals to expand. This is termed as the “indirect relativistic effect.” The last effect is spin orbital splitting that occurs for electrons in levels with  $l > 0$  (p, d, f, ... electrons) into  $j = l \pm 1/2$  states. Originating in the nucleus, spin orbit coupling becomes similar or even larger in size than typical bond energies. Since this effect arises from the nucleus, the spin-orbit splitting lessens

with higher number of subshells. These effects has the same significance and increases correspondingly to  $Z^2$ .<sup>16</sup>

### 1.2.3 Solvent Extraction

Solvent extraction (SX) is a separation technique by which a compound can be concentrated more readily between two immiscible liquid phases in based on its solubility preference. While these phases can be any two liquids, the majority of solvent extractions are aqueous and organic based. When the solubility of an analyte varies greatly between the two phases, then this property can be exploited to selectively separately the solute from other undesired impurities.<sup>41</sup>

To quantitatively measure the performance of a SX system, the distribution ratio, D, is used. It compares the solubility of the solute in the organic phase with its solubility in the aqueous phase at equilibrium. Mathematically, it can be represented by:

$$D = \frac{A_{org}}{A_{aq}}$$

where  $[A_{org}]$  described as the concentration of the solute in the organic phase, whereas  $[A_{aq}]$  is the concentration of the solute in the aqueous phase.<sup>42</sup> The D value is temperature dependent since solubility and equilibrium rates are greatly affected by the heat present in the solution.

The phase boundary between the solvents is where the solute interacts and is transported between the two solutions. If the phase boundary area is increased, the time necessary to reach equilibrium will also be decreased. One of the simplest ways to achieve this is by robust mixing of the solvents. To easily manipulate the extraction to possibly extract a variety of different solute, the formation of the extracted complex can be controlled to selectively extract certain solutes into the organic phase. The concentration of an acid in the aqueous phase can affect the



concentration of the complex. For systems with lower distribution ratios, the SX may have to be performed multiple times to achieve satisfactory separation.<sup>43</sup>

Generally, higher distribution ratios are desired to achieve higher separation factors from the undesired products. To accomplish this, an additional extractant may be added to the organic to increase its performance. This solid or viscous extractant may require a solvent to be able to operate as a functioning liquid phase. The appropriate solvent must be selected with respect to its polar properties, as a solute may not dissolve in the right solvent or the solvent may not be nonpolar enough to form an immiscible phase with the aqueous solution. Diluents should generally exhibit the properties of having a low viscosity and a high surface tension to shorten the length of time an emulsion occurs after mixing the two phases.

Because elements can have different solubilities in the two phases, a mixture of different solutes can be separated by relying on their different distribution ratios in the phases. The desired element can either be extracted in the organic phase leaving the impurities behind, or the impurities can be extracted into the organic phase leaving the desired element behind. The separation factor is the measure of the efficacy of this operation and can be expressed by the following:

$$SF = \frac{D_A}{D_B}$$

where  $D_A$  and  $D_B$  are the distribution ratios of the particular solutes of interest.

Formation of a third phase is a problematic feature that can occur when a diluent and extractant are contacted with the aqueous phase. The diluent with a small concentration of extractant are contained in the lighter phase; the heavier third phase consists of a much higher percentage of the extractant with little diluent. Generally, the third phase forms because of the

polar nature of the more polar metal-extractant molecules and the nonpolar diluent. Because solvent extraction processes have strict flow and mixing requirements, the formation of a third phase can form an additional obstacle to the separation. For example, in separations for the nuclear fuel cycle, plutonium can become more concentrated in the third phase, which prompts criticality concerns. The addition of a modifier chemical, such as an alcohol, can dissipate the third phase by making the solute a slightly more polar environment for the metal extracted complex to become dissolved.<sup>44</sup> However, this should be avoided as modifiers generally decrease the extraction capability.

#### 1.2.4 Extraction Chromatography

Chromatography is a process where two substances can be separated, based on their attraction for a solid or mobile phase. Extraction chromatography is a branch of this technique, where a ligand bound to a solid support is considered the stationary phase and a liquid passes along the solid as the mobile phase. This is analogous to the liquid-liquid extraction where the organic phase would be placed onto resin bead and the aqueous phase would be the liquid moving through the column. The organic extractant can be placed on the resin bead by dissolving it in a volatile solvent (such as dichloromethane (DCM)) and allowing it to slowly evaporate while in the presence of a support backbone. This method leads to a uniform and even coat of extractant on the resin bead. After this method, the resin can be packed into a column and the aqueous phase can be varied at various points in the extraction to manipulate the elution of different substances. If the analyte of interest has a stronger affinity for the stationary phase, then the elution time is longer for that substance, whereas other analytes with less attraction for the resin will travel more quickly through the column. These components can then be separated by collecting them in different fractions. Figure 1.51 shows the basic schematic of an extraction

chromatographic system. The advantages of EXC are the ease, speed, and performance of a column is paired with the selectivity of a solvent extraction, while also eliminating the production of organic waste.<sup>45</sup>

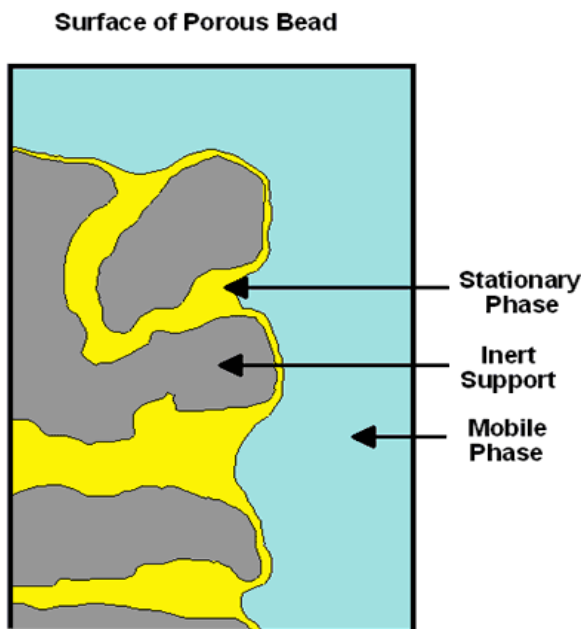


**Figure 1.5** Diagram of the components of an extraction chromatographic system.<sup>46</sup>

Column chromatography is governed by theoretical plates, the zone where two phases establish an equilibrium with each other. For solvent extraction, this is one step for the extraction. In extraction chromatography, the height equivalent of a theoretical plate, HETP, is measured by the following equation:<sup>47</sup>

$$\text{HETP} = \frac{(L)(W^2)}{8(V_{\text{max}}^2)}$$

For Equation 1.4.1, L is the length of the column, W is the width of the peak at 1/e times the maximum value and  $V_{\text{max}}$  is the elution volume to peak maximum. The advantage of EXC is that, instead of one theoretical plate occurring in an experimental run, many extractions occur as the mobile phase interacts with the solid phase. The number of theoretical plates can be determined by dividing the HETP by the length of the column, L. A variety of parameters can

influence the performance of an extraction chromatographic column's elution profile. Horwitz and Bloomquist considered many of these factors such as particle size of the inert support, extractant weight loading, temperature, cross section of the column, elution rate, and the column bed length and found that all can affect the HETP value. As such, lowering the HETP causes higher retention times and larger elution volumes.

As stated previously with solvent extraction, Equation 1.5.2 defines the distribution ratio.

$$D = \frac{A_{org}}{A_{aq}}$$

The difference between the distribution ratios of two analytes allows for the separation to occur.<sup>47</sup> In EXC, the number of free column volumes to peak maximum,  $k'$ , is used to describe the attraction of the solutes to the stationary phase. The equation 1.5.3 shows how the  $k'$  is calculated:<sup>47</sup>

$$k' = \frac{V_{max} - v_m}{v_m}$$

$V_{max}$  is the elution volume to peak maximum and  $v_m$  is the column void volume (or space within the column not occupied by the stationary phase). The higher the  $k'$  for a substance is, the more affinity it shows for the stationary phase. Because  $k'$  is dependent on volume and is a dimensionless number, it is independent of the large variance of column parameters. With the  $k'$  values, the separation factor between 2 analytes can be determined:

$$SF = \frac{k'_A}{k'_B}$$

The width of the elution band can be calculated by:<sup>48</sup>

$$SR = \frac{1}{4} \left( 1 - \frac{1}{SF} \right) (N^{1/2}) \frac{k'_2}{1 + k'_2}$$

Values such as  $k'$  are also obtained in batch experiments where free resin is placed in an aqueous solution instead of a column. Radiochemical tracers are often utilized in these studies because they can be performed at high speed and are a simple setup. The weight distribution ratio can be described by the following equation:

$$D_w = \left( \frac{A_o - A_s}{A_s} \right) \left( \frac{\text{mL}}{\text{g}} \right)$$

$A_o - A_s$  is the activity sorbed on a known weight of resin, g.  $A_s$  is the activity in a known volume of solution, mL. The  $k'$  value can be derived by converting from  $D_w$  to the volume distribution ratio:

$$D_v = D_w \times \frac{d_{\text{extr}}}{w_{\text{load}}}$$

$$k' = D_v \times \frac{v_s}{v_m}$$

The  $d_{\text{extr}}$  is the density of the extractant, and  $w_{\text{load}}$  is the extractant loading in grams of extractant per gram of resin. The  $v_s$  and  $v_m$  values are the volumes of the stationary and mobile phases respectively. The  $k'$  value can also be calculated directly by multiplying the  $D_w$  by the resin factor,  $F_c$ :

$$k' = D_w \times F_c$$

The  $F_c$  is a constant provided from the resin manufacturer that considers the various parameters in the calculation of  $D_v$ .<sup>47-48</sup>

### 1.2.5 Atom-at-a-Time Chemistry

Experiments to study the chemistry of the transactinide elements are difficult due to the atom-at-a-time production. For an effective trial, a highly sensitive detection system is necessary to correctly identify the presence of a transactinide. The ideal method to confirm a positive nucleus production is to measure the successive  $\alpha$ -decays of the transactinide and its daughters

all the way to a nuclide with a known  $\alpha$ -decay energy. However, due to the various decay branches and nuclear instability, the transactinide or its daughter may also undergo spontaneous fission. Although this outcome is not preferable, the  $\alpha$ -decay energies of the previous nuclides can be used for identification. Because of the low production rates and short half-lives, the process of separation and identification must be rapid, selective and efficient. These chemical studies can be carried out in two phases, either liquid or gas. Chemical studies for rutherfordium through seaborgium (104-106) as well as hassium (108) have been carried out in both the gas and as well as the liquid phases, whereas the chemistry of copernicium (112) and flerovium (114) has only been studied in the gas phase. Gas phase studies are inherently more abundant due to a lack of a solvent evaporation step. This gives a speed boost to the experiment because the solvent does not need to be evaporated down before the detection of the transactinide.

Atom-at-a-time chemistry poses a challenge to chemical thermodynamics and kinetics. Macroscopic chemistry is based on the assumption of many atoms undergoing a chemical reaction or equilibrium, but transactinide studies do not have the luxury of having a large number of atoms to perform reactions. Current macroscopic chemical equilibria is based on the law of mass action:

$$K = \frac{a^c(C)a^d(D)}{a^a(A)a^b(B)}; \quad \text{For} \quad aA + bB \leftrightarrow cC + dD$$

K is defined as the equilibrium constant. If the metal ion is both a constituent of A and C, then at the equilibrium point, the metal ions exchange at each site at a constant rate. However, if only one atom of the metal ion exists, it cannot be present in A and C simultaneously. Therefore, an equilibrium constant cannot be defined because the activity for A or C is zero. Guillaumont et. al. have proposed a law of mass action for atom-at-a-time by substituting the concentration with

the probabilities of finding an atom in a given phase, deriving a formula for transactinide studies.<sup>49-51</sup>

For the reaction,  $MA + B \leftrightarrow MB + A$ , the forward and reverse reaction rate is governed by the height of the activation energy barrier. The higher the barrier the slower the reaction rate and the slower the equilibrium will be established. This is because more energy is required to overcome the resulting barrier. For transactinide chemical systems, the equilibrium must be established on the order of seconds due to the short half-life of the transactinide of interest. Activation energies less than 60 kJ provide enough time for the equilibrium to be reached compared to the half-life of the transactinide element.<sup>51</sup>

Prior to performing an online transactinide chemistry experiment, the chemical system must be tested with the homologs and pseudo-homologs of the transactinide element. Batch studies are used to investigate the best parameters and performance of the resin with the homologs for separation. Dynamic column studies are used to study the transport of the radiochemical tracer or flow conditions of the resin. The kinetics of both these types of experiments are also examined to ensure that the chemistry happens fast enough for the transactinide chemical system. After the specifications are optimized, on-line studies at accelerators are performed with the homologs and pseudo-homologs. Online experiments are necessary because they provide invaluable data regarding the kinetics of the chemical system and the species that form during the nuclear reaction and transport.

The chemical system must be very selective for the desired element. In the nuclear reaction of the projectile and target foil, a large number and variety of transfer products are created other than the transactinide of interest. These transfer reaction production rates are orders of magnitude higher than the production of the transactinide and can interfere with the

identification of the transactinide element. Therefore, magnetic pre-separators, such as the TransActinide Separator and Chemistry Apparatus (TASCA) at Gesellschaft für Schwerionenforschung (GSI), and the Berkeley Gas-filled Separator (BGS) at Lawrence Berkeley National laboratory (LBNL) can be used as an effective instrument to separate out the unwanted transfer products. They work by using the magnetic rigidities of the transfer products:<sup>52</sup>

$$B\rho = \frac{mv}{q}$$

$B\rho$  the magnetic rigidity of a particle of mass,  $m$ , velocity,  $v$ , and charge,  $q$ . The dipole region of the separator is filled with a dilute gas, such as He, and the moving ions change energy, direction, and charge from their interactions with the gas (see Figure 1.6).

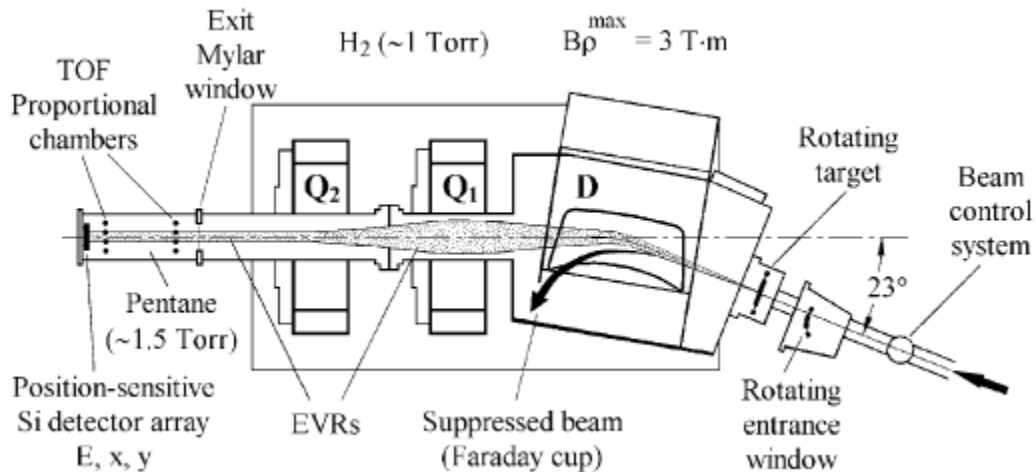


**Figure 1.6** Schematic of the Dubna Gas-filled Recoil Separator (DGFRS).<sup>53</sup>

The beam will split into components based on different charge values, reaching an equilibrium mean charge after colliding with many gas atoms. With a Gaussian distribution centered at  $\bar{q}$ , the equilibrium of the charges can be approximated calculated by:

$$\bar{q} \approx \frac{v}{v_0} Z^{1/3}$$



Z is the ion atomic number and  $v_0 = 2.19 \times 10^6$  m/s (Bohr velocity). Combining Equations 1.5.2 and 1.5.3 yields:

$$B\rho = 0.02267 \frac{A}{Z^{\frac{1}{3}}}(Tm)$$

For the online chemistry, the experiments can be operated in two different methods. A static method measures the distribution coefficient of a single atom between two phases. This experiment is performed repeatedly to get enough data to perform a statistical analysis. Some of the earliest transactinide chemistry experiments were performed this way by using solvent extractions and determining in which phase the superheavy element resided by alpha counting. As an example, SISAK (Short-lived Isotopes Studied by the AKUFVE technique) has been used as a continuous liquid-liquid extraction system.<sup>54</sup> The other method is a dynamic study where there are several successive static experiments performed. An example of this is a column chromatography experiment where the atom undergoes hundreds of exchange steps between the mobile and stationary phases. Both methods can be performed continuously or discontinuously. ARCA (Automated Rapid Chemistry Apparatus), an extraction chromatography system, is a dynamic system but it is also discontinuous because the system requires maintenance at regular intervals.<sup>55-56</sup>

### 1.2.6 Zirconium and Hafnium Aqueous Chemistry

Zirconium and hafnium have such a similar chemical behavior that they are very difficult to separate. Considering the electron configuration's for both elements (Zr is  $[\text{Kr}]5s^24d^2$  and Hf is  $[\text{Xe}6s^24f^{14}5d^2]$ ), both should have notably different chemical behaviors due to the addition of the f shell for hafnium. However, the lanthanide contraction and relativistic effects shield the nuclear charge for hafnium so that the atomic and ionic radius shrink to about the same size as

for zirconium. Having only the +IV oxidation state available, zirconium's and hafnium's similarities in the structure of the electron orbitals prevents a great disparity in reaction rates and complexation formation.

**Table 1.6:** Atomic properties of the group IV elements and pseudohomologs.

Property	Ti	Zr	Hf	Th	Pu
Atomic number	22	40	72	90	94
Electronic structure	[Ar]3s <sup>2</sup> 4d <sup>2</sup>	[Kr]5s <sup>2</sup> 4d <sup>2</sup>	[Xe]4f <sup>14</sup> 5d <sup>2</sup> 6s <sup>2</sup>	[Rn]6d <sup>2</sup> 7s <sup>2</sup>	[Rn]6f <sup>6</sup> 7s <sup>2</sup>
Number of naturally occurring isotopes	5	5	6	1	1
Atomic weight	47.867	91.224	178.49	232.03806	207.2
Ionic radius/pm	60.5	72	71	94	86
M(IV)					
M(III)	67.0	-	-	-	100
M(II)	86	-	-	-	-
Metal radius/pm	147	160	159	179	159
Melting point	1667	1857	2222	1750	640
Boiling point	3285	4200	4450	4788	3228
Pauling electronegativity	1.5	1.4	1.3	1.3	1.3

One of the challenges posed by the group IV elements is that they hydrolyze in dilute acidic solutions. These hydrolysis products create an obstacle when trying to study the speciation and behavior of mononuclear species. The presence of only mononuclear species is essential

since rutherfordium will only be created at an atom-at-a-time. Zr and Hf also form polynuclear species in metal concentration of greater than  $10^{-4}$  M and in less than 2 M acidic solutions.<sup>57</sup> Therefore, even the addition trace amounts of Zr and Hf can greatly influence the chemical speciation in solution. In column studies, these species cause the adsorption behavior to change and may even block the active sites.

In chloric, nitric, hydrofluoric and perchloric acidic matrices ( $\gg 6$  M acid), the hexa complex predominates and is the main anionic species for extraction studies. However, at low acid concentrations ( $< 2$  M), cationic species are formed. For HCl, neutral complexes are the major species from 4-8 M HCl.<sup>58</sup> Theory predicts that the complex formation strength between the group IV elements follows this trend:  $Zr \geq Hf > Rf$ .<sup>59</sup>

#### 1.2.7 Group IV Liquid Phase Online Chemistry

Initial chemical studies of rutherfordium were carried out to determine its chemical behavior and to confirm its placement on the periodic table. In 1970, R.J. Silva et. al. used cation exchange chromatography and  $\alpha$ -hydroxyisobutyric acid ( $\alpha$ -HiB) for the first liquid phase chemistry experiment.<sup>60</sup> The isotope  $^{261}\text{Rf}$  was produced at the Berkeley Heavy Ion Linear Accelerator (HILAC) by bombardment of a  $^{248}\text{Cm}$  target on a Be foil with a 92 MeV  $^{18}\text{O}$  beam. After being transported from the target assembly in helium gas, the recoil products then were placed on a Pt foil coated with ammonium chloride from the gas jet. This residue was washed with ~50 microliter of 0.1 M ammonium  $\alpha$ -HiB and dropped into 2 mm x 2 cm long heated Dowex 50 x 12 cation resin. Three two drop fractions were then collected: the first fraction contained the free column volume of liquid and had approximately no activity. The next two fractions were collected onto platinum discs and measured on  $\alpha$ -detectors. These two fractions possessed activity attributed to  $^{261}\text{Rf}$  and chemically followed Zr and Hf behavior on the column resin, whereas the

lanthanides and trivalent actinides stuck strongly to the column. In 1980, E. K. Hulet et. al. conducted a study with an extraction chromatographic resin using the ligand Aliquat 336 (trioctylmethyl ammonium chloride) because the extractant had faster thermodynamics. Due to the anionic complex that forms and bonds with the resin, the recoil products were placed on the column in 12 M HCl, and eluted off in 6 M HCl. They were then counted on  $\alpha$  detectors. They found that Rf showed the same behavior as Zr and Hf.<sup>61</sup>

Fluoride complexes have also been studied for rutherfordium and its homologs in a variety of conditions. Rajan et. al. have used Amberlite IRA 400 and Dowex 2 to separate a small amount of Hf from a large amount of Zr base on the hexafluoro complex.<sup>62</sup> Using a multicolumn system (an anion column between two cationic exchange columns), Pfrepper et. al. successfully showed that Rf displayed similar behavior like Hf in an on-line experiment.<sup>63</sup> Trubert et. al. used a Bio-Rad AG-MP1 resin to separate all the group IV elements at low concentrations of HCl with 0.02 M HF.<sup>64</sup> Since this separation was at low concentrations of acid, the group IV element should be extracted as a neutral or cationic species. Employing a similar experiment, Strub et. al. found with a Dowex 1x8 anion exchange column the group IV elements can be loaded with a 0.1 M HNO<sub>3</sub>/0.1 M HF solution and eluted off with 5 M HNO<sub>3</sub>/0.001 M HF.<sup>65</sup> Rutherfordium was eluted at an HF concentration an order of magnitude higher than Zr and Hf. However, they also investigated the elution of Th and found that it took an even higher concentration of HF to elute off than Rf. Toyoshima and Ishii discovered a similar behavior, but determined that the formation of the fluoro complex of Rf is weaker than Zr and Hf.<sup>66-67</sup> Kronenberg et. al. found that for a mixed nitric and hydrofluoric system on an anion exchange column the Rf adsorption diminishes due to the nitric acid.<sup>68</sup> Rutherfordium then does not stick to the column and elutes quickly. This contradicts the previous work of the other scientists. Initially, it is possible to

believe that with the presence of nitric acid that Rf does not form a hexafluoro complex, but the authors cite that the nitric acid may be increasing competition for the exchange sites.

For pure and mixed chloride systems, Huffman, Street and Kraus et. al. have looked into the chemical behavior for the group IV elements (excluding Rf). Huffman et. al. used an anion exchange column and an Amberlite IRA 400 column.<sup>69</sup> The group IV elements can be separated in a mixture of hydrochloric and hydrofluoric acids. On the Dowex 2 column, this is due to the formation of the hexachloro complex (only hydrochloric acid was used). For the Amberlite IRA 400, the separation was based on the fluoro-chloro complex.<sup>70</sup> Hf and Zr can also be separated using 6 M HCL to elute the elements off the 50 Dowex cation exchange column. With 1 M HCl/0.5 M HF, Zr and Hf can be separated using a Dowex 1 column.

Group IV's behavior can also be examined with sulfuric acid. Szeglowksi et. al. and Li et. performed experiment with H<sub>2</sub>SO<sub>4</sub>.<sup>71</sup> Szeglowksi used a multi-column system of (a Dowex 50WX8 column between two Dowex 1X8 exchange columns) and found that the system could be used due to the metal cation formation in dilute sulfuric acid. In Li et. al.'s study, a mixed sulfuric and nitric system was used to separate the group IV elements and thorium. They found the resulting trend for the sulfate complex formation:  $Zr \geq Hf > Rf \gg Th$ .<sup>72</sup>

## 2. MATERIALS AND INSTRUMENTATION

### 2.1 Offline Studies

#### 2.1.1 Tris(2-ethylhexyl)amine and tris(2-ethylhexyl)phosphate

In 2010, Banda et. al. demonstrated that zirconium and hafnium could be separated successfully with TEHA and TEHP in kerosene.<sup>73</sup> Since TEHA and TEHP have not been used before in studies of rutherfordium, these two ligands were selected as prime candidates for super heavy element chemistry. Banda et. al. focused on separating milligram to gram quantities of the group 4 elements, possibly for the separation of zirconium and hafnium for the production of zircalloy, the primary material for nuclear fuel rods. Gaudh and Shinde reported that tri 2-ethyl hexyl (TEHP) phosphate can also separate Zr and Hf in hydrochloric acid.<sup>74</sup> TEHA and TEHP's chemistry with tracer level of zirconium and hafnium had however not been investigated. No literature is available for any extraction data neither for plutonium in a chloride matrix nor for the production of a resin coated with these ligands. Both TEHA and TEHP used for experiments were purchased from Sigma-Aldrich.

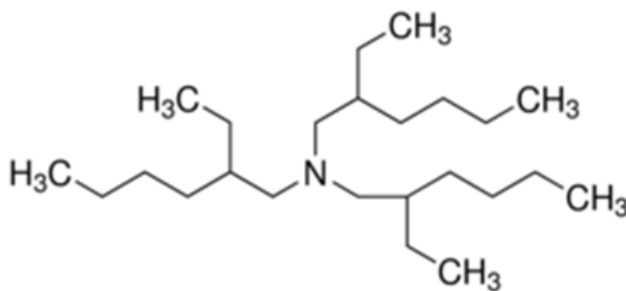


**Figure 2.1** Structure of Tris(2-ethylhexyl)amine

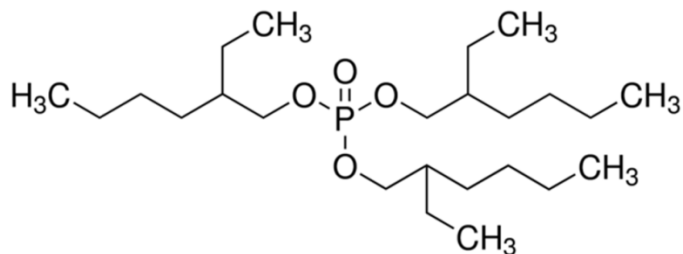


**Figure 2.2** and tris(2-ethylhexyl)phosphate

Tertiary amines have been found to extract forming an ammonium salt with the metal complex. This reaction is represented by the following equation:



where  $R_3N$  is the tertiary amine,  $H^+$  is the proton from an acidic solution,  $M^-$  is the metal anion complex, and  $R_3NH^+M^-$  is the extracted species. Metals that have high oxidation states generally are present in high concentrations of HCl as anionic chloride species, which helps facilitates this reaction. Trivalent metals do not form these species and do not readily extract with tertiary amines.<sup>75</sup> These two properties can be exploited for a separation.

Organophosphate ligand such as TEHP form adducts to extract the metal complexes. Adducts are the formation of neutral metal complexes and the organic extractant. The reaction is shown as:



where  $M^{n+}_{aq}$  is the metal in solution,  $nA^{-}_{aq}$  is the acid, and  $MA_nTEHP_x$  is the extracted complex.

The doubled bonded oxygen is where the complex interfaces with the metal complex species.

Although charged species may exist in solution, only neutral complexes can be extracted.

Neutral acidic species may also participate in the extraction.<sup>76</sup>

### 2.1.2 Radionuclide tracers

### 2.1.2.1 $^{89}\text{Zr}$ Solution

A solution of carrier-free  $^{89}\text{Zr}$  tracer was used in all experiments. It was obtained either from Perkin-Elmer or from the cyclotron at the University of Wisconsin. All  $^{89}\text{Zr}$  was received as a  $\sim 2$  mCi solution in  $\sim 10$   $\mu\text{L}$  oxalic acid solution. To convert the oxalate to the chloride, a conversion procedure was required.

First, the oxalic acid solution was mixed with 2 mL of a solution containing 10mg/mL lanthanum nitrate. Next, about five drops of ammonium hydroxide were added to the solution to turn the solution basic. This causes the precipitation of lanthanum hydroxide, which appears white and grainy. After this step, the solution was centrifuged for 15 minutes to cause the  $^{89}\text{Zr}$  to become trapped between the spaces of the precipitate, effectively separating out the  $^{89}\text{Zr}$  from the oxalate. After the centrifugation, the solution was decanted from the precipitate and counted to ensure that no activity was left with the oxalate. The precipitate was rinsed vigorously with 2 mL of deionized water and centrifuged again for 10 minutes. Then, the supernatant solution was counted again, and the precipitate was only lightly rinsed with deionized water. The deionized water was removed and 3 mL of concentrated hydrochloric acid was added. Now exposed to acidic conditions, the precipitate was dissolved and required further purification from the lanthanum.

To achieve this, the solution was passed through an ion exchange column for separation. A Dowex 1X8 column was prepared by first washing the column with 10 to 15 mL deionized water. Next, the column was conditioned with 4 mL of 12 M hydrochloric acid, added in 1 mL increments. The stock solution of  $^{89}\text{Zr}$  was then added to the column. A load fraction was collected and counted. Next, the column was washed with 2 mL of 12M hydrochloric acid. This wash fraction was also collected and counted to ensure no  $^{89}\text{Zr}$  was eluting. Finally, 6 mL of 2 M



hydrochloric acid was added to the column, with fractions being collected at 1 mL intervals. The  $^{89}\text{Zr}$  content in each fraction was counted, and the fractions were then dried down and combined into one stock solution.

#### 2.1.2.2 $^{175}\text{Hf}$ solution

The  $^{175}\text{Hf}$  used was produced at the Center for Accelerator Mass Spectrometry (CAMS) at Lawrence Livermore National Laboratory (LLNL). The setup at the accelerator consisted of a natural lutetium foil placed as a catcher foil in another experiment that was bombarded by photons. With a proton beam energy of  $\sim 12$  MeV the  $^{175}\text{Lu}(p,n)^{175}\text{Hf}$  reaction was used to make the no carrier added  $^{175}\text{Hf}$ . An approximate total activity of  $\sim 1000$  cps was produced. The foil was then partially dissolved in concentrated hydrochloric acid, leaving behind some black residue. The solution was decanted and the residue was counted to ensure that none of the  $^{175}\text{Hf}$  was remaining in the residue. This was followed by a purification step on a Dowex 1X8 column. The same column procedure as described in section 2.1.2.1 was followed, with the exception of the elution step (instead of eluting the  $^{175}\text{Hf}$  with 2 M hydrochloric acid, a solution of 7 M hydrochloric acid was used).

#### 2.1.2.3 $^{239}\text{Pu}$ solution

The  $^{239}\text{Pu}$  was purchased as a stock solution from Eckert-Zeigler Isotope Products in 4M nitric acid. An amount containing approximately 15,000 cpm was obtained from the stock and converted to hydrochloric acid through multiple evaporations of the solution, and reconstituting the  $^{239}\text{Pu}$  in concentrated hydrochloric acid to drive off the  $\text{NO}_3^-$  present in the solution. The oxidation state was controlled by adding a 1:10 HI/HCl solution to the plutonium and again evaporating the solution drive off the HI remaining in solution.

Ultimately,  $^{239}\text{Pu}$  was chosen rather than Th as the homolog to study. While natural thorium is abundant and cheap, carrier-free solutions are required for transactinide homolog studies. The  $^{232}\text{Th}$  isotope has too long of half-life to be measured on a radiation detector and a carrier-free  $^{228}\text{Th}$  isotope would require production at an accelerator. Therefore,  $^{239}\text{Pu}$  was chosen as its accessibility was easier despite the more complex chemistry.

### 2.1.3 Other reagents used

Reagent grade acids and organic solvents were purchased from Sigma-Aldrich. Acid solutions were prepared by diluting concentrated acids with deionized water from an 18M $\Omega$  cm purification system, such as a Millipore or Milli Q, The Ultima Gold AB liquid scintillation cocktail was obtained from Perkin Elmer. The different concentrations of acid and organic solutions were prepared using volumetric pipettes and volumetric flasks.

The TEHA and TEHP resins utilized were created in-house using a rotovap procedure. First, the resin backbones (Amberchrome CG71, XAD4, and XAD7HP) were washed with water through a filtration setup to remove sodium chloride, sodium bicarbonate, or isopropyl alcohol used to prevent bacterial formation in storage. The resin was dried in an oven for one week at 40°C. Then, an amount of dry resin backbone was added to a round bottom flask along with the appropriate amount of TEHA or TEHP to achieve the desired weight loading in a 25 mL to 100 mL of toluene or methanol slurry. The solution was allowed to mix on the rotovap for two hours at ambient temperature and pressure so that the ligand was evenly coated on the resin particles. Afterwards, the temperature of the water bath was increased to 30°C and the pressure was lowered to ~45 torr. The solution was allowed to evaporate overnight. The remaining residue was then placed in an oven at 40°C for 2 days to ensure complete evaporation of the solvent.

This dry weight was stored in plastic Nalgene container bottles at ambient temperature until use in batch studies.

## 2.2 Instrumentation

### 2.2.1 Sodium Iodide Detector

Sodium iodide crystals doped with thallium (NaI(Tl)) detectors are useful gamma detectors with excellent efficiencies and reasonable resolution of energy peaks. The NaI(Tl) detector detects gamma rays through the interaction of the photon with the electrons of the crystal. The incoming gamma photon causes the excitation and ionization of the electrons in the K or L shells of the NaI(Tl) crystal (lasting around 0.2  $\mu$ s), which give off a quantity of light whose intensity is directly proportional to the energy of the initial gamma photon. The light can be detected by a photomultiplier tube (PMT), which senses the flash of light photons and convert it into an interpretable voltage pulse to be measured and analyzed by electronics.

Due to the three unique ways that a gamma photon can interact with matter, each type of interaction must be understood in how the NaI(Tl) will provide output pulses from these exchanges. With the photoelectric effect, the height of the pulse is directly proportional to the original gamma ray energy. For this interaction, all of the energy of the incoming photon is deposited within the detector. However, effects such as the actual amount of gamma ray energy that is converted to light, the amount of light collected by the PMT, the efficiency of the PMT at ejecting electrons, and the gain of the PMT can cause statistical fluctuations in the data and affect the energy resolution. These variances do however not noticeably affect the net counts for the total absorption peak. These counts are therefore used to calculate the absolute activity.

With Compton scattering, a gamma photon only gives up a portion of its energy to the crystal. This fraction may vary from zero to the amount that can be transferred in a single

interaction. This is because the scattering angle determines how much of the energy from the photon will be deposited. As a result, a Compton continuum (an area of elevated counts) is created with an edge corresponding to the maximum kinetic energy of a Compton electron. A single peak will not arise, but rather a broad spectrum due to the variance of the angle in each Compton scattering (see Figure 2.1).

A gamma photon with an energy above 1.02 MeV can undergo pair production. This interaction results in a photon creating an electron/positron pair. The positron will deposit its kinetic energy within the crystal and then annihilate itself with an electron, giving rise to two 0.511 MeV photons. It is important to note because pair production with the materials surrounding the detector can especially interfere with the analysis of spectrums, in particular when expecting to have a gamma of ~0.511 MeV recorded. Also, the annihilation gammas (one or both) may escape the detector giving rise to a voltage pulse of a single escape peak or double escape peak.

Other characteristic peaks may also appear in the gamma spectrum that is produced. A backscatter peak arises from the complete absorption of gammas scattered 180 degrees from the shield. Other peaks can correspond to X-rays arising from the interactions of photons with the shield surrounding the crystal. These interactions can be traced to the internal conversion in the shield or surrounding materials.

One piece of the electronics that is used to evaluate these pulses' energies and convert them into a spectrum is a multichannel analyzer. It is different from the single channel analyzer in that it can take the voltage pulse and transform it into a Gaussian shape. It then takes the shape and begins placing the different pulse values into bins.

The primary gamma detector used for experiments at UNLV was a 2480 wizard automatic gamma counter. It contained a 3 inch NaI(Tl) well detector shielded by a 75 mm thick lead. Sample count time varied from 1 minute to 4 hours depending on the activity present in solution. All samples were counted in 13 mm diameter culture tubes.



**Figure 2.3** Wizard 2480 automated gamma counter

### 2.2.2 Germanium detectors

High purity germanium crystal (HPGe) detectors are gamma detectors with excellent resolution of energy peaks and are available with reasonable efficiencies. HPGe's are the cutting edge detectors and are used to identify unknown nuclides in samples because their ability at resolving peak to <1%.

The interaction of a gamma ray photon in the HPGe detector results in the production of electron-hole pairs in the crystal. Within the material, there are two bands: the conduction band and the valence band. The conduction band is where the electrons are allowed to move within the material, whereas the valence band is where the electrons are in the ground state. Between the

two states exists a region known as the band gap. No electrons are allowed to exist in this region unless the material contains impurities that allow the electron to exist in the impurities' energy states. The band gap can be measured and is shown to be about 5 MeV for insulators and about 1 MeV for semiconductors. For metals, the band gap is either very small or nonexistent because the bands can actually overlap. Because the band gap is close for semiconductors, it is necessary to cool the detector (at least for germanium semiconductors) to avoid having electrons become thermally excited and cross the band gap. A temperature of 77 K is used to stop the development of a leakage current.

When radiation enters the germanium detector, it causes electron hole pairs to form in the crystal matrix. Under the influence of an electric field, the electrons head to the anode and the holes move towards the cathode. Due to the fast drift velocity and small size, these detectors are among the fastest on the market. Its peak resolution is also very low because the large number of information carriers decreases the statistical variation. As with the Na(Tl) detectors, they share the same type of peak spectrum characteristics that are associated with the different interaction mechanism gamma photons, albeit with better peak resolutions. For a review of how gamma radiation interacts with matter, see the previous section.

### 2.2.3 Liquid Scintillation Counting

Liquid scintillation counting is an important technique used to examine the composition of mono-radioisotope samples. It is especially useful for beta emitters such as  $^3\text{H}$ ,  $^{14}\text{C}$ ,  $^{32}\text{P}$ , and  $^{35}\text{S}$  in the medical industry and in life sciences.

A liquid scintillator relies on the fact that the organic molecules contained in the solution emits light when it is excited by radiation. The mechanism that causes this process to happen can be described as follows: when the beta or alpha emitter gives off radiation, the resulting energy

deposition lead to an excitation of the solvent. This excitation energy is then passed on to an organic molecule, typically an aromatic compound such as toluene, which causes it to become excited and emit a photon. Thus, the interaction travels from the ionizing radiation to the solvent and then from the solvent to the scintillator. Then the solvent emits a photon and then the wavelength shifter absorbs and reemits that photon to a different wavelength. However, for the detector to see the fluorescence, a wavelength shifter is needed to better identify the light emitted. Additionally, the cocktail contains surfactants to form a more homogenous mixture for a variety of aqueous or chemically digested samples.

The primary advantage of liquid scintillation is the 100% efficiency of the instrument since the “detector” completely surrounds the source of radiation, greatly aiding in achieving superior counting statistics. Most LSC’s are also automated so that large numbers of samples can be measured quickly. Since so many devices are used in the medical industry, LSCs also have the advantage of being relatively inexpensive instruments compared to other detectors.

A drawback to a LSC is the extremely low resolution that it provides, making it a poor instrument to use when measuring mixed isotope samples. Another large disadvantage is associated with the disposal of LSC samples; the cocktail become mixed organic waste after use. The high cost of this mixed waste may cause the consideration of another nondestructive sample analysis.

LSC data may also be affected by the amount of quenches occurring in samples. A quench is anything that reduces the number of photons that are being recorded by the photomultiplier tube. Quenches are divided into two categories: chemical and color. A chemical quench is one that interferes with the first steps of the scintillating process where another chemical competes with the transfer of excitation energy. A common chemical quench is caused

by oxygen because it will absorb the excitation energy and then will release that energy through vibration. Color quench occurs when the output of photons is absorbed by another interfering agent. For example, if the solution is colored violet, blue, green, or can absorb ultra-violet, then some of the photons will be absorbed by the solution and decrease the total amount of light emitted from the sample.

However, it is possible to quantify the amount of quench in solution by spectral analysis. There are several ways of doing this. Two of the more common ones are based on the Spectral Index of the Sample (SIS) and the transformed Spectral Index of the External Standard (tSIE). The SIS uses the sample isotope spectrum to monitor the quench. The tSIE uses the Compton spectrum induced in cocktail by the external  $^{133}\text{Ba}$  source. The source is placed under the sample to induce a Compton spectrum. The instrument makes a calculation on a scale of 0 (most quenched) to 1,000 (unquenched).



### 3 METHODS

The performance of both TEHA and TEHP in extracting Zr, Hf, and Pu was measured in solvent extraction, batch studies, and column studies. Experiments are typically first conducted with solvent extractions, as the reaction responsible for the extraction is not limited by steric and size interferences that might present themselves in batch studies and column studies. Batch studies with free resin are then performed prior to the column studies as they allow the ability to process a large number of samples under a variety of test conditions in a short amount of time. Then the optimal conditions determined in the batch studies can be applied and tested in a dynamic flow environment of the column.

#### 3.1 Solvent Extraction

For the solvent extraction experiments involving Zr and Hf, the organic and aqueous volumes used were 2 mL each in a 15 mL centrifuge tube. For studies involving the Pu, the volumes were lowered to 0.7 mL to reduce the amount of LSC cocktail used and subsequent waste generated. The solution with spiked was 50  $\mu$ L of the individual radionuclide in either 8 M or 12 M HCl and prior to its addition to the solution, the volume of acid in the vial was adjusted to bring the total solution volume up to either 2 mL or 0.7 mL (meaning the pre-spike volume would be 1.95 mL or 0.65 mL, respectively). These volumes were mixed on a mixing table for 30 minutes at ~1200 rpm for the general solvent extraction and the speciation study. After removal from the mixing table, an aliquot equaling half of the initial volume of each phase was taken with a volumetric pipette. For the determination of Zr and Hf, these aliquots were then placed in plastic 5 mL gamma counting tubes for analysis on an automated counter or a 2 mL microcentrifuge for measurement on a HPGe detector. For Pu measurements, the aliquot was

placed into a 5 mL LSC vial and counted on a LSC instrument after ~5mL of LSC cocktail had been added.

### 3.2 Batch Studies

For the batch studies conducted, ~50  $\mu\text{g}$  of resin was weighed out into a 2 mL microcentrifuge tube. Then, 1.45 mL of acid with a preselected concentration was added to the vial to precondition the resin for extraction. The microcentrifuge tube was placed on tilt table and the resin was allowed to mix with the acid for at least 30 minutes. After 30 minutes, 50  $\mu\text{L}$  of the radionuclide in 9 M hydrochloric acid was added to the solution. The vial was then mixed on a vortex mixer for an additional 30 minutes at ~1200 rpm. The contents of the vial were then transferred into a syringe and passed through a 0.45  $\mu\text{m}$  PTFE syringe filter. A 1 mL aliquot of this solution was then taken and added to either counting tubes or LSC vials filled with cocktail for analysis.

#### 3.2.1 Batch Study Corrections

When taking only an aliquot of the entire filtered solution, a verification is required to determine whether the volume can be corrected back to the original volume after contact with the resin. To conclude whether the matrix's physical properties have changed, the density of the acid before and after contact with the resin is measured to ensure no change has transpired. To do this, a volumetric pipette was first calibrated by measuring the weight of 1 mL of water 10 times on a scale. Using the known density of water at room temperature, the pipette's delivery volume was accurately determined. Then, knowing the pipette's delivery volume, the weight of 1 mL of acid was determined 10 times on the scale and recorded. After contacting the acid with the resin, a 1 mL aliquot from those samples was then weighed and recorded. Since no density difference

was apparent between the before and after resin contact, no volume correction was required to be made to the measurements.

Since the resin can also extract the acid, a correction may also be required to determine the actual acid concentration after conditioning of the resin. A titration experiment was performed to check the acid concentration before and after contact with the resin without any radionuclides present in solution. To do this, trials with samples of acid were performed where one group of samples was placed in contact with resin and another set with acid was not. The samples were then diluted with deionized water and 1% phenolphthalein was added in preparation for the titration. A 25 mL burette was filled with 1 N of sodium hydroxide, which was then added dropwise to the samples until a pink color was observed in solution. Based on the results of the titration, the concentration of acid did not change and therefore no correction was necessary for all further calculations.

### 3.3 Column Studies

The first step was to prepare a 4 mm inner diameter Konte glass column for the studies. The columns used had a 20 cm height and included a 15 mL reservoir on top of the column. Prior to each use, the columns were washed with deionized water and dried. Glass wool was then added to form a porous barrier, which provides a base for the resin to sit on but allows for the solution to pass through. Resin was then measured directly into the column and weighed on a scale. The column was filled with enough resin to achieve a bed height of 3 cm. Water was then added, and acid washed sand was placed on the top of the resin to prevent the column bed from being disturbed by future additions of solution. Air bubble formation was closely monitored, and the column was resettled if any was observed. The free column volume (FCV) was subsequently measured by adding 11 M hydrochloric acid to the column and monitoring the drops by placing

tiny strips of litmus paper near the exit of the column. The FVC was estimated to be ~ 150  $\mu\text{L}$  for a column with a 3 cm bed height. The columns were then conditioned with an additional 1 mL of 11 M hydrochloric acid. After the conditioning, a load solution of 50  $\mu\text{L}$  of 11 M hydrochloric acid containing a spike of the radionuclide of interest was added. A volume of hydrochloric acid was then added to the column and fractions were collected until the volume of acid reached the height of the resin bed. Fractions of 200  $\mu\text{L}$  and 1 mL were taken and measured. The volume used to collect was determined by preliminary column studies; the 200  $\mu\text{L}$  fractions were taken when elution of the radionuclide was expected to occur, and the 1 mL fractions were collected when no elution was expected. These fractions were then prepared for counting.

## 4 SOLVENT EXTRACTIONS

### 4.1 Exploratory Extractions

Prior to the selection of tris(2-ethylhexyl)amine (TEHA) and tris(2-ethylhexyl)phosphate (TEHP) as viable ligands, a variety of other substances were tested for extraction with zirconium. It must be noted that only zirconium was used during these exploratory extractions. Previously, dicyclo-18-crown-6 ether had shown extraction of zirconium and hafnium in hydrochloric acid, so a solvent extraction using nitric and sulfuric acid was attempted with a spectrum of concentration ranging from 0.1 M to concentrated acid. However, no extraction was observed over the entire concentration range. Calixarenes, similar in structure and chemistry to the crown ethers, were also investigated as a possible candidate for extraction. Over a range from 0.1 M to concentrated, calix[4]arene showed no extraction behavior in hydrochloric, sulfuric, and nitric acids. Likewise, thiacycrown ethers were further considered as possible ligands; however, another concurrent research project discovered that thiacycrown ethers extract soft acids/bases (lead and mercury). It was therefore extremely unlikely that an extraction would occur with hard acids such as zirconium and hafnium. TEHA and TEHP were then tested for extraction from nitric and sulfuric acid. Neither were found to have extracted zirconium and these acid systems were therefore not pursued.

### 4.2 Solvent Extraction from Hydrochloric Acid

#### 4.2.1 Solvent Selection

Before fully evaluating the extraction capabilities of TEHA and TEHP in more detailed studies, a variety of solvents were examined to ensure the best conditions for the separation of zirconium and hafnium. Solvent properties can affect the separation in different ways; its viscosity, dipole moment, and measure of solubility in the polar phase are some examples how

the ligand can be inhibited or enhanced by the solvent in its extraction capability. Dichloro methane (DCM), hexanes, diethyl ether (DEE), kerosene, and toluene were all chosen as prospective solvents due to the high variability of their properties and commercial availability. All of these solvents were tested over the range of 6 M to 12 M hydrochloric acid in 1 M or 0.5 M increments. Each data point was done in pentuplicate. The concentration for TEHA and TEHP was at a 0.05 M concentration for all these experiments. Both the aqueous and organic phase volumes were set at 2 mL in a 15 mL centrifuge tube and were mixed for 30 minutes on a timed mixer. After the mixing, 1 mL of liquid was extracted from each phase and counted on an automated gamma counter. With the DMC and DEE, a direct displacement pipette was used to measure volumes for the organic phase.

#### 4.2.1.1 Kerosene as a Solvent

Kerosene is a mixture of hydrocarbons chains ranging from 6 to 16 carbons per molecule and is often used as solvent in industrial size separations due to the low cost and availability. It also has the added benefit of not being as volatile at room temperature as other common solvents used in solvent extraction. However, as noted from Banda et. al., a third phase forms between the kerosene and aqueous phase. This third phase increased in volume as the acid concentration increased. In preliminary experiments, it was noted that the zirconium increasingly extracted into this third phase as the acid concentration rose. To avoid this third phase formation, dodecanol was added to the kerosene stock solution at a concentration of 10% v/v.

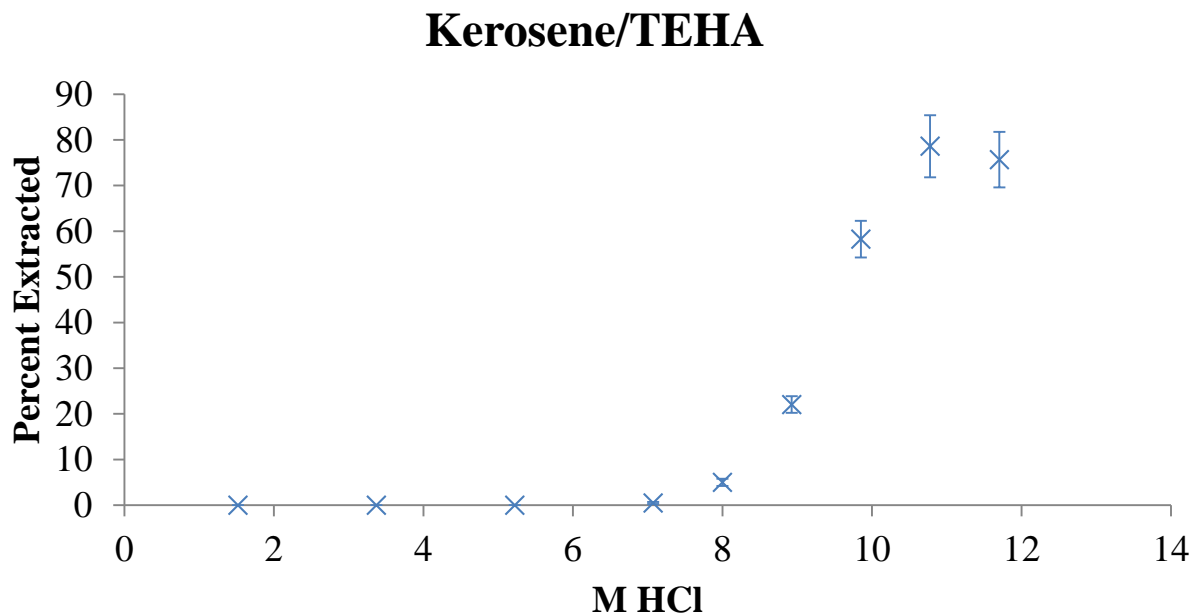


**Figure 4.1** Percent Extraction of  $^{89}\text{Zr}$  with 0.05 M TEHA in kerosene.

The results of the extraction of zirconium with TEHA into kerosene are shown in Figure 4.1. Extraction begins at 8 M and peaks at 11 M with 78.6%. Compared to the rest of the solvents, kerosene extracted the least when extracting zirconium; it extracts the lowest peak percentage (~80%) and requires a higher acid concentration to begin extraction. Extraction over 50% also only occurs once 10 M hydrochloric acid is reached. This outcome may be due to the purity of kerosene, as it is a mixture of hydrocarbons. With this low extraction and the third phase formation affecting its performance, experiments with TEHP in kerosene were not performed due to the other solvents' higher extraction ability with TEHA and TEHP.

#### 4.2.1.2 Dichloro Methane as a Solvent

Dichloro methane (DCM) is often used as a solvent for dissolving nonpolar compounds. However, its high volatility means that it is difficult to work with when volume determinations can greatly influence the accuracy of the measurement being made. Its high vapor pressure

makes it unsuitable for an air displacement pipette, so a direct displacement pipette was used for measuring the volumes of DCM. Centrifuge tubes were sealed with Parafilm when mixing to prevent evaporative losses.

As can be seen from Figure 4.2, the zirconium extraction with TEHA in DCM as the solvent begins at around 8 M and reaches its maximum extraction power at 12 M with 95.6%. The DCM had no third phase formation occur over the range of hydrochloric acid concentrations studied.

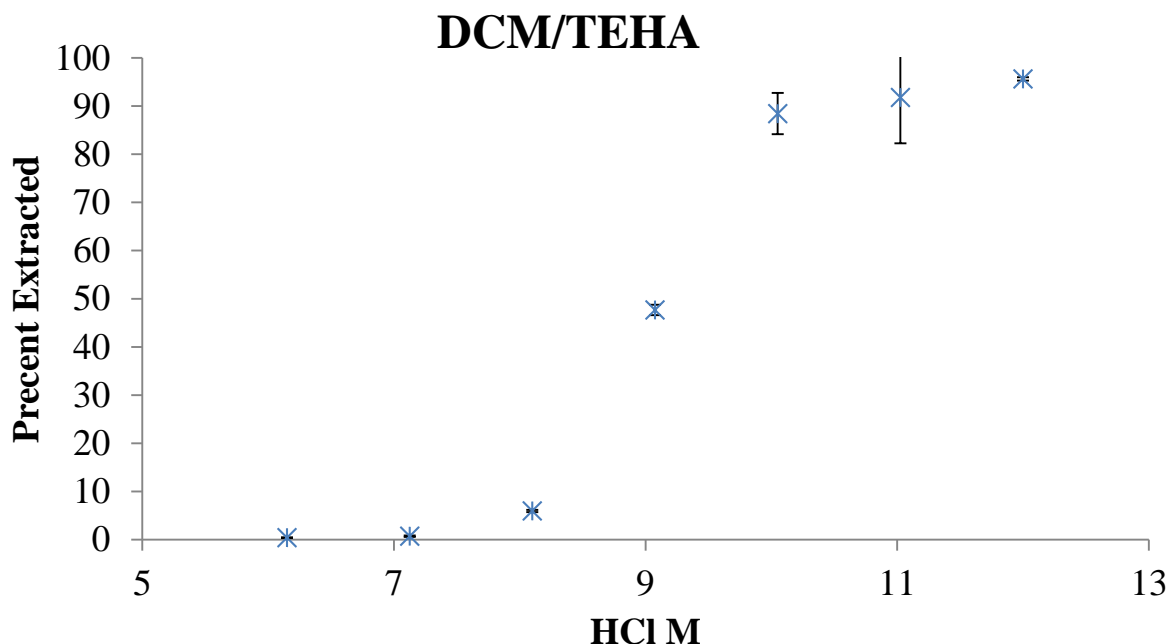


**Figure 4.2** Percent Extraction of  $^{89}\text{Zr}$  with 0.05 M TEHA in DCM

TEHP showed similar results over the concentration range investigated (see Figure 4.3). It begins its extraction slightly earlier at 7 M and levels off at 9 M with a peak extraction of 84.0% at 12 M. The smaller retention of zirconium on the TEHP is unique to DCM as TEHP typically has a larger extraction capability with zirconium than TEHA.



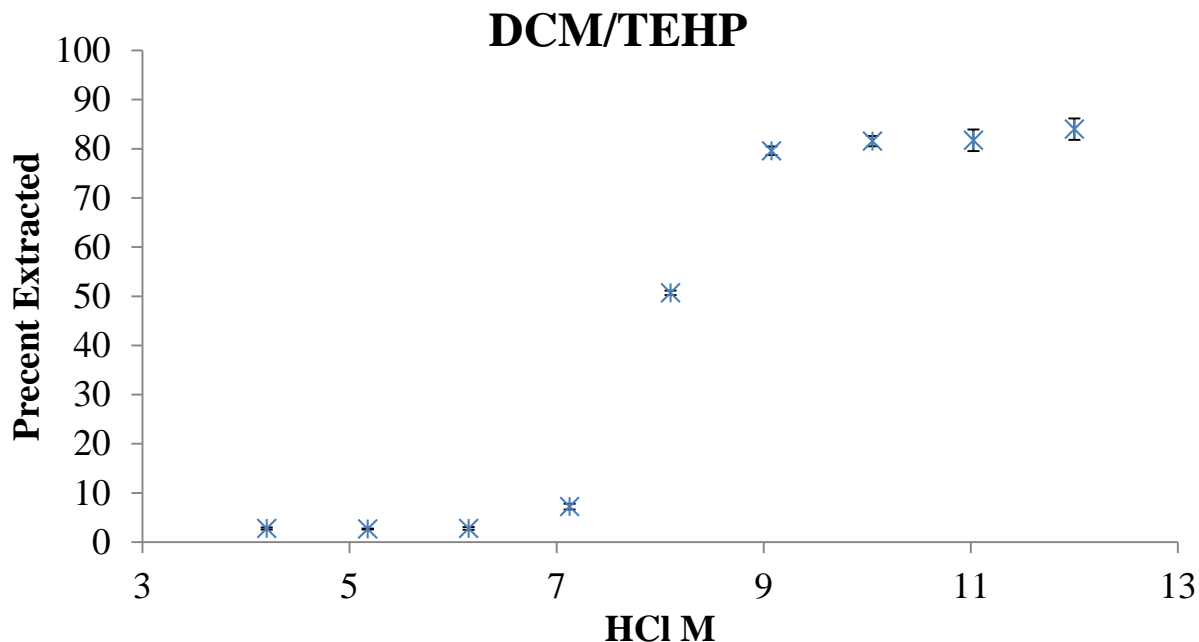


**Figure 4.3** Percent Extraction of  $^{89}\text{Zr}$  with 0.05 M TEHP in DCM.

#### 4.2.1.3 Hexanes as a Solvent

In solvent extractions, hexanes are also a commonly used solvent. Hexanes, rather than “hexane”, are used in the name as hexanes contain all the available isomers rather than a single atomic arrangement of the hydrocarbon. Due to the high vapor pressure of the compound, the direct displacement pipette was used and all centrifuge tubes were sealed with Parafilm when being mixed. As with the kerosene, hexanes also experienced formation of a third phase. Dodecanol was added to make a 10% v/v solution, which eliminated the emulsion.

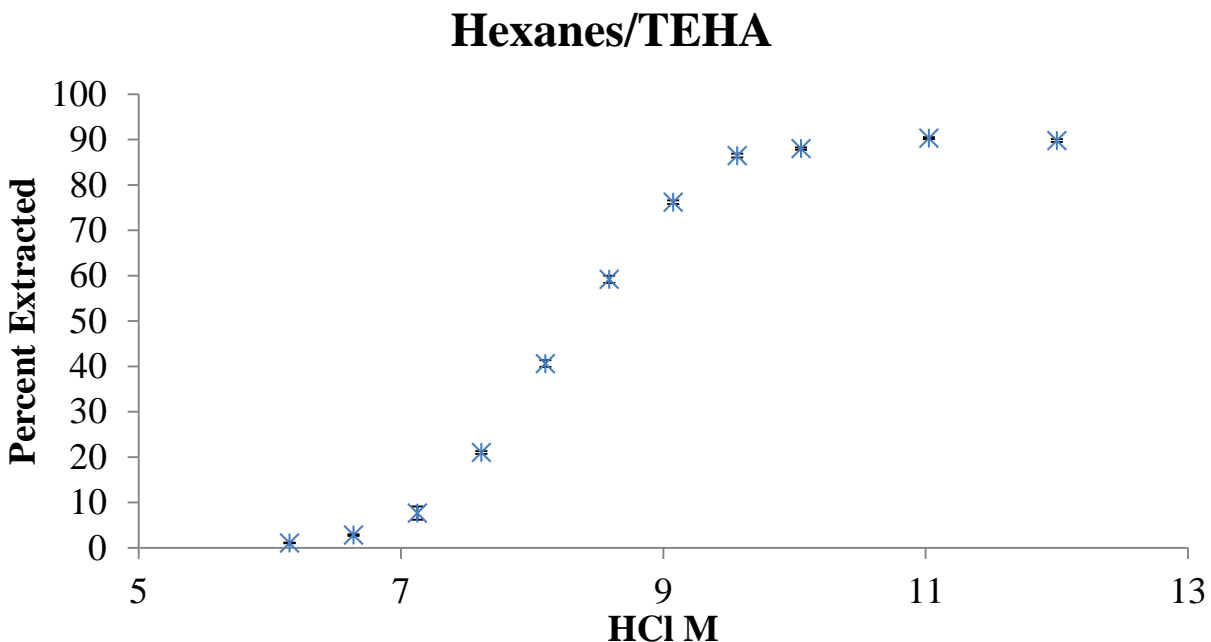


**Figure 4.4** Percent Extraction of  $^{89}\text{Zr}$  with 0.05 M TEHA in hexanes.

With the TEHA, the zirconium started extracting earlier than with other solvents at around 7 M and had a peak extraction of 90.3% at 11 M hydrochloric acid (see Figure 4.4). Although the TEHA in hexanes extracts earlier than in some solvents, it still requires a concentration of at least 9 M to reach a 90% extraction level. For the TEHP (see Figure 4.5), the zirconium shows a similar extraction curve, slowing increasing its percent extracted at concentration of 8 M and greater and extracting 99.5% at 12 M. Its performance was extremely satisfactory as almost all the zirconium was transferred into the organic phase at high hydrochloric acid concentrations.

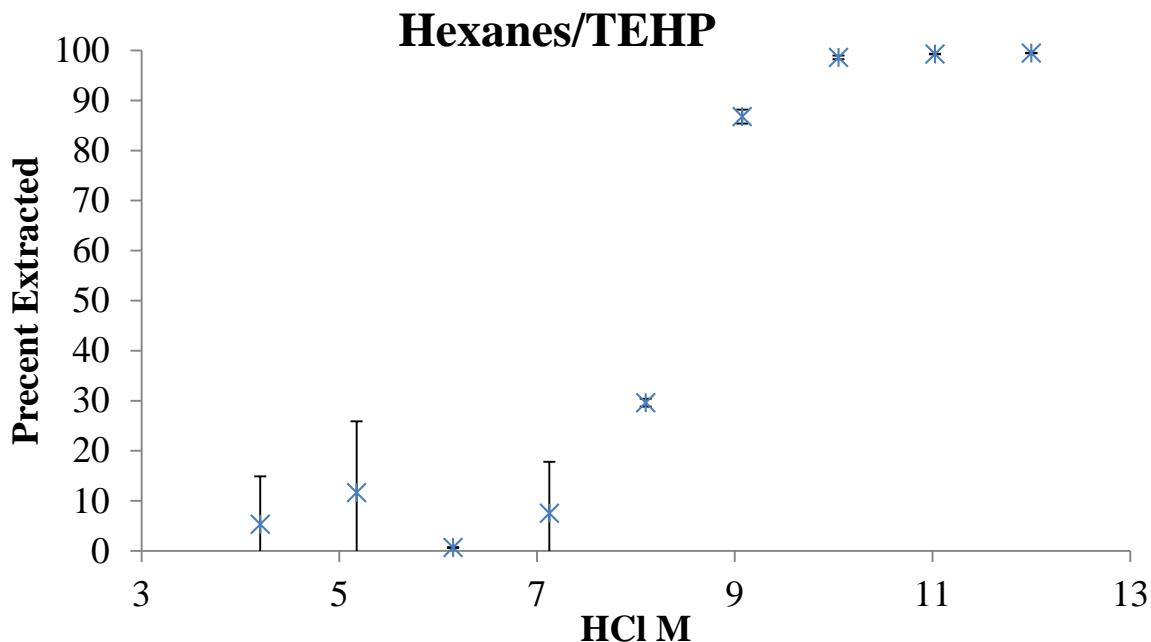


**Figure 4.5** Percent Extraction of  $^{89}\text{Zr}$  with 0.05 M TEHP in hexanes.

#### 4.2.1.4 Diethyl Ether as a Solvent

Diethyl ether (DEE) can be an appropriate solvent when the ligand does not completely dissolve due to its polar nature. However, because of its polar nature, DEE must be contacted with the aqueous phase to allow it to reach equilibrium since a portion of the DEE will also dissolve in the aqueous phase. In attempting to use diethyl ether, this preconditioning of the aqueous phase was not adhered to in the preliminary trials. This resulted in the organic phase dissolving into the aqueous phase. Due to the performance and ease of the other solvents, diethyl ether was not further pursued as a solvent.

#### 4.2.1.5 Toluene as a Solvent

Toluene can perform as useful solvent in liquid-liquid extractions. Its low vapor pressure and nonpolar properties to dissolve organic ligand allow for convenient use in the lab. It also

does not require the use of a displacement pipette. One drawback to toluene is its toxicity and the obstacles for its disposal.

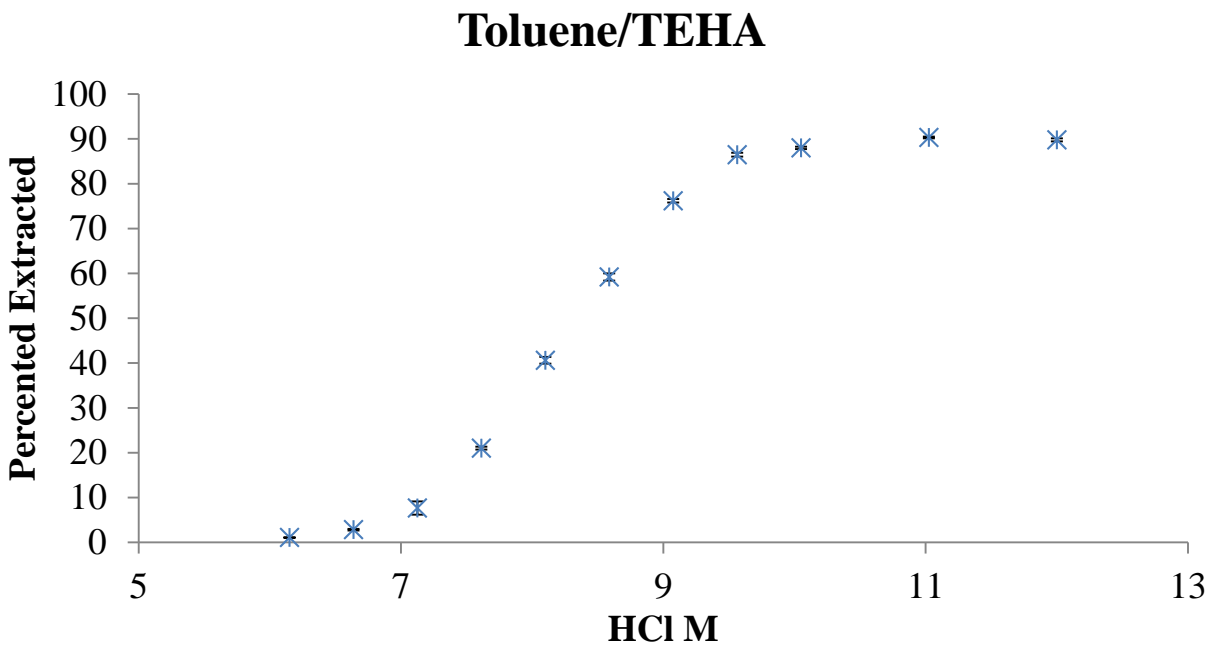


**Figure 4.6** Percent Extraction of  $^{89}\text{Zr}$  with 0.05 M TEHA in toluene

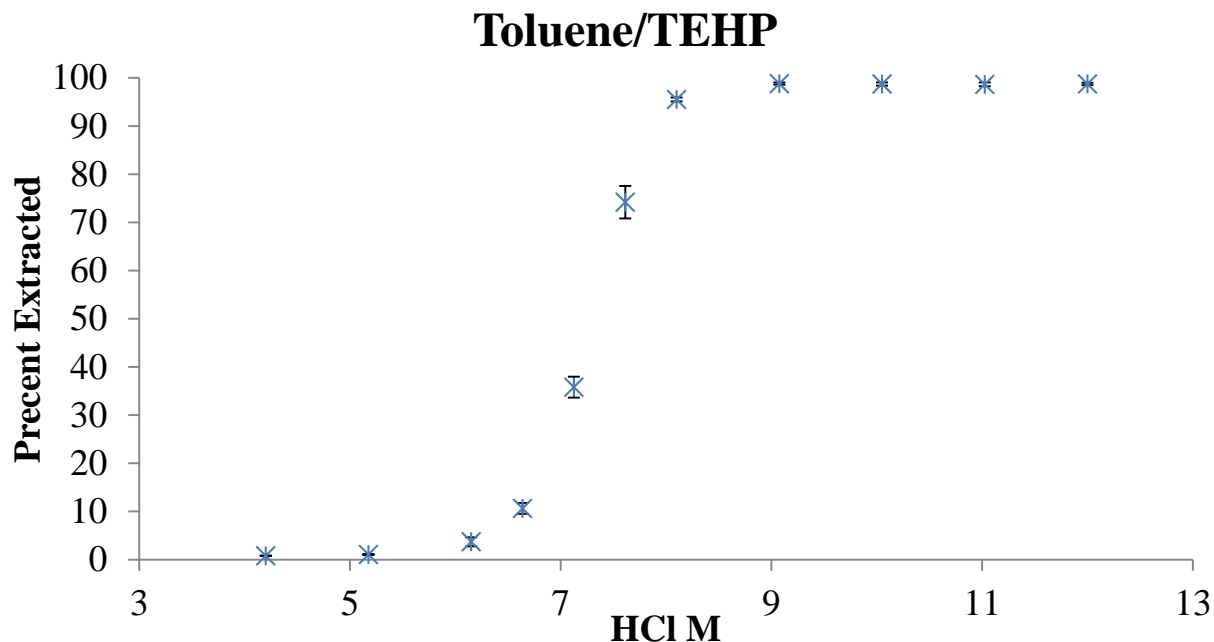


**Figure 4.7** Percent Extraction of  $^{89}\text{Zr}$  with 0.05 M TEHP in toluene

As can be seen from Figure 4.6, with TEHA in toluene, the extraction begins at 7 M and reaches a peak extraction of around 90% extraction at 9.5 M. TEHP begins its extraction at 6 M and reaches a peak extraction of around 99% extraction at 9 M (see Figure 4.7). Since the extraction with TEHP in toluene did not completely drop to 0% at 6 M hydrochloric acid, data points at 4 M and 5 M were added to show the complete curve of extraction.

#### 4.2.1.6 Discussion

From all the solvents tested, ultimately toluene was chosen as the best for future solvent extraction studies. Many of the solvents showed the same two problems: high vapor pressure and third phase formation. For DMC, kerosene, and diethyl ether, their extraction performance was more than 10% than that of hexanes and toluene and those three solvents were no longer considered. While hexanes showed marginally better performance, the formation of a third phase and the high vapor pressure made it unsuitable for these experiments with large numbers of

samples. While the third phase formation could be solved using dodecanol, the high vapor pressure would make the results questionable; as the hexane evaporates, it increases the concentration of the radionuclide in the organic phase and makes the comparison with the aqueous phase difficult with higher error. Also, the higher vapor pressure of hexanes requires the use of a direct displacement pipette. Toluene has neither of these challenges and thus was chosen as the appropriate solvent.

#### 4.2.2 Solvent Extractions with $^{89}\text{Zr}$ , $^{175}\text{Hf}$ , $^{239}\text{Pu}$

After selecting toluene as the solvent, a range of different concentrations of hydrochloric acid was contacted with an organic phase containing 0.05 M TEHA or TEHP. This value was selected because a higher concentration of TEHA or TEHP in the organic phase caused formation of an emulsion that lasted longer than a minute. For online experiments, it is required to have fast resolution of the emulsion into the separate phases to be able to detect the transactinide of interest. Use of a centrifuge for the dissipation of the emulsion is not preferable on such a short timetable. Also, when higher concentrations of TEHA and TEHP were contacted with hydrochloric acid greater than 10 M, the organic phase's viscosity increased to the point where the phase transformed into a "gel-like" consistency. Again, this chemical behavior made higher organic concentration unsuitable for extraction purposes.

##### 4.2.2.1 TEHA

As seen with Figure 4.8, plutonium extracts extremely well with TEHA, showing an extraction over the entire range of the hydrochloric acid concentrations studied. Concentrations below 4 M hydrochloric acid were not pursued as all three elements of interest can begin to hydrolyze around 2 M hydrochloric acid. Zirconium follows the commonly observed trend of beginning extraction at 7 M and hafnium commences at around 9 M. A separation between all

three can be achieved at any point in the concentration range, although the 6 M to 10 M hydrochloric acid range can be manipulated to exploit the best separation factors. The  $^{239}\text{Pu}/^{175}\text{Hf}$  pair in particular showed extremely good separation with a peak separation factor of  $\sim 800$  at 9 M hydrochloric acid as seen in Figure 4.9.

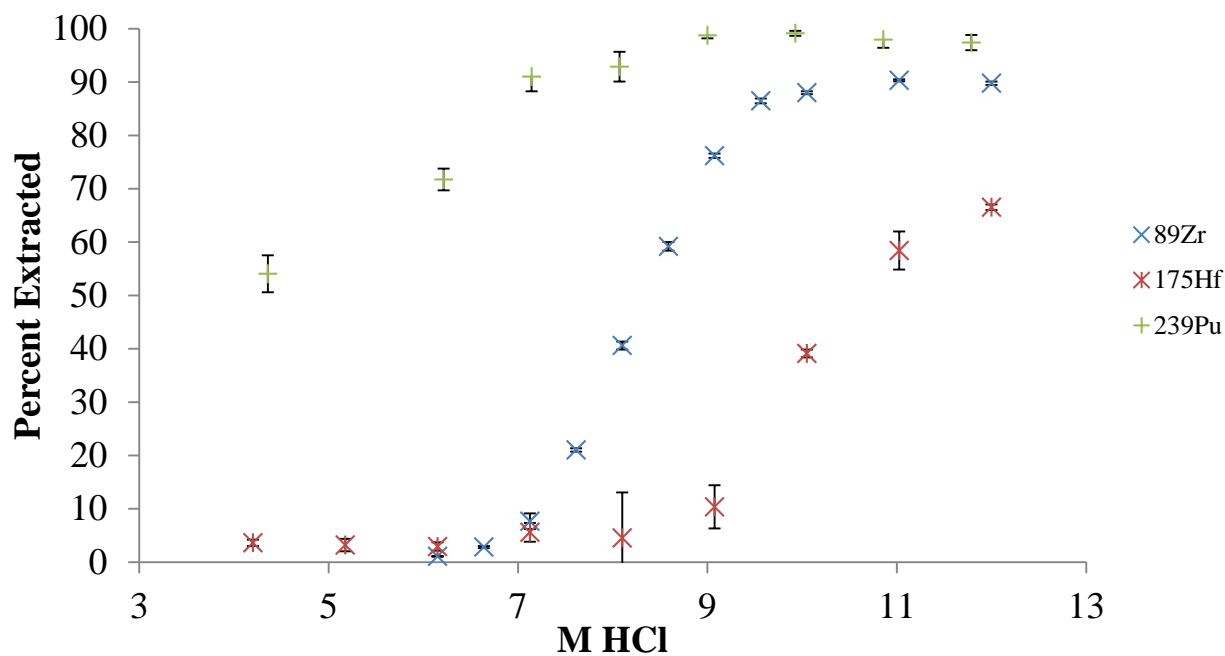


**Figure 4.8** Percent Extraction of  $^{89}\text{Zr}$ ,  $^{175}\text{Hf}$ , and  $^{239}\text{Pu}$  with 0.05 M TEHA

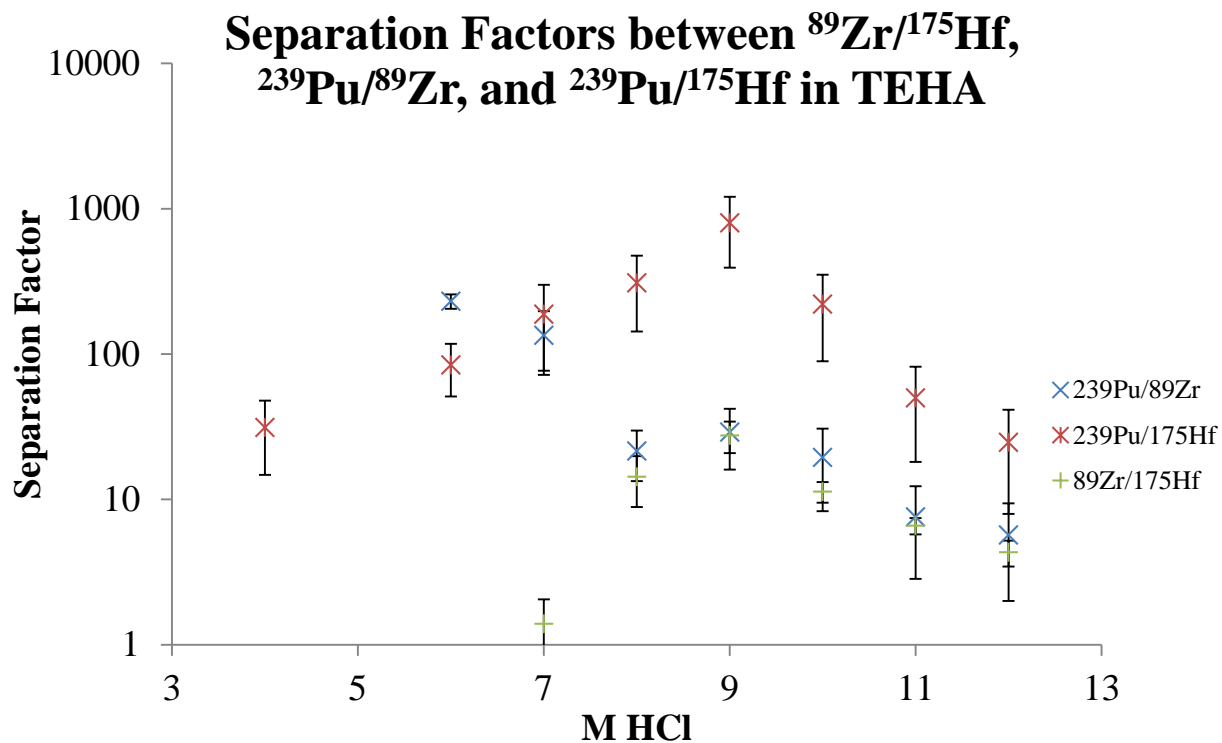


**Figure 4.9** Separation factors of  $^{89}\text{Zr}$ ,  $^{175}\text{Hf}$ , and  $^{239}\text{Pu}$  with 0.05 M TEHA

#### 4.2.2.2 TEHP

In TEHP, plutonium followed the opposite trend and extracted less at higher acid than zirconium and hafnium (see Figure 4.10). Antagonistically, zirconium and hafnium extracted at lower hydrochloric acid concentrations and at higher percentages in the TEHP. Hafnium also matches the extraction level that zirconium does and the extraction curves are much similar, making it a more difficult separation. At 12 M HCl, all three elements are almost completely extracted into the organic phase.

For the separation factors in Figure 4.11,  $^{89}\text{Zr}/^{239}\text{Pu}$  illustrated a high separation from 7 M to 10 M with a peak of 363.6 at 8 M. For the  $^{175}\text{Hf}/^{239}\text{Pu}$ , the best separation factors were from 8 M to 12 M having a high value of 33.8 at 8 M. The best separation factors between



$^{89}\text{Zr}/^{175}\text{Hf}$  spanned from 7 M to 9 M, with a peak of 42.5. While these numbers are not as high as TEHA, the potential for separation of the nuclides is possible.

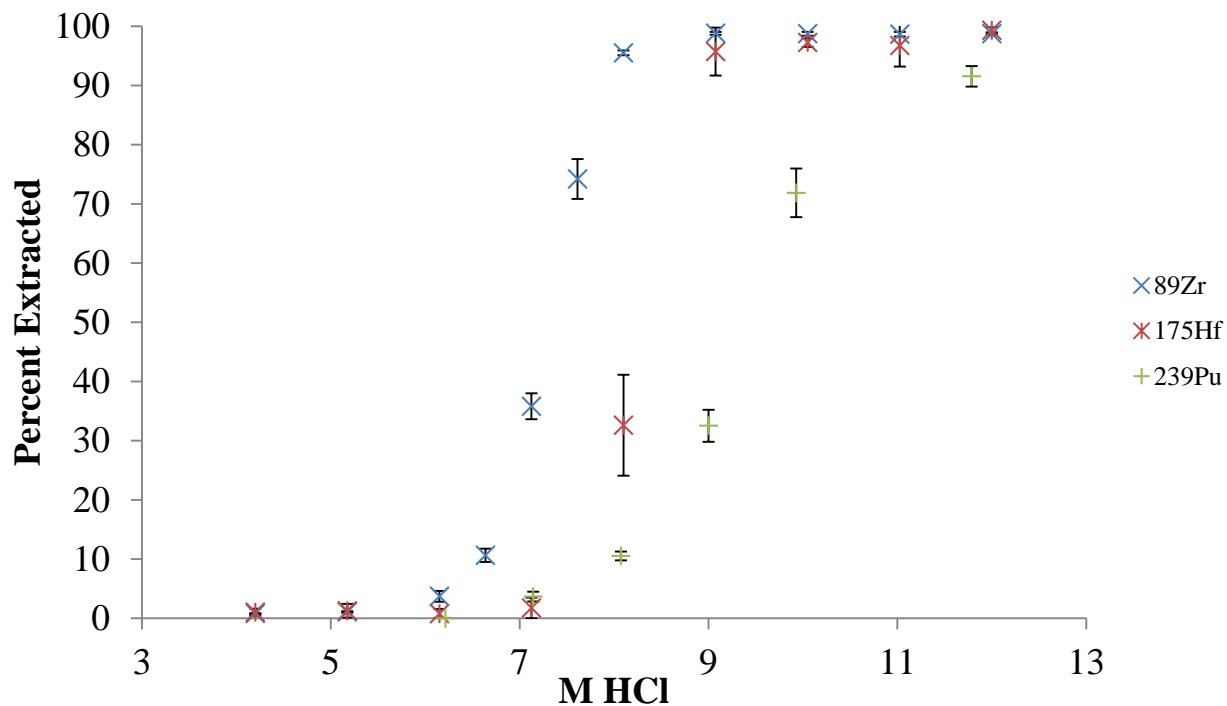


**Figure 4.10** Percent Extraction of  $^{89}\text{Zr}$ ,  $^{175}\text{Hf}$ , and  $^{239}\text{Pu}$  with 0.05 M TEHP

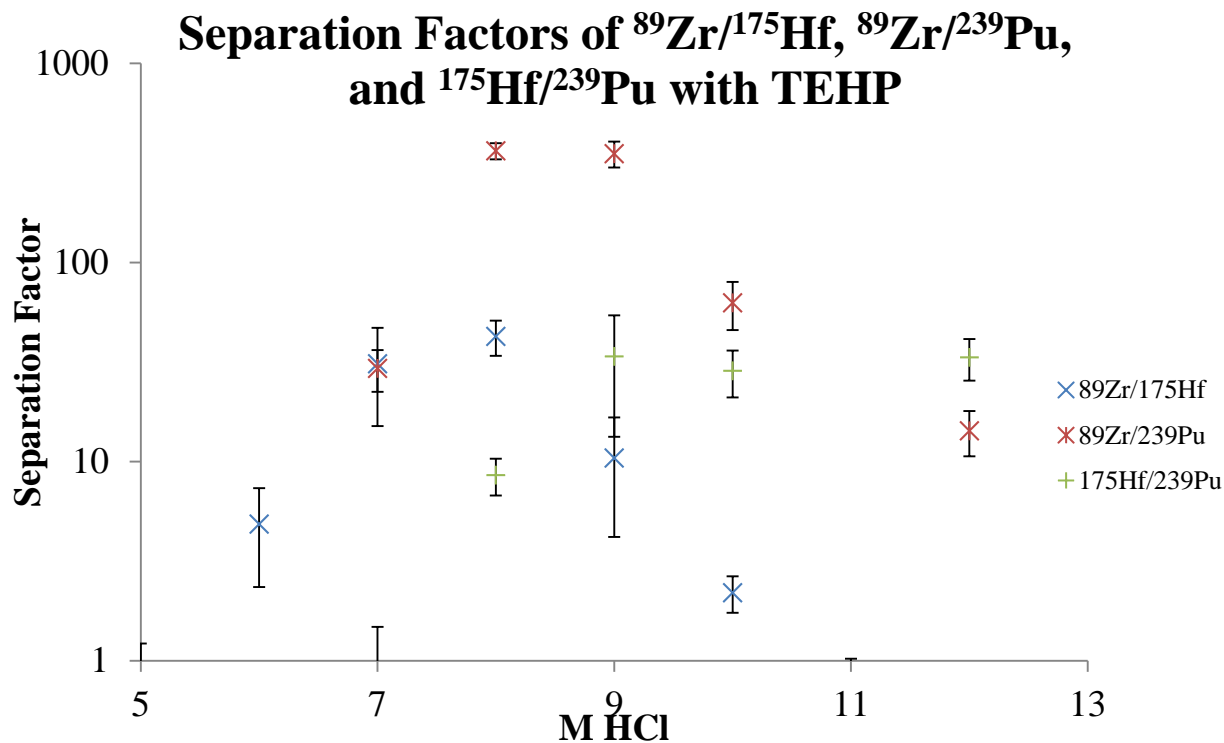
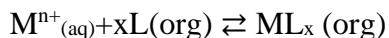


**Figure 4.11** Separation factors of  $^{89}\text{Zr}$ ,  $^{175}\text{Hf}$ , and  $^{239}\text{Pu}$  with 0.05M TEHP

#### 4.2.3 $^{89}\text{Zr}$ , $^{175}\text{Hf}$ , $^{239}\text{Pu}$ speciation

To determine the amount of ligands coordinating with the metal being extract, the logarithm of the distribution ratios can be plotted against the logarithm of a variety of organic concentrations where the slope identifies the number of organic molecules required to extract the metal. This idea can be derived by knowing the general equilibrium equation involved in a solvent extraction:



This reaction can be mathematically represented by:

$$K = \frac{[\text{ML}_x]}{[\text{M}^{n+}][\text{L}]^x}$$

Where K is the equilibrium constant. By manipulating both sides of the equation with a logarithm, the equation can be changed to the equation of a line:

$$\log D = x \log [L] + \log K$$

The acid concentration for these studies was kept constant at 8 M hydrochloric acid for each experiment with the organic concentration varied from 0.001 M to 0.5 M for both TEHA and TEHP. The rest of the procedure was carried out as outlined in the methods sections.

#### 4.2.3.1 TEHA

For the TEHA,  $^{89}\text{Zr}$  and  $^{175}\text{Hf}$  showed very similar slope numbers at 1.81 with reasonable  $R^2$  values. This seems to indicate that these two elements are extracted by 2 TEHA molecules as seen in Figures 4.12 and 4.13. The  $^{239}\text{Pu}$  experiment was repeated three times at different hydrochloric acid concentrations; however, a consistent slope was not achieved at any conditions. Therefore, no information about the speciation of the  $^{239}\text{Pu}$  could be obtained.

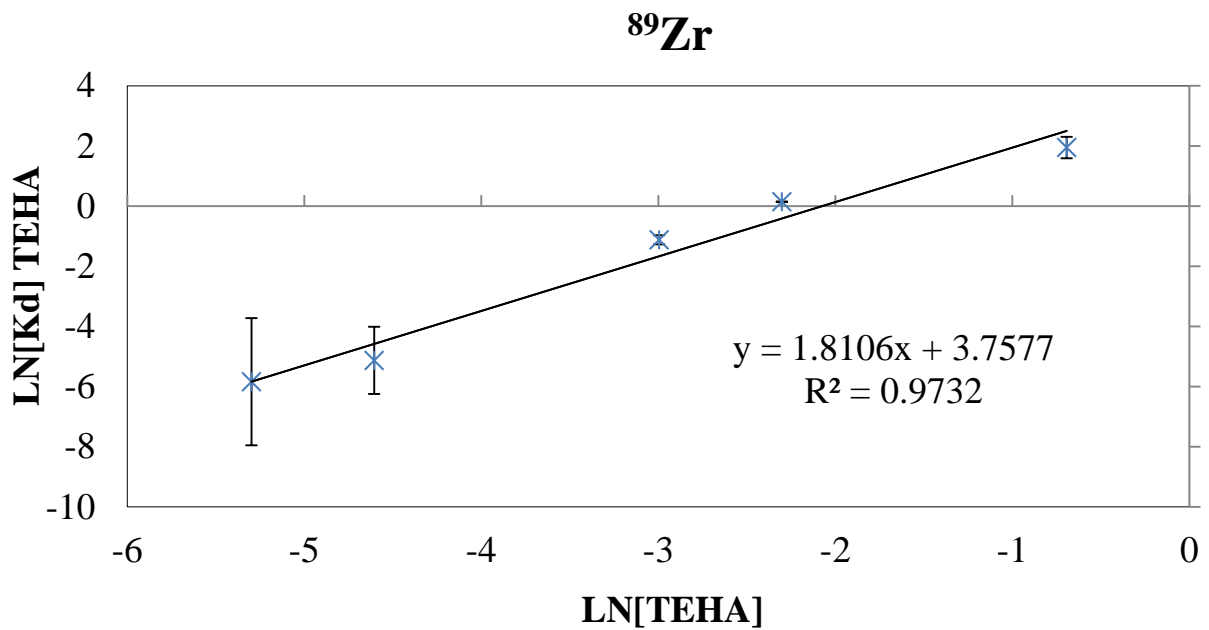


**Figure 4.12** The natural log of the distribution ratios for <sup>89</sup>Zr as a function of the natural log of the concentration of TEHA in toluene at 8 M HCl.

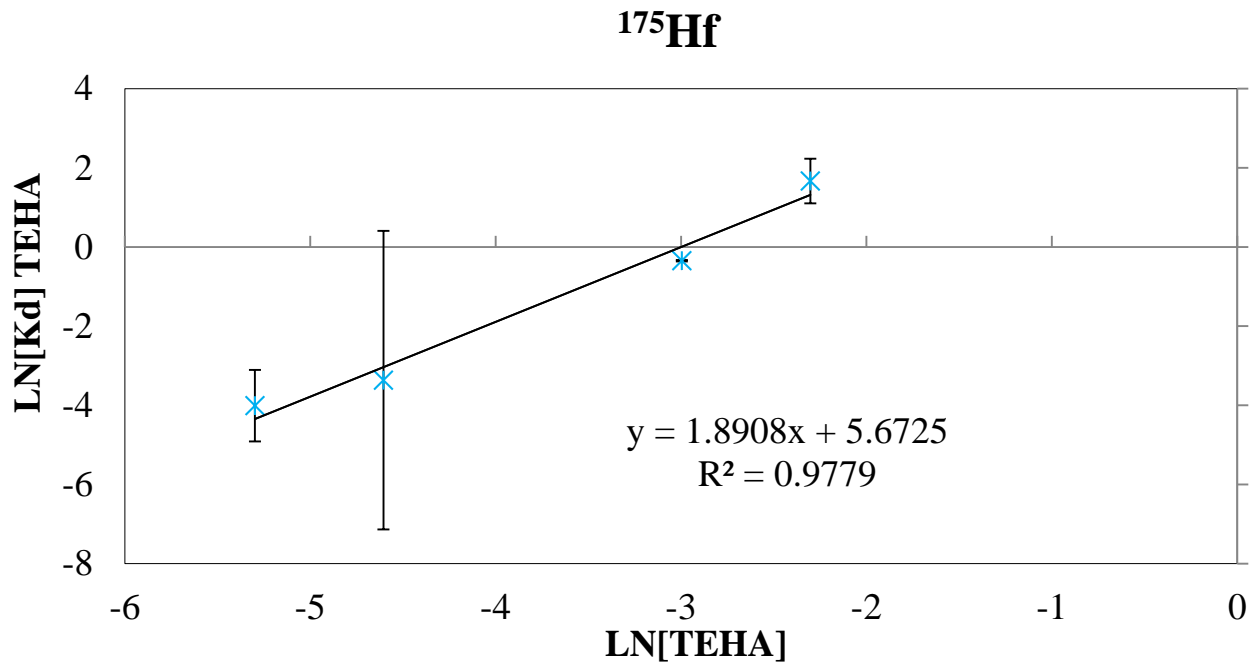


**Figure 4.13** The natural log of the distribution ratios for <sup>175</sup>Hf as a function of the natural log of the concentration of TEHA in toluene at 8 M HCl.

#### 4.2.3.2 TEHP

For the TEHP, the extraction slope for the  $^{89}\text{Zr}$  and  $^{175}\text{Hf}$  was approximately 1 corresponding to a 1:1 ligand to radionuclide extraction ratio as seen in Figures 4.14 and 4.15. The  $^{239}\text{Pu}$  showed a slightly lower result at around 0.8 in Figure 4.16; however, it is assumed that this also indicates a 1:1 extraction. The higher error in the  $^{175}\text{Hf}$  corresponds to the lower activity used compared to the smaller error bars seen in the  $^{89}\text{Zr}$  and  $^{239}\text{Pu}$ .

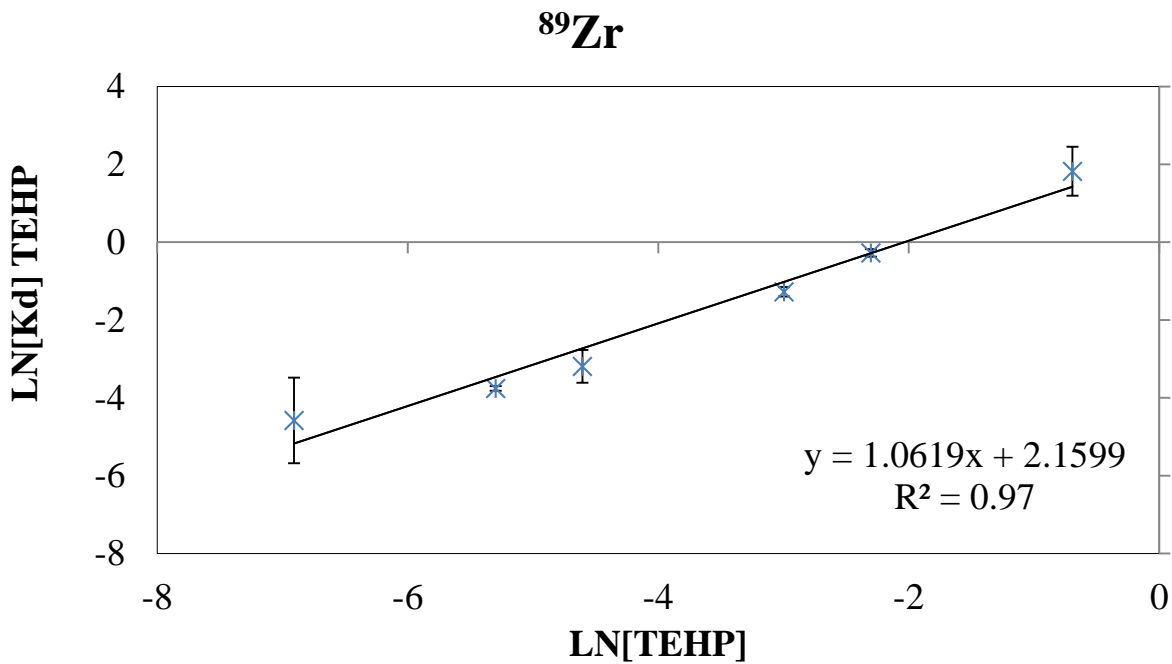


**Figure 4.14** The natural log of the distribution ratios for  $^{89}\text{Zr}$  as a function of the natural log of the concentration of TEHP in toluene at 8 M HCl.

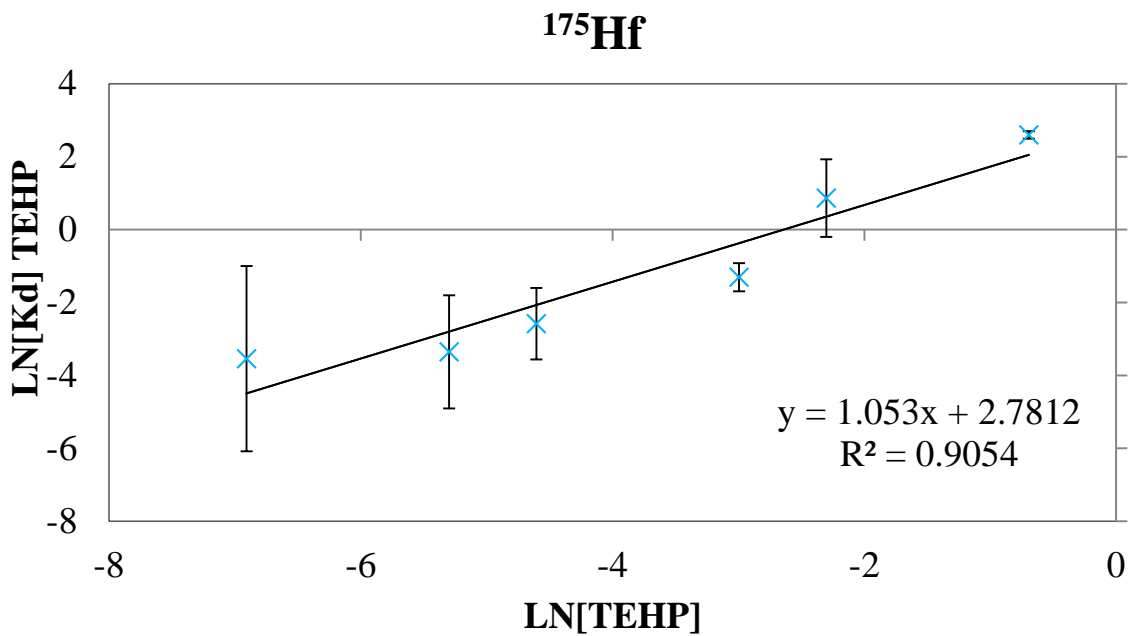


**Figure 4.15** The natural log of the distribution ratios for <sup>175</sup>Hf as a function of the natural log of the concentration of TEHP in toluene at 8 M HCl.

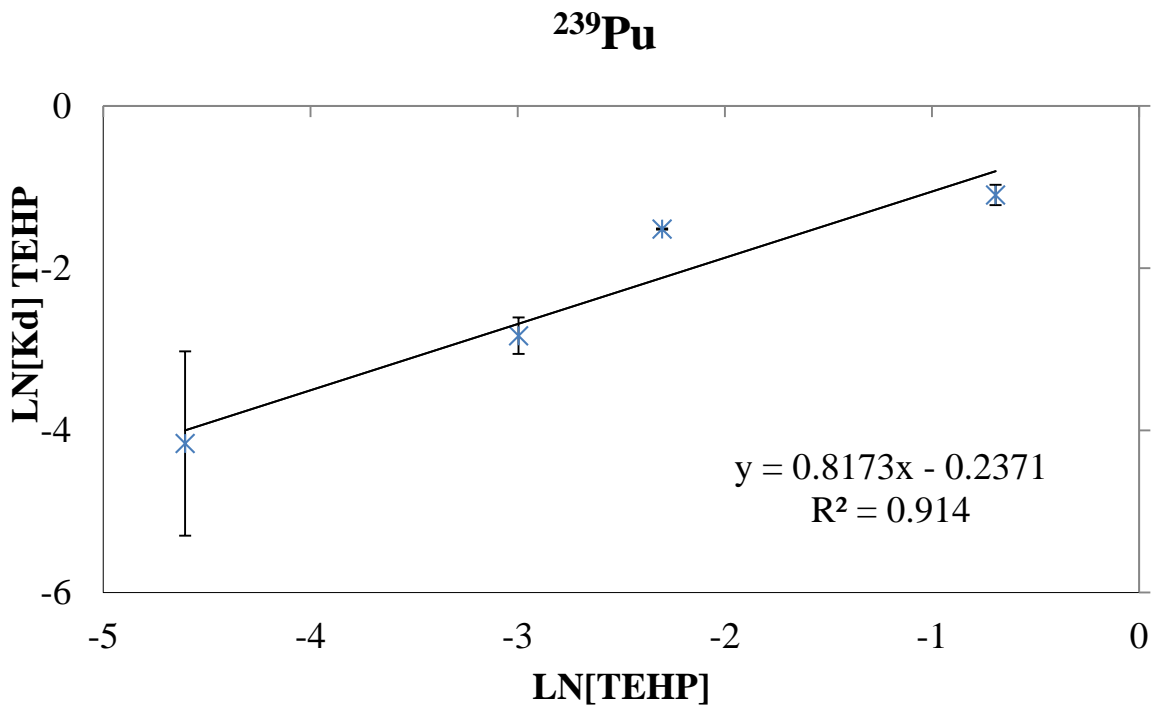


**Figure 4.16** The natural log of the distribution ratios for <sup>239</sup>Pu as a function of the natural log of the concentration of TEHP in toluene at 8 M HCl.

#### 4.2.4 Kinetics of $^{89}\text{Zr}$ , $^{175}\text{Hf}$ , and $^{239}\text{Pu}$ Extraction

To ensure compatibility for transactinide experiments, kinetic studies were undertaken to guarantee that chemical equilibrium is achieved within the half-life of the transactinide. For this work, equilibrium is defined as the point in the separation when the extraction has reached a consistent percent extracted (typically at the highest percent extracted). For preparing the system for rutherfordium, an equilibrium time of less than 60 seconds is generally seen as the cutoff for any chemistry to be observed, corresponding with the length of its half-life; however, faster kinetics would be desirable. The longer the equilibrium time forces more rutherfordium atoms to be produced to get statistically significant data. The procedure used to test this is similar to the one listed in the Chapter 3.1; however, instead of keeping the mixing time constant at 30 minutes, it was varied from 5 seconds up to 15 minutes. For extractions under 2 minutes, the shaking of the sample was performed on a vortex mixer, while a shaking table was used for all other times. Consequently, the slight decrease in extraction at 120 or 210 seconds in the extraction is due to the higher shaking power that the vortexer provides.

##### 4.2.4.1 TEHA

The extraction of the  $^{89}\text{Zr}$  into TEHA was extremely fast with an equilibrium reached within 30 seconds as seen in Figure 4.17. In Figure 4.18, the  $^{175}\text{Hf}$  was slightly slower arriving at equilibrium at about 60 seconds. Figure 4.19 shows that the kinetics of  $^{239}\text{Pu}$  took the slowest with equilibrium not being reached until after 30 minutes. This assumption is based on the fact that the  $^{239}\text{Pu}$  had not finished extracting in the 15 minute timescale of the kinetic study and the mixing time used for the original extraction of  $^{239}\text{Pu}$  was 30 minutes.

### **$^{89}\text{Zr}$ Kinetic Study of TEHA**

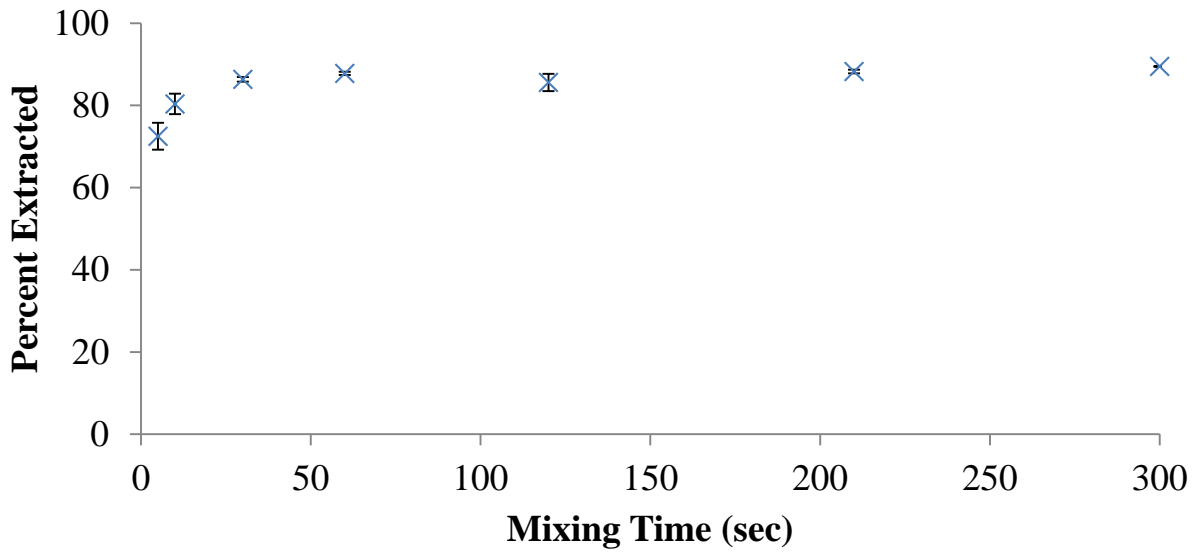


**Figure 4.17** Kinetics of  $^{89}\text{Zr}$  in 0.05 M TEHA/12 M HCl

### **$^{175}\text{Hf}$ Kinetic Study of TEHA**

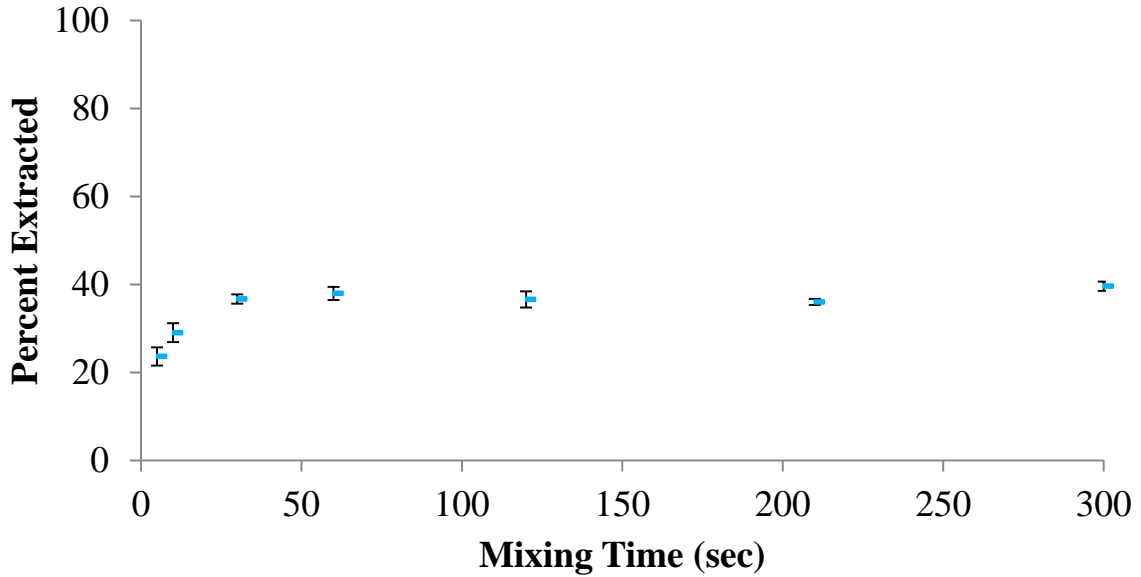


**Figure 4.18** Kinetics of  $^{175}\text{Hf}$  in 0.05 M TEHA/12 M HCl



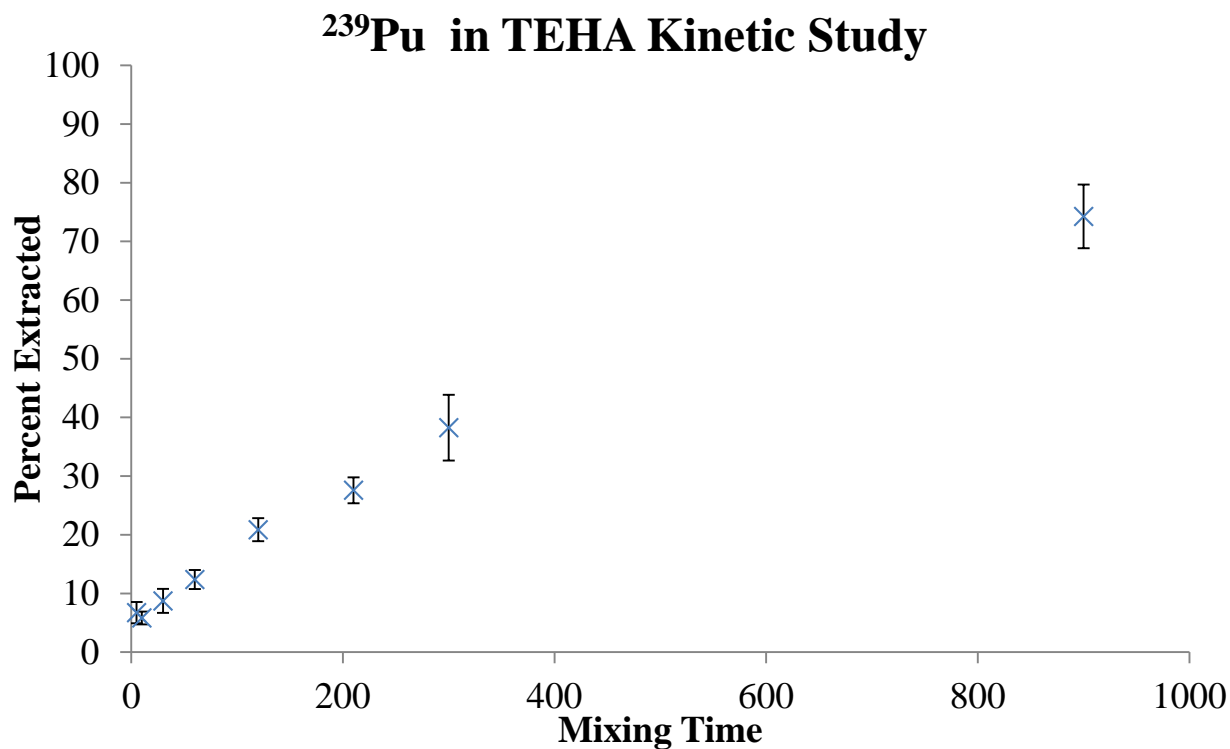


**Figure 4.19** Kinetics of  $^{239}\text{Pu}$  in 0.05 M TEHA/12 M HCl

#### 4.2.4.2 TEHP

The kinetics of extraction with TEHP proved to be similar kinetics with TEHA between all three radionuclide with some slight differences. The  $^{89}\text{Zr}$  extraction into TEHP was the fastest with its equilibrium reached in 10 seconds (see Figure 4.20). In Figure 4.21, the  $^{175}\text{Hf}$  was slower, having to take 210 seconds to arrive at equilibrium (see Figure 4.21). Again, the kinetics of  $^{239}\text{Pu}$  required the longest equilibrium time with 30 minutes (see Figure 4.22). This assumption is based on the fact that the  $^{239}\text{Pu}$  had not finished extracting in the 15 minute timescale of the kinetic study and the mixing time used for the original extraction of  $^{239}\text{Pu}$  was 30 minutes.

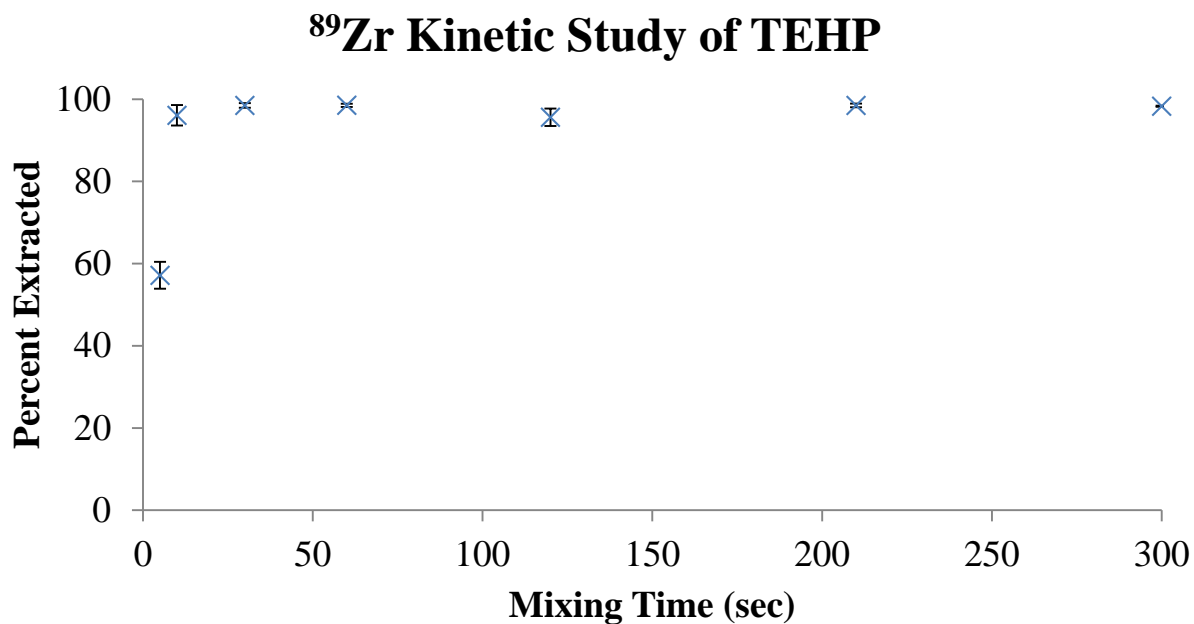


**Figure 4.20** Kinetics of  $^{89}\text{Zr}$  in 0.05 M TEHP/12 M HCl

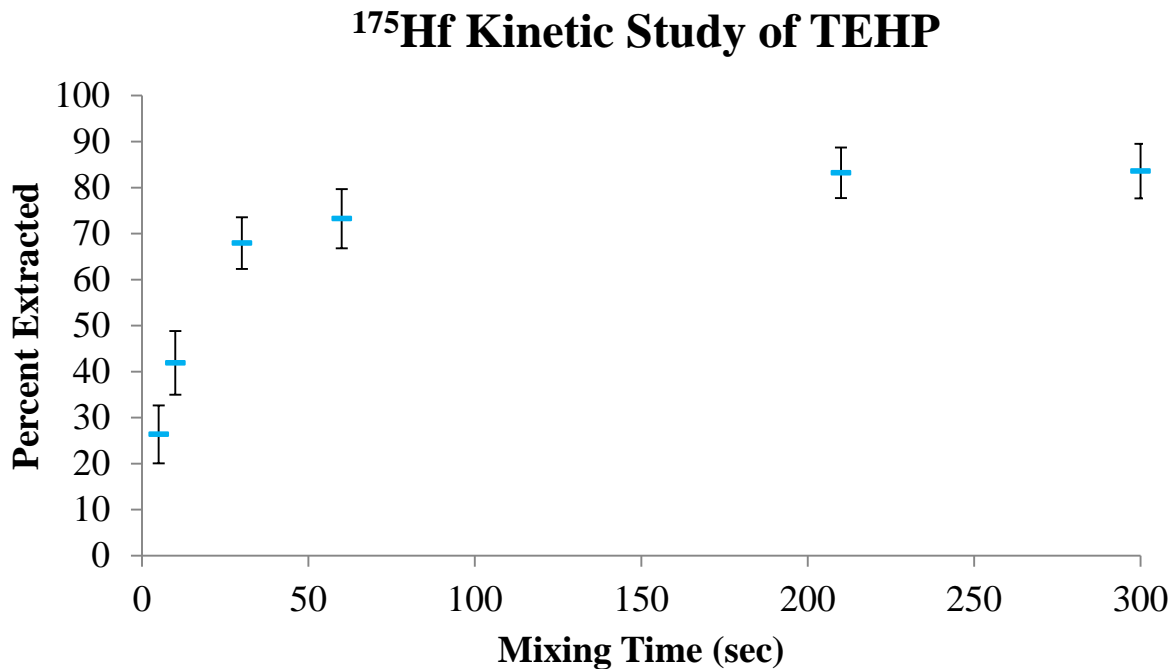


**Figure 4.21** Kinetics of  $^{175}\text{Hf}$  in 0.05 M TEHP/12M HCl

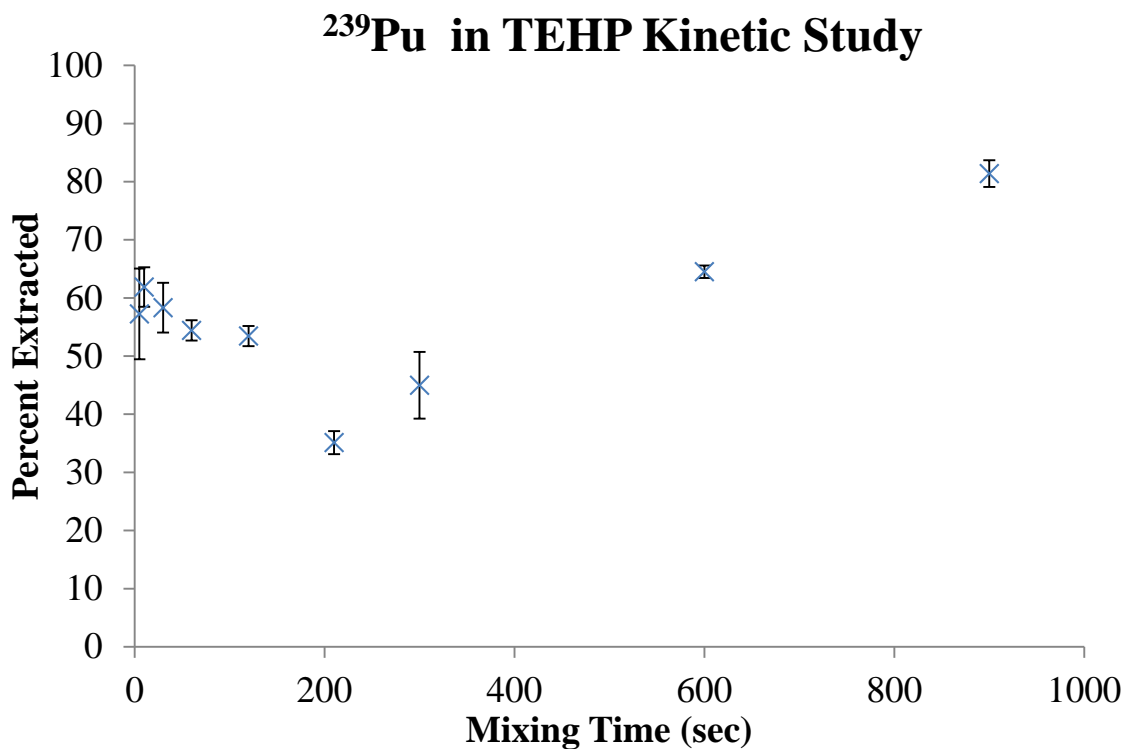


**Figure 4.22** Kinetics of  $^{239}\text{Pu}$  in 0.05 M TEHP/12M HCl

#### 4.2.5 Discussion

The solvent selection experiments showed that toluene was the best solvent to use for extraction. The rest of the solvents investigated were either difficult to use due to the high vapor pressure or formation of a third phase. Since toluene had neither of these problems and had excellent extraction (only marginally second to DCM), it was the solvent of choice.

As shown in the results, a good separation between all three radionuclides can be found for both TEHA and TEHP. In particular, the region between 6 M to 9 M hydrochloric acid shows the greatest potential for separation. This initial separation shows the ideal curve for extracting super heavy elements. The ideal separation concentrations for the three elements with TEHA are the following: 9 M for  $^{89}\text{Zr}/^{175}\text{Hf}$  (27.5 separation factor); 7 M for  $^{239}\text{Pu}/^{89}\text{Zr}$  (29.0 separation factor); and 9 M for  $^{239}\text{Pu}/^{175}\text{Hf}$  (800.9 separation factor). For TEHP, the best concentrations for

separations are: 8 M for  $^{89}\text{Zr}/^{175}\text{Hf}$  (42.5 separation factor); 8 M for  $^{89}\text{Zr}/^{239}\text{Pu}$  (363.6 separation factor); and 9 M for  $^{175}\text{Hf}/^{239}\text{Pu}$  (33.8 separation factor). In solvent extraction, a separation factor of greater than 2 between the two species is the generally cutoff for determining whether a species can be extracted for practical purposes (although multiple separations will be required). There is enough separation between the radionuclides to differentiate rutherfordium's behavior when running online studies.

In the speciation studies, the TEHA extracts the  $^{89}\text{Zr}$  and  $^{175}\text{Hf}$  at a 2:1 ratio. This corresponds to the formation of the hexachloro-metal complex for each element with the 2 amine coordinating with the complex. Since the zirconium anion complex forms at a lower acid concentration than the hafnium complex, it extracts at the lower acid concentration that correlates with metal complex formation. Since hafnium does not completely extract into TEHA, it does not completely exist as the hexachloro-complex in solution and most likely has neutral complexes present. Although information about the speciation of  $^{239}\text{Pu}$  was not obtained (possibly due to polymerization), the  $^{239}\text{Pu}$  hexachloro-complex is assumed to have been the extracted complex.

For TEHP, all three elements are extracted at a 1:1 ratio. This follows the expected complex extracted, as organophosphate compounds form adducts. The extracted complex is possibly a mixture of the neutral complexes that the three elements form as well as the neutral acidic species in solution as the extraction continues into the higher acid concentrations. Plutonium forms these neutral complexes more readily and at lower acid concentrations than hafnium and zirconium. Zirconium and hafnium form neutral complexes at higher acid concentrations and completely extract into TEHP.

One concerning result when looking at the applicability of these ligand systems to transactinide studies are the kinetic result for  $^{175}\text{Hf}$  and  $^{239}\text{Pu}$ . While the TEHA equilibrium for  $^{175}\text{Hf}$  is reached at just under a minute, the TEHP results for  $^{175}\text{Hf}$  and both the TEHA and TEHP results for  $^{239}\text{Pu}$  are longer than a minute, even more so for the  $^{239}\text{Pu}$ . This delay could possibly be due to the complex formation of the hexachloride complex in solution, which means that only the  $^{89}\text{Zr}$  results of TEHA and TEHP and the  $^{175}\text{Hf}$  results of TEHP could be used in online studies of rutherfordium to further elucidate its behavior.

Since  $^{239}\text{Pu}$  results could not be reproduced reliably, there are a number of possible reasons that the chemistry could be more complicated. The  $^{239}\text{Pu}$  could extract differently than the  $^{89}\text{Zr}$  and  $^{175}\text{Hf}$ , possibly as a different chemical species. This may be the reason why it begins extracting at lower hydrochloric acid concentration than the  $^{89}\text{Zr}$  and  $^{175}\text{Hf}$ . In the TEHP extractions, all three of  $^{89}\text{Zr}$ ,  $^{175}\text{Hf}$ , and  $^{239}\text{Pu}$  show an approximate 1:1 ligand to element extracted ratio. Another possibility may be due to the treatment of the  $^{239}\text{Pu}$  solution during the solution preparation. While initially a tracer level solution, the  $^{239}\text{Pu}$  concentration in the solution may have increased to the point that some of the  $^{239}\text{Pu}$  had undergone polymer formation. This would explain some of the nonlinear trends seen in Figure 4.22.

Despite some incompatible results for online studies, a separation between  $^{89}\text{Zr}$ ,  $^{175}\text{Hf}$ , and  $^{239}\text{Pu}$  can be reliably achieved if the extraction required does not rely on fast kinetics. This separation can be used for stable separation between zirconium and hafnium reliably.

## 5 BATCH STUDIES

### 5.1 Exploratory Batch Studies with Resin Backbones and Ligand Loading

Prior to columns studies, batch studies must be performed to determine the optimal loading conditions for the desired separation between the elements. These conditions can be tested for columns; however, when compared to column studies, batch studies can provide the same conclusions as the columns on a much faster time scale for a much larger sample volume.

Different types of polymer backbone for the resin as well as weight percent loading for the ligand were tested for each radionuclide. The types of resin backbones tested are Amberchrome CG71, XAD7HP, and XAD4. All of these polymer beads have been used previously with other extraction chromatographic resins and are viable candidates for providing support in radionuclide separations. The weight percent loading of the ligand was also varied from 10% to 40%. Previous studies have shown that loading above 40% can result the extractant bleeding from the column. Therefore, it is desired to have the loading as low as possible to prevent the extractant from bleeding off the column. On the other hand, loading the column with less extractant usually leads to a smaller extraction. It is imperative to balance these two conditions if possible; if increasing the load of the resin does not lead to more extraction, then the lower loading percentage should be used to avoid bleeding from the column.

#### 5.1.1 TEHA

##### 5.1.1.1 $^{89}\text{Zr}$

Among the exploratory batch studies performed with  $^{89}\text{Zr}$ , the Amberchrome CG71 resin showed the greatest potential for highest extraction. As seen from Figures 5.1, 5.2, and 5.3, it performed almost two orders of magnitude better the other two backbones and the following trend was established: Amberchrome CG71>XAD7HP>XAD4. Amberchrome CG71 extracted

a  $D_w$  value of 10,000 on TEHA where as XAD4 and XAD7HP highest values did not go over 600. Generally, the 40% loading also showed the greatest extraction compared to the other two loadings with the following trend of  $D_w$ : 40% > 20% > 10%. As such, the 40% loading on Amberchrome was chosen and more data points were added. The XAD4 performed particularly poorly relatively to the other two backbones as seen in Figure 5.3, only showing  $D_w$  of 100 at 12 M hydrochloric acid.

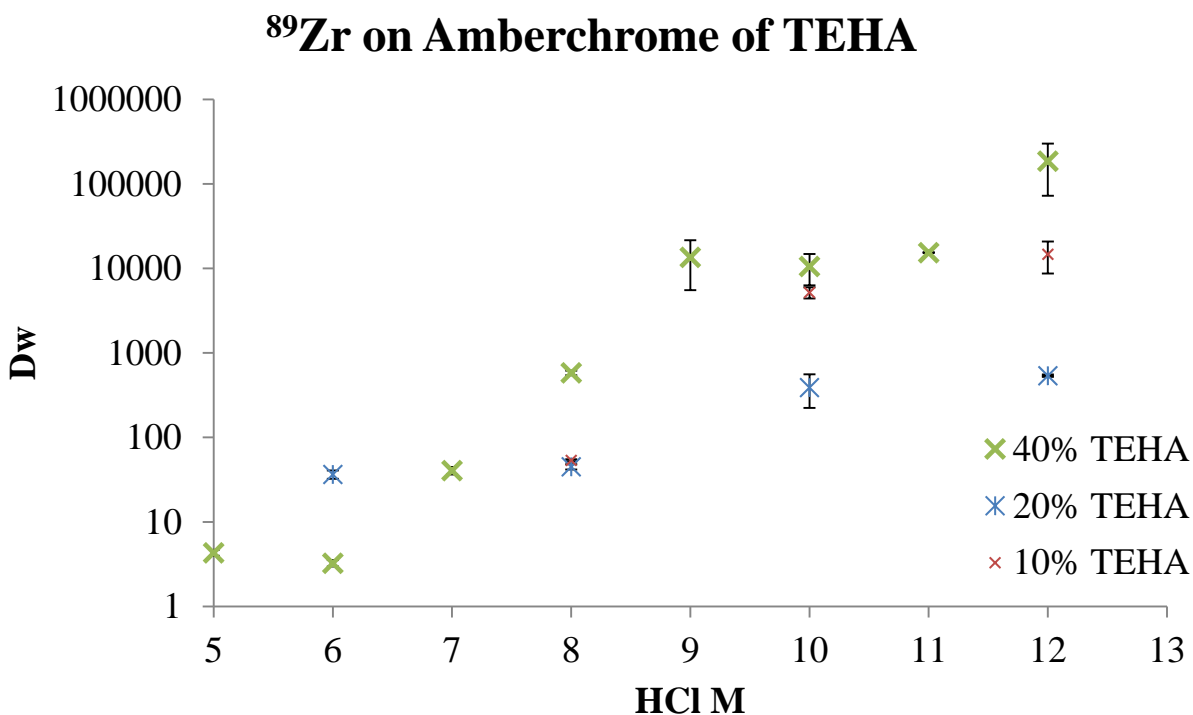


**Figure 5.1** Batch study of  $^{89}\text{Zr}$  on different percent loadings TEHA loaded Amberchrome backbone

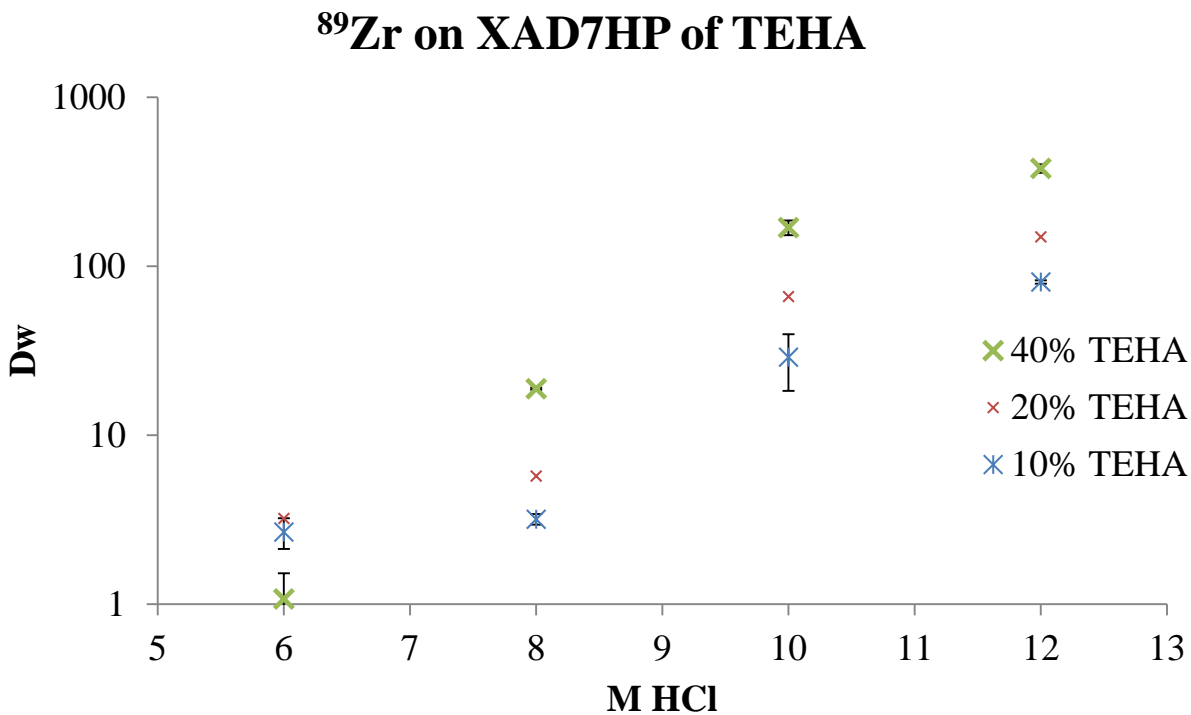


**Figure 5.2** Batch study of  $^{89}\text{Zr}$  on different percent loadings TEHA loaded XAD7HP backbone

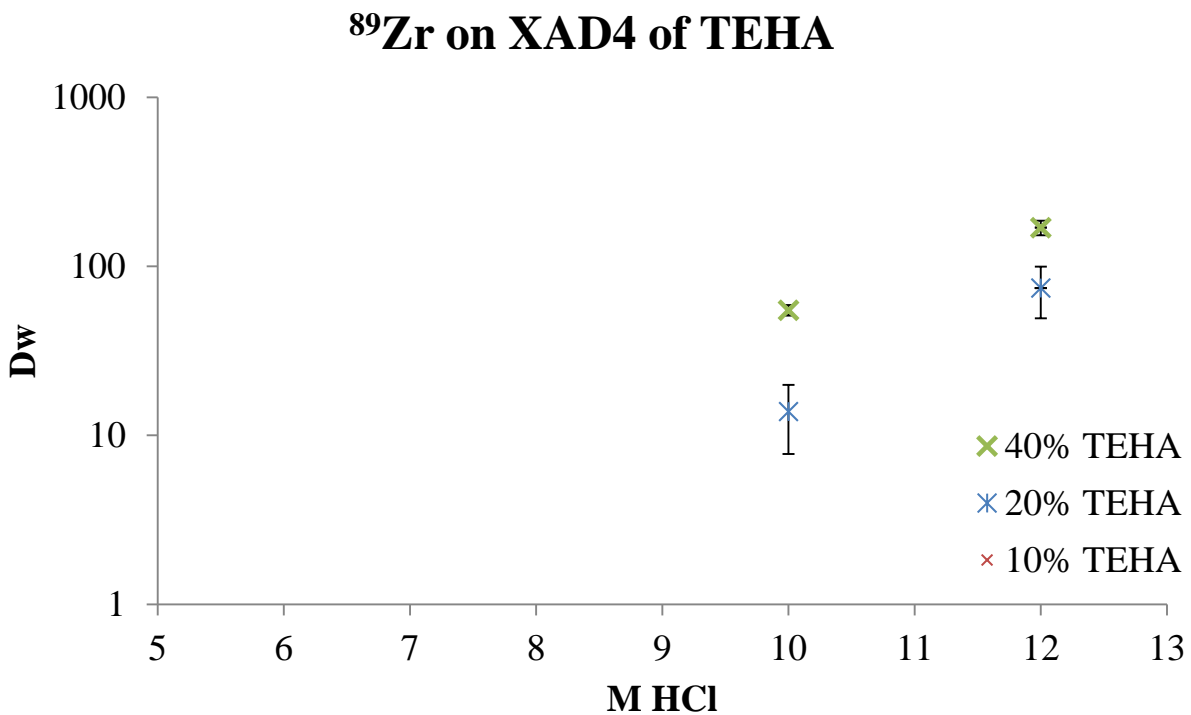


**Figure 5.3** Batch study of  $^{89}\text{Zr}$  on different percent loadings TEHA loaded XAD4 backbone



### 5.1.1.2 $^{175}\text{Hf}$

Since the available  $^{175}\text{Hf}$  stock had such low activity (100 Bq), an extension study testing each backbone and each loading as the ones performed for  $^{89}\text{Zr}$  and  $^{239}\text{Pu}$  was not feasible. Instead, a scaled back version was carried out in which only the 40% loading of the three backbones was tested. It was found that the  $D_w$  measured followed this trend: Amberchrome CG71>XAD7HP>XAD4 (see Figure 5.4). For the XAD4, only the 12M hydrochloric acid data point was done due to the poor performance of the resin on  $^{89}\text{Zr}$ . Since it extracted lower than both the XAD7HP and Amberchrome CG71, no further trials were performed as the other two backbones had greater extraction performance. Between the two other backbones, the Amberchrome outperformed the XAD4HP by a small percentage. Consequently, Amberchrome was chosen as the backbone and additional trials were added at the 7 M, 9 M, and 11 M hydrochloric acid points along the extraction curve.

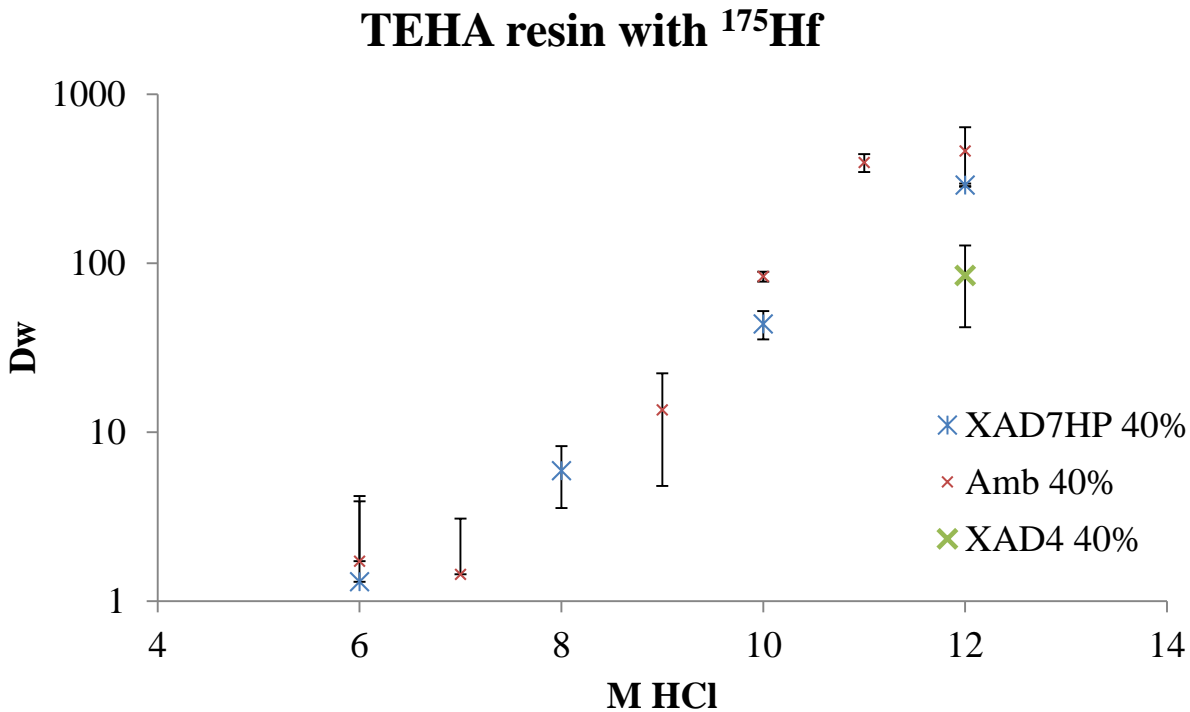


**Figure 5.4** Batch study of  $^{175}\text{Hf}$  on TEHA loaded Amberchrome, XAD7HP, and XAD4 backbone

#### 5.1.1.3 $^{239}\text{Pu}$

The behavior of  $^{239}\text{Pu}$  showed similarities to the  $^{89}\text{Zr}$  batch studies with the same general trends of  $D_w$ : Amberchrome CG71 > XAD7HP > XAD4 and 40% > 20% > 10%. One small exception to the trend was found on the Amberchrome CG71 20% at concentrations of 6 M and 8 M HCl, respectively. These data points saw an increased extraction of  $^{239}\text{Pu}$  of the Amberchrome CG71 20%, whereas the Amberchrome CG71 40% showed no extraction at all. Despite these two deviant results, the 40% Amberchrome CG71 eventually surpassed the 20% loading at 10 M and 12 M HCl. On the XAD7HP, the results between weight loadings were very similar, although the 40% was only nominally higher. The XAD4 again resulted in relative low extraction across the hydrochloric acid concentration range studied, although the 10% showed the most extraction of all the weight loadings.

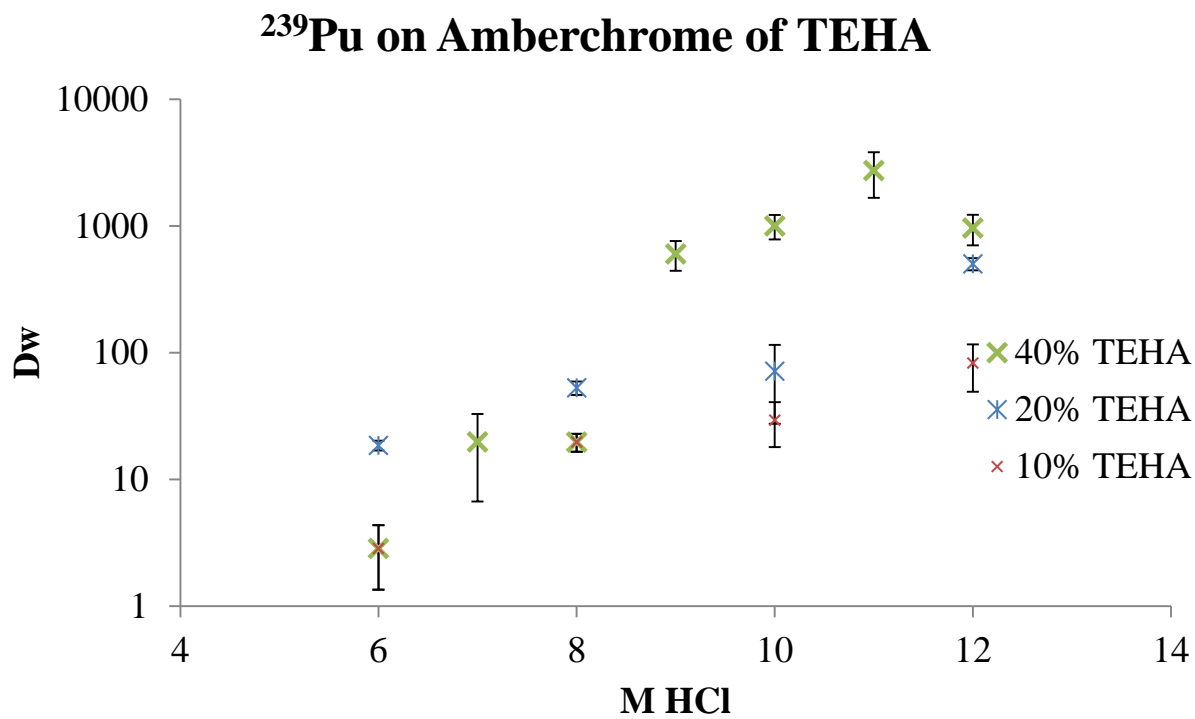


**Figure 5.5** Batch study of  $^{239}\text{Pu}$  on different percent loadings TEHA loaded Amberchrome backbone

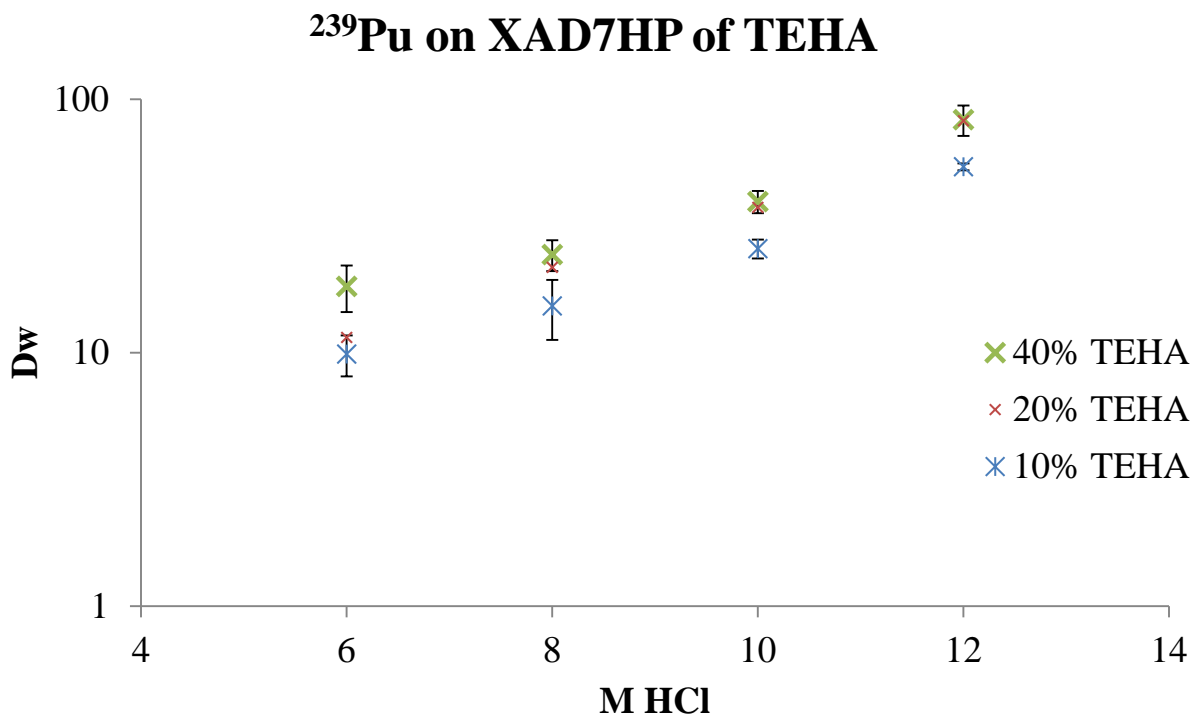


**Figure 5.6** Batch study of  $^{239}\text{Pu}$  on different percent loadings TEHA loaded XAD7HP backbone

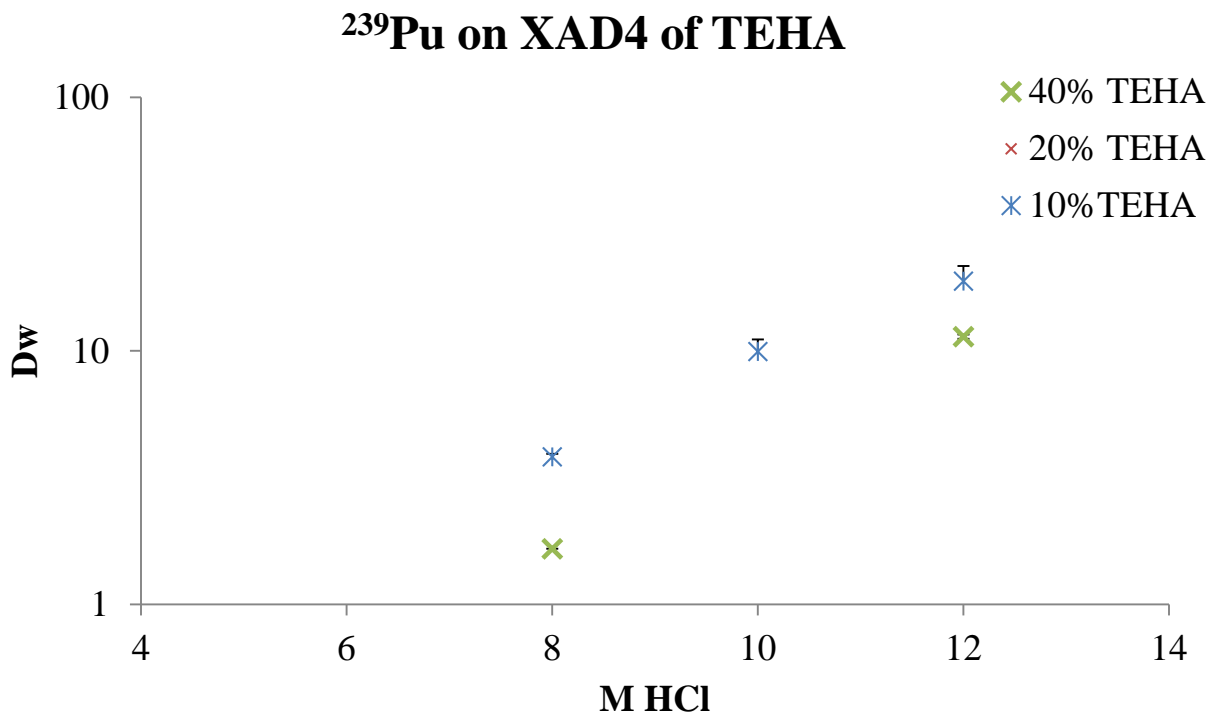


**Figure 5.7** Batch study of  $^{239}\text{Pu}$  on different percent loadings TEHA loaded XAD4 backbone

#### 5.1.1.4 Discussion of $^{89}\text{Zr}$ , $^{175}\text{Hf}$ , and $^{239}\text{Pu}$ Batch Studies with TEHA

From the previous results, the Amberchrome CG71 40% showed the greatest retention of all the radionuclides to be separated and was chosen as the ideal candidate for column studies. The behavior of  $^{89}\text{Zr}$  and  $^{175}\text{Hf}$  mirrors the solvent extraction results; however, the  $^{239}\text{Pu}$  batch studies show a lower extraction potential than the  $^{89}\text{Zr}$ . In the solvent extraction, the  $^{239}\text{Pu}$  extracted higher and at a lower hydrochloric acid concentrations than both the  $^{89}\text{Zr}$  and  $^{175}\text{Hf}$ . The solvent extraction studies should typically predict a similar extraction behavior than is seen in the resin batch studies. Since this is not the case, an interference, such as a steric hindrance or plutonium polymer formation, may be inhibiting the extraction. Having two TEHA compounds with a larger plutonium complex size may be preventing the plutonium extraction from showing the same performance as the  $^{89}\text{Zr}$  and  $^{175}\text{Hf}$ .

Prior to the column studies, the separation factors between each radionuclide were also determined and shown in Figure 5.8. These values help in judging how to construct the column procedure by showing the greatest separation between the elements within the hydrochloric acid concentration range. Also,  $^{89}\text{Zr}$  showed the highest retention at the lower acid concentrations and best separation factor of 994.0 with  $^{175}\text{Hf}$ ; this indicates that  $^{89}\text{Zr}$  should be eluted off last. The  $^{239}\text{Pu}$  also exhibited the second highest  $D_w$  and should be preferably eluted off next at a slightly higher acid concentration. Therefore,  $^{175}\text{Hf}$  should be eluted first and at the highest concentration possible without the  $^{89}\text{Zr}$  and  $^{239}\text{Pu}$  bleeding through.

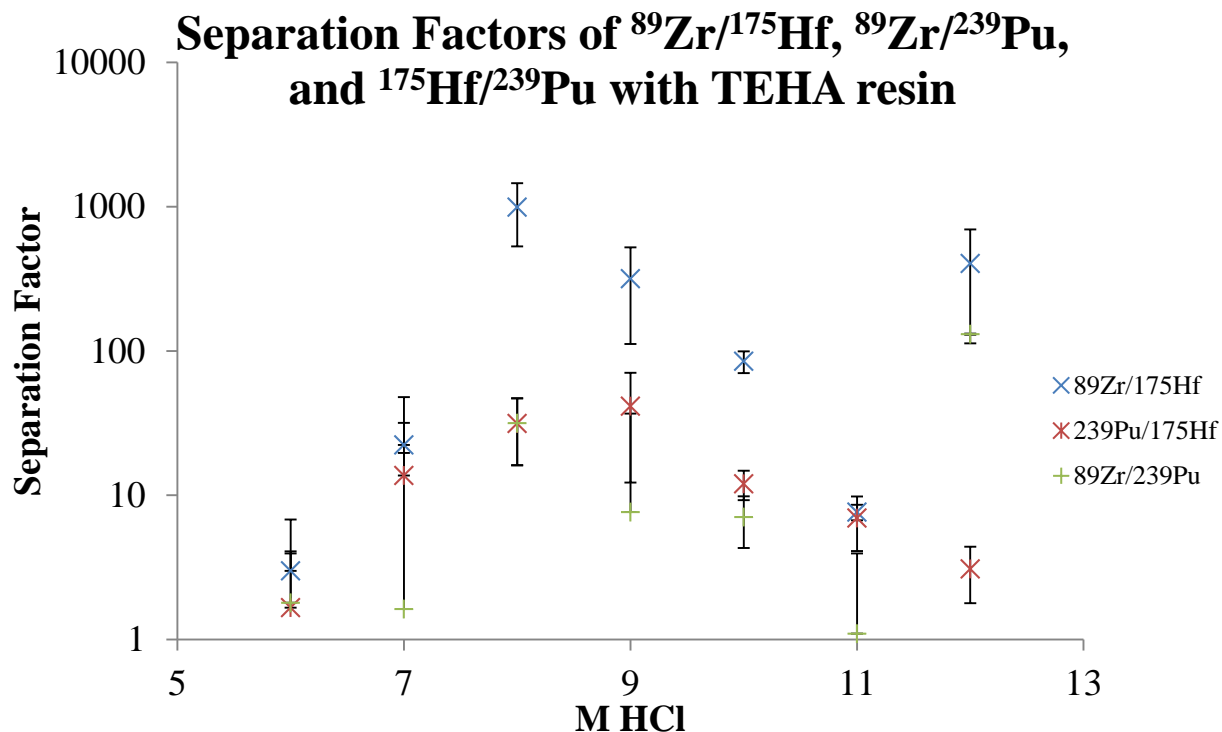


**Figure 5.8:** Separation factors of  $^{89}\text{Zr}$ ,  $^{175}\text{Hf}$ , and  $^{239}\text{Pu}$  on TEHA 40% Amberchrome resin

### 5.1.2 TEHP

#### 5.1.2.1 $^{89}\text{Zr}$

For  $^{89}\text{Zr}$  in TEHP, the Amberchrome CG71 again showed the greatest potential for extraction by at least an order of magnitude over the other two backbones and the following trend was established: Amberchrome CG71>XAD7HP>XAD4. Additionally, the 40% loading also showed the greatest extraction compared to the other two loadings as well with the following trend of  $D_w$ : 40%>20%>10%. As with the TEHA, the 40% loading on Amberchrome was chosen for the kinetic and column study. Addition trials of batch studies were also performed on the 40% Amberchrome CG71 to further develop the extraction curve. While the XAD7HP extracted at lower  $D_w$ 's across the HCl range, the XAD4 showed slight sorption at 10M and 12M HCl.

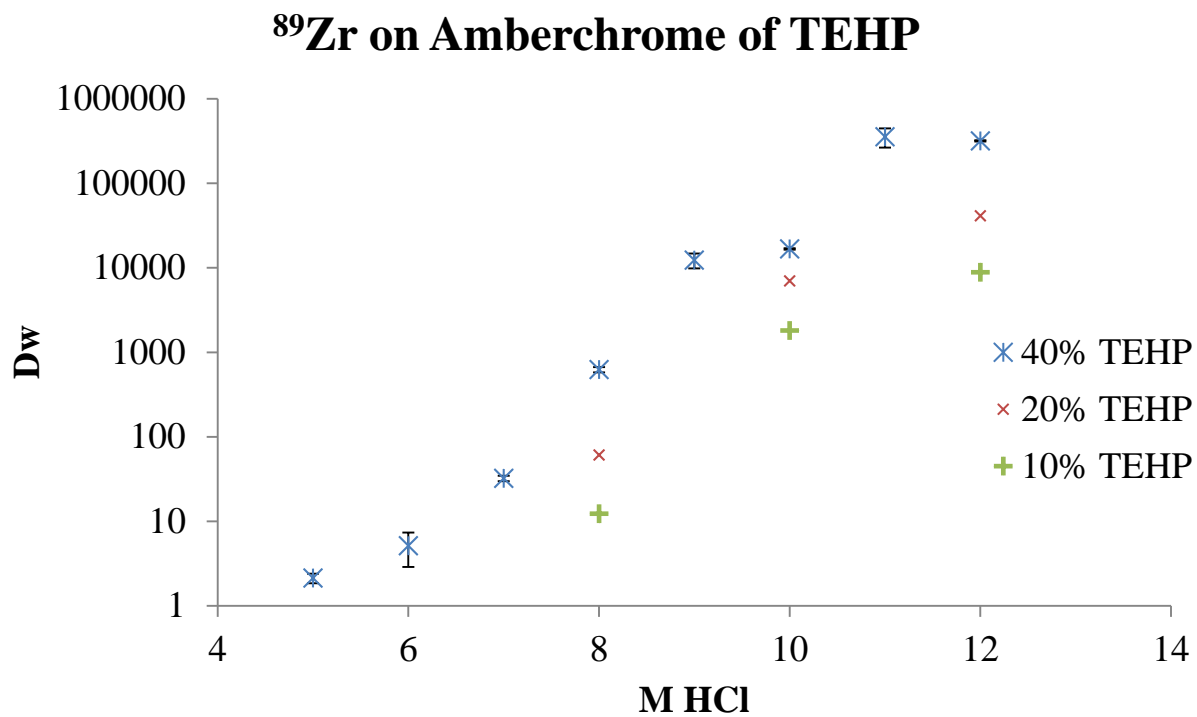


**Figure 5.9** Batch study of  $^{89}\text{Zr}$  on different percent loadings TEHP loaded Amberchrome backbone

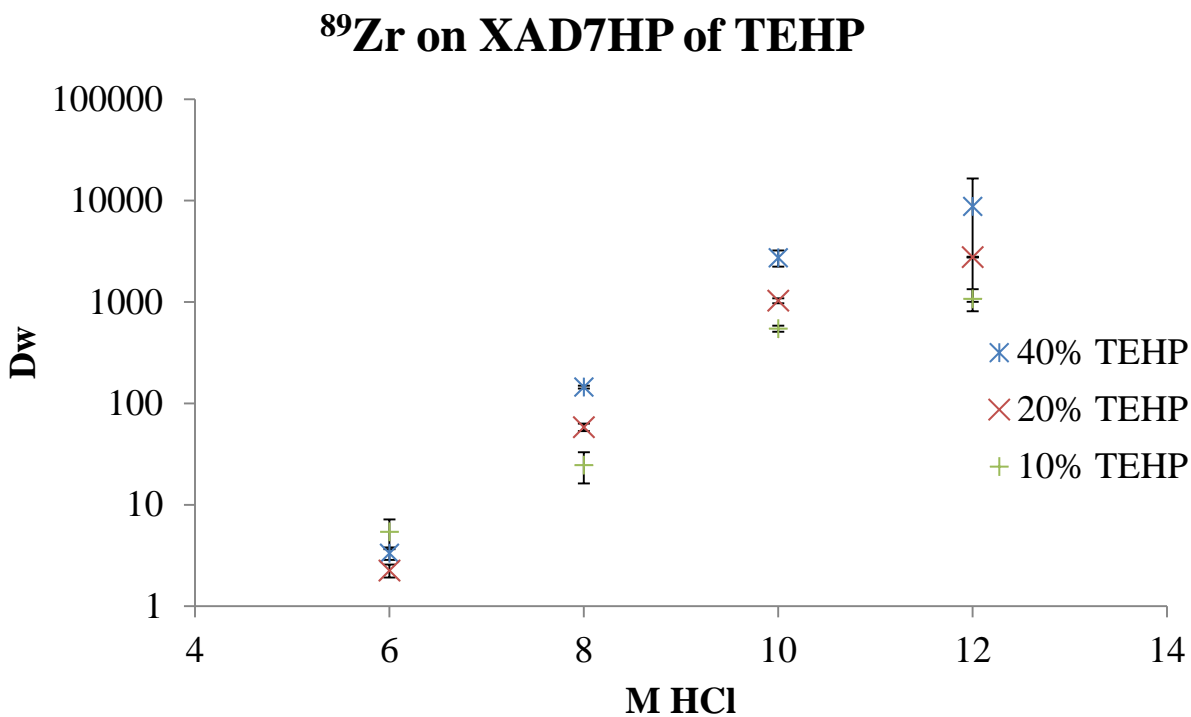


**Figure 5.10** Batch study of  $^{89}\text{Zr}$  on different percent loadings TEHP loaded XAD7HP backbone

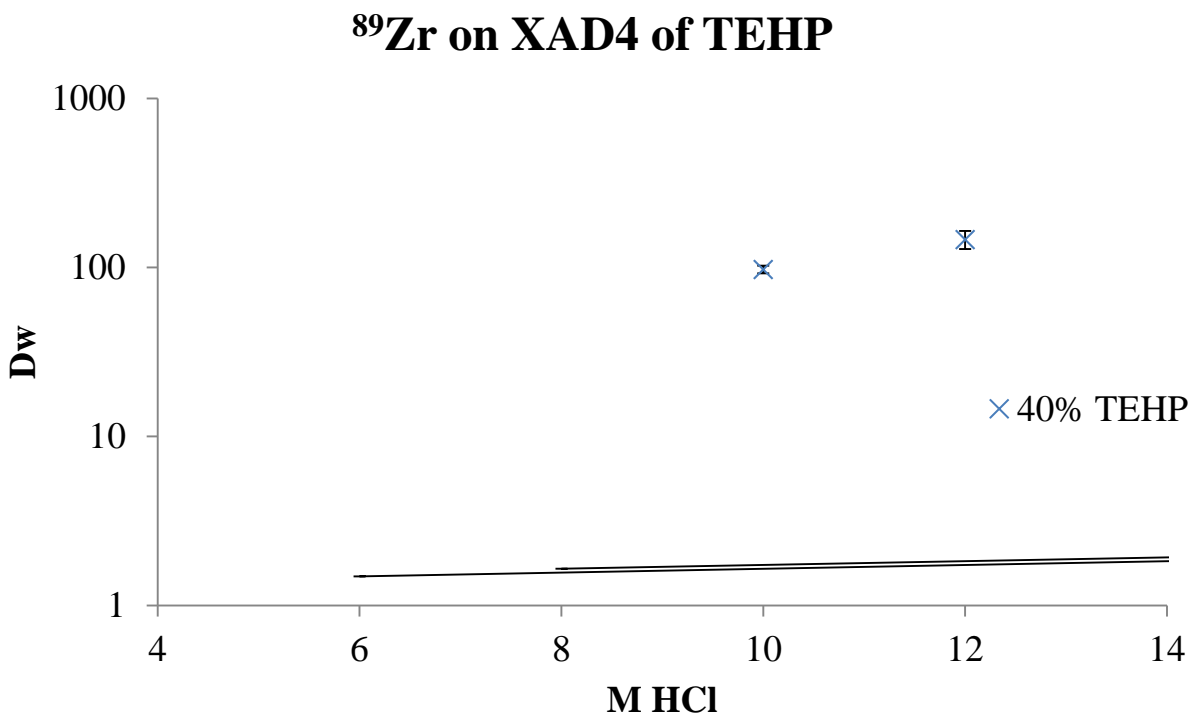


**Figure 5.11** Batch study of  $^{89}\text{Zr}$  on different percent loadings TEHP loaded XAD4 backbone



### 5.1.2.2 $^{175}\text{Hf}$

As previously with the TEHA, the  $^{175}\text{Hf}$  extraction was only attempted with the 40% loading of the backbone due to the low amount of activity available in the stock solution (see Figure 5.12). Hafnium on the Amberchrome CG71 showed an extraction with a  $D_w$  over 100,000 at 11 M. Continuing the same trend in the batch studies, the XAD4 and XAD7HP extracted lower than the Amberchrome CG71. Since the Amberchrome CG71 trials were performed first, when it became apparent that the XAD4 would not outperform this resin, no further trials were attempted except the 12 M HCl to conserve the stock solution. Since XAD7HP backbone had been comparable to the Amberchrome CG71 in previous results, batch studies were performed with the 6 M, 8 M, and 10 M HCl for comparison.

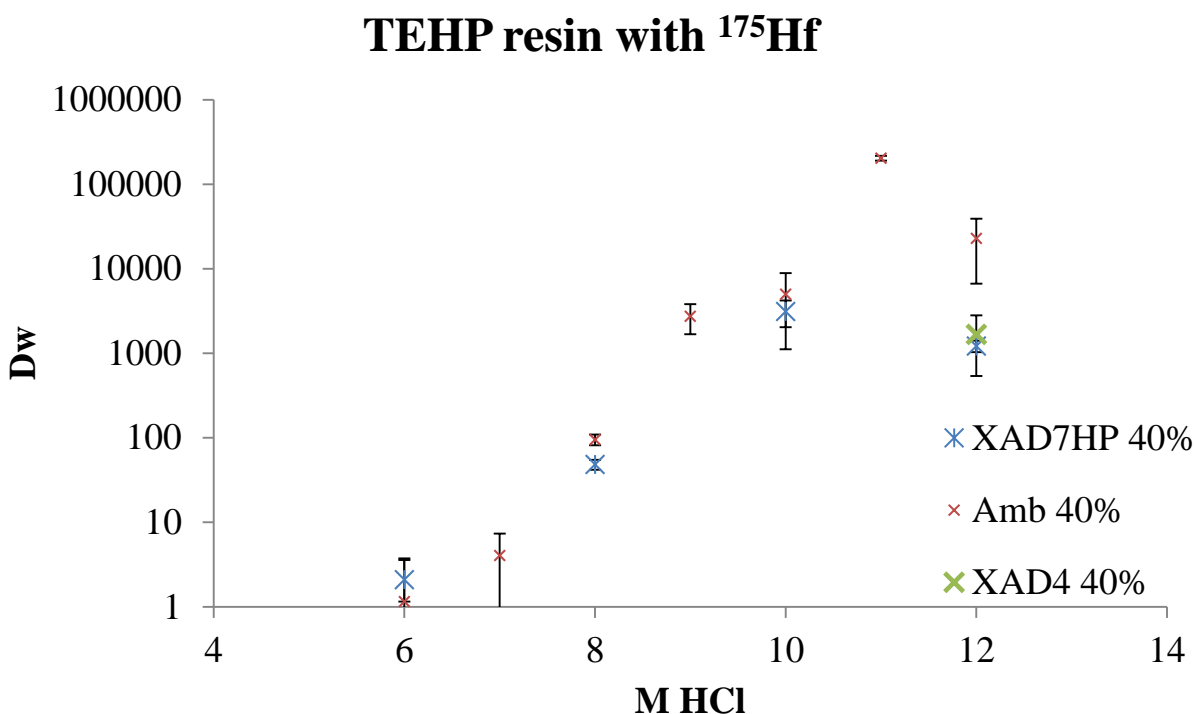


**Figure 5.12** Batch study of  $^{175}\text{Hf}$  on a TEHP loaded Amberchrome, XAD7HP, and XAD4 backbone

### 5.1.2.3 $^{239}\text{Pu}$

The  $^{239}\text{Pu}$  showed a much lower extraction in batch studies but with the same general trends of  $D_w$  as observed before (see Figure 5.13, 5.14, and 5.15): Amberchrome CG71>XAD7HP>XAD4 and 40%>20%>10%. The lower extraction was expected since the  $^{239}\text{Pu}$  extracted the lowest in the solvent extraction. On the XAD7HP, the sorptions between weight loadings were essentially the same, although the Amberchrome CG71 had a much higher  $D_w$ . The XAD4 resulted in a similar extraction to the XAD7HP with a greater differentiation between the weight loadings.

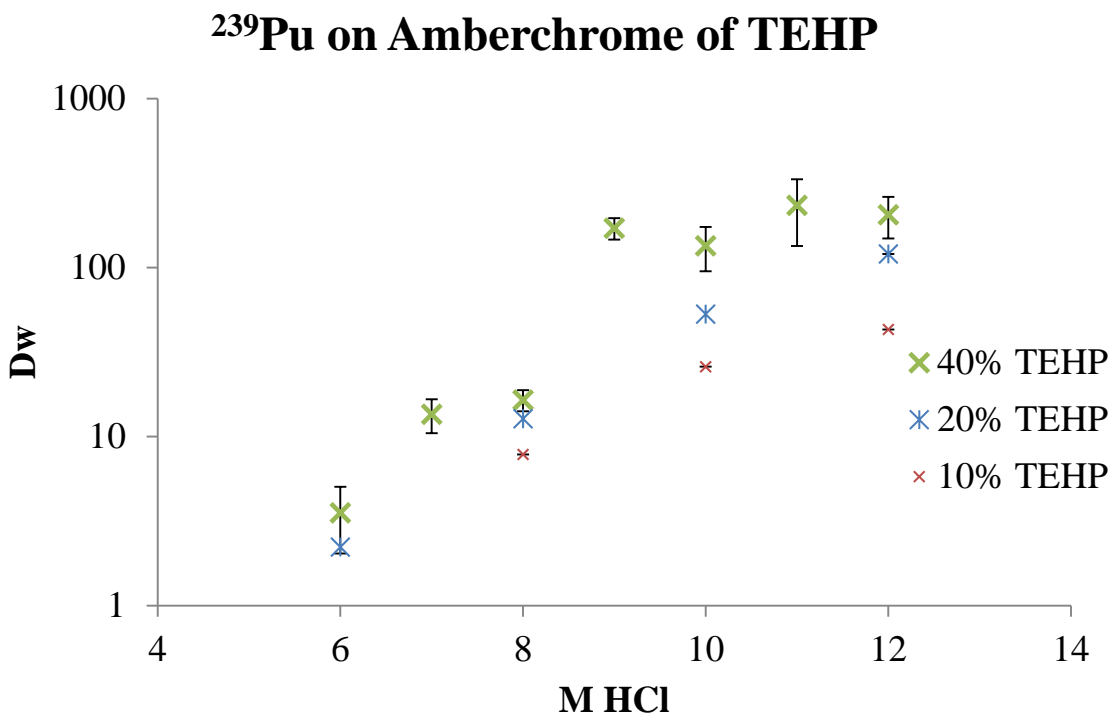


**Figure 5.13** Batch study of  $^{239}\text{Pu}$  on different percent loadings TEHP loaded Amberchrome backbone

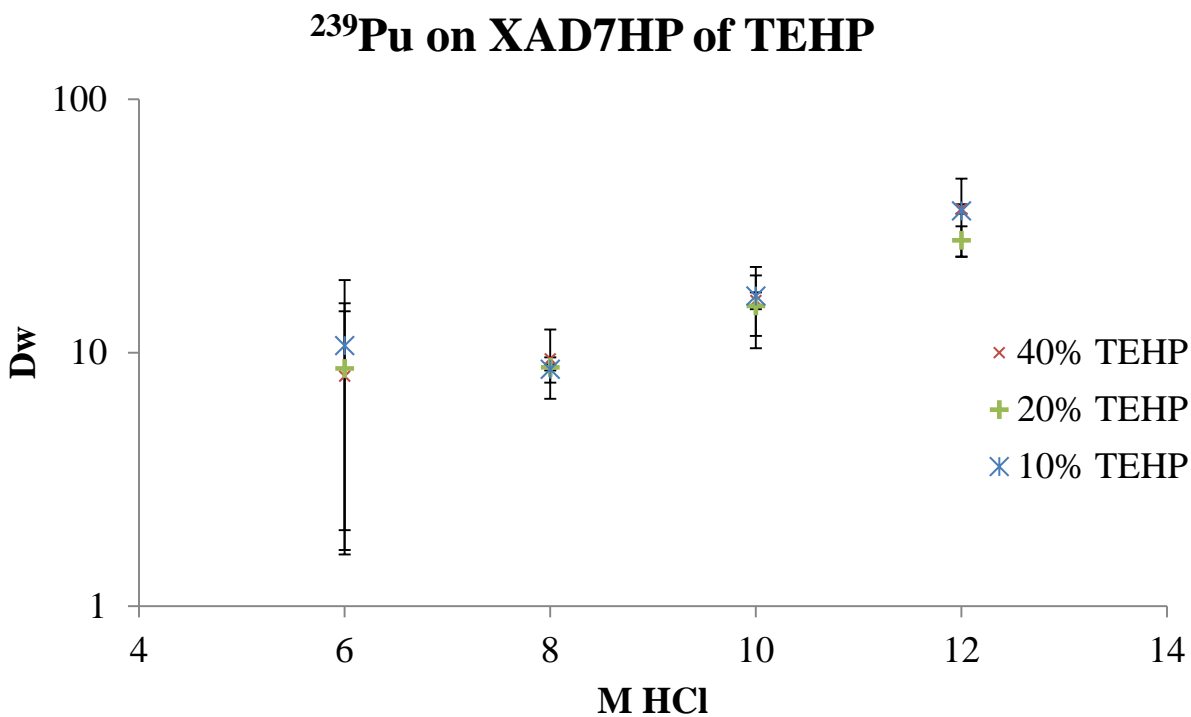


**Figure 5.14** Batch study of  $^{239}\text{Pu}$  on different percent loadings TEHP loaded XAD7HP backbone

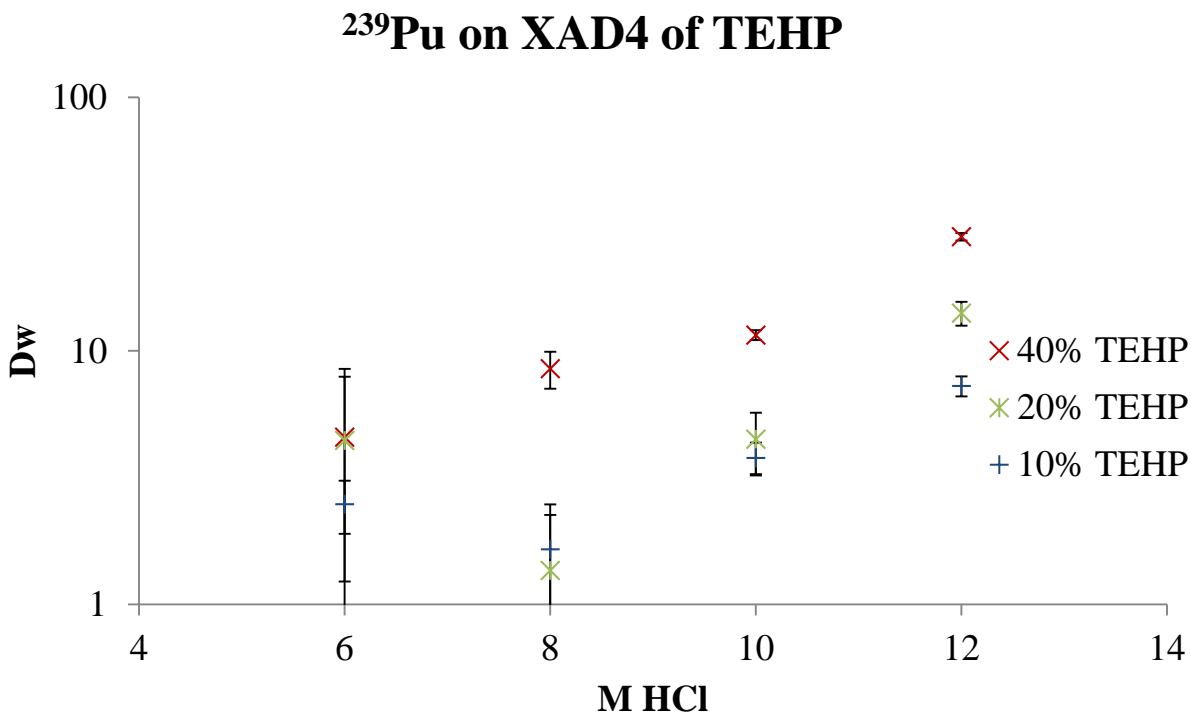


**Figure 5.15** Batch study of  $^{239}\text{Pu}$  on different percent loadings TEHP loaded XAD4 backbone

#### 5.1.2.4 Discussion of $^{89}\text{Zr}$ , $^{175}\text{Hf}$ , and $^{239}\text{Pu}$ Batch Studies with TEHP

Accounting for all the previous results, the Amberchrome CG71 40% again demonstrated the greatest retention of all the radionuclides to be separated and was chosen for column studies. The  $^{89}\text{Zr}$ ,  $^{175}\text{Hf}$ , and  $^{239}\text{Pu}$  mimicked the TEHP solvent extraction results, following the extraction trend of  $^{89}\text{Zr} > ^{175}\text{Hf} > ^{239}\text{Pu}$ . Since it has the lowest affinity for the resin,  $^{239}\text{Pu}$  should be eluted first and at the highest acid concentration possible. Next,  $^{175}\text{Hf}$  should be next at a slightly lower acid concentration. The  $^{89}\text{Zr}$  showed the highest retention at the lowest acid concentration and, preferably, should be eluted off last.

When comparing back to solvent extraction studies, the TEHP resins showed a very similar trend unlike the TEHA. Since TEHP forms an adduct with the radionuclides at a 1:1 ratio, the different complex size and steric interferences do not greatly decrease the similarities of separation from the solvent extraction studies. This in theory makes TEHP a better ligand for extraction chromatography because it does not have to deal with those obstacles.

Figure 5.16 shows the various separation factors between the three isotopes. Since  $^{89}\text{Zr}$  and  $^{175}\text{Hf}$  extraction curves are so close together, they do not show as much extraction (with the highest separation factor of  $\sim 10$ ) as the separations with  $^{239}\text{Pu}$ . From 9 M to 12 M, the other two separation factors,  $^{89}\text{Zr}/^{239}\text{Pu}$  and  $^{175}\text{Hf}/^{239}\text{Pu}$ , show excellent performance with peak separation factors of 1546.8 and 787.3 respectively.

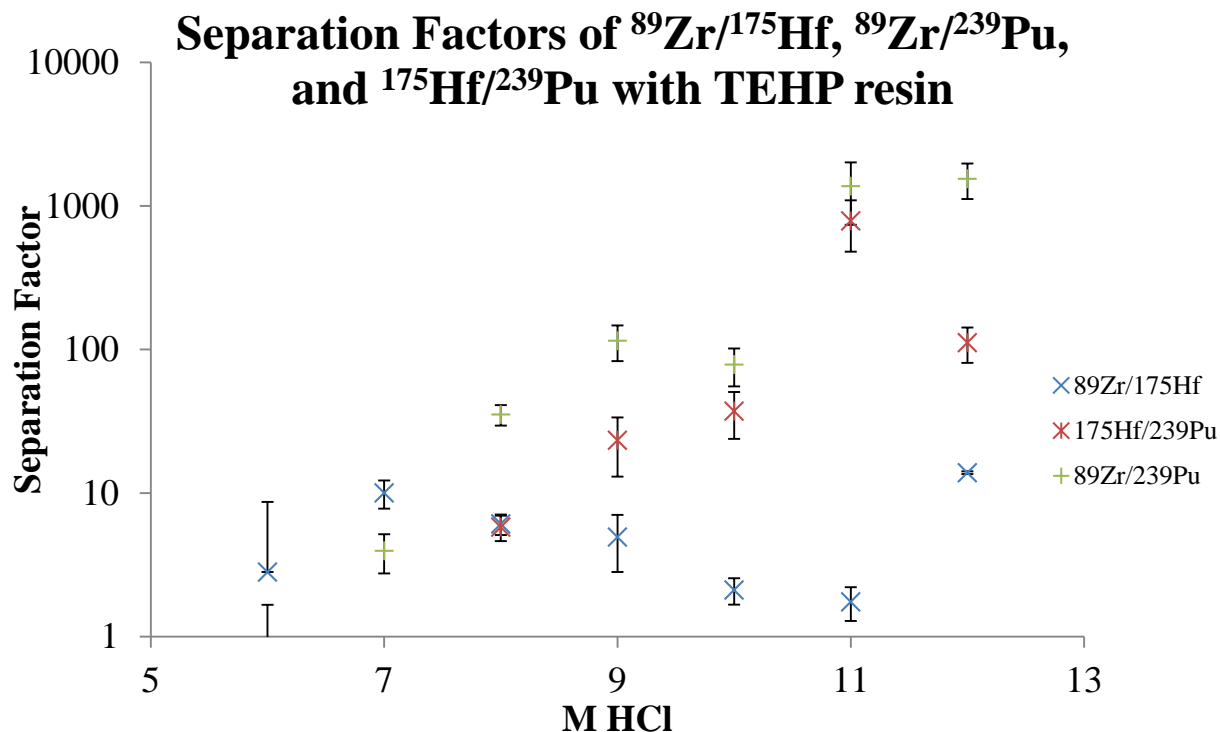


**Figure 5.16** Separation factors of  $^{89}\text{Zr}$ ,  $^{175}\text{Hf}$ , and  $^{239}\text{Pu}$  on TEHP 40% Amberchrome resin

## 5.2 Kinetic Studies

The final experiments that had to be completed before moving to a column system were kinetic studies for the resin. Not only are fast kinetics on a resin important for transactinide experiments due to the short half-lives, but it is also required that the radionuclides absorb quickly before they pass through the entire column. Theoretically, resins should have faster kinetics than solvent extraction because the increased surface area of the resin bead increases the theoretical plate height.

### 5.2.1 TEHA

As seen from Figure 5.17, the extraction of the  $^{89}\text{Zr}$  into TEHA 40% Amberchrome CG71 resin reached equilibrium within 60 seconds. The  $^{175}\text{Hf}$  was slightly faster arriving at equilibrium in 30 seconds as seen in Figure 5.18. Kinetics of  $^{239}\text{Pu}$  were the slowest with

equilibrium not being reached until 30 minutes (see Figure 5.19). This is assumed from the fact that the  $^{239}\text{Pu}$  had not matched the extraction levels in the kinetics study that were reached in the batch study with a mixing time of 30 minutes.

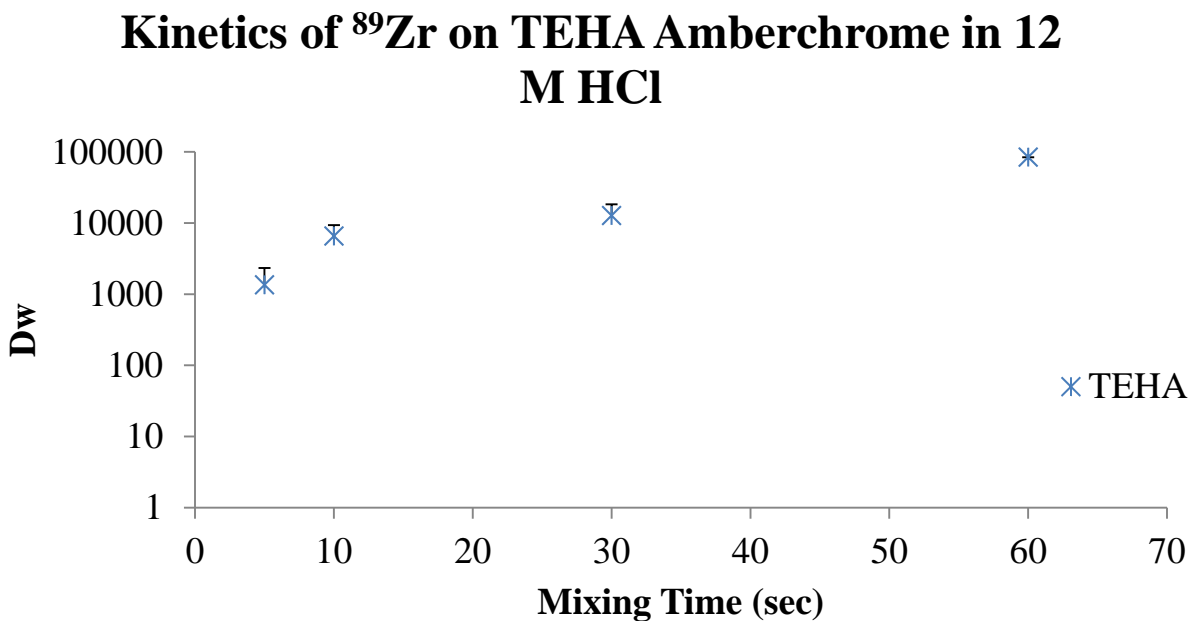


**Figure 5.17** Kinetics of  $^{89}\text{Zr}$  on TEHA Amberchrome in 12 M HCl

### Kinetics of $^{175}\text{Hf}$ on TEHA Amberchrome in 12 M HCl

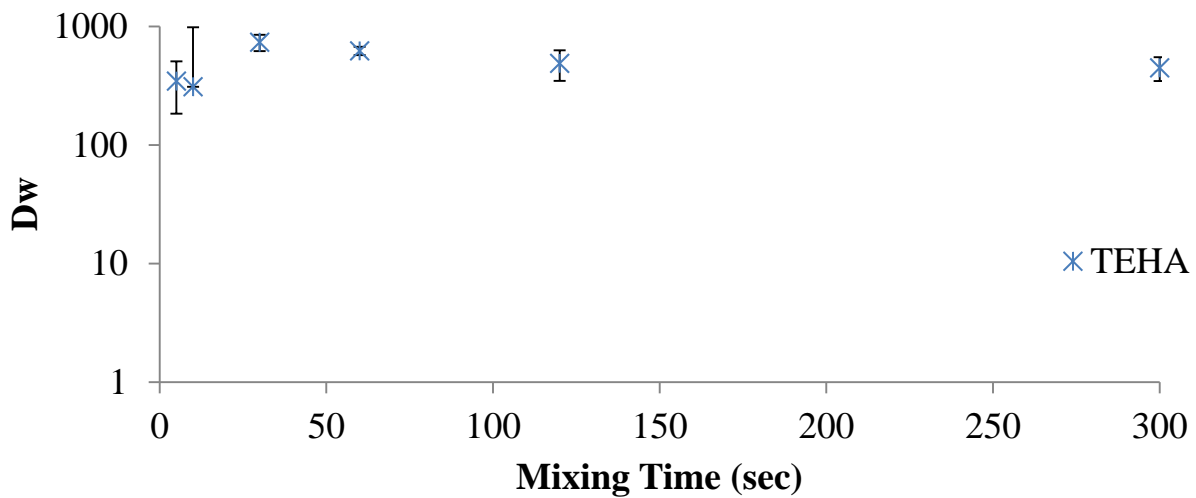


Figure 5.18 Kinetics of  $^{175}\text{Hf}$  on TEHA Amberchrome in 12 M HCl

### Kinetics of $^{239}\text{Pu}$ on TEHA Amberchrome in 12 M HCl

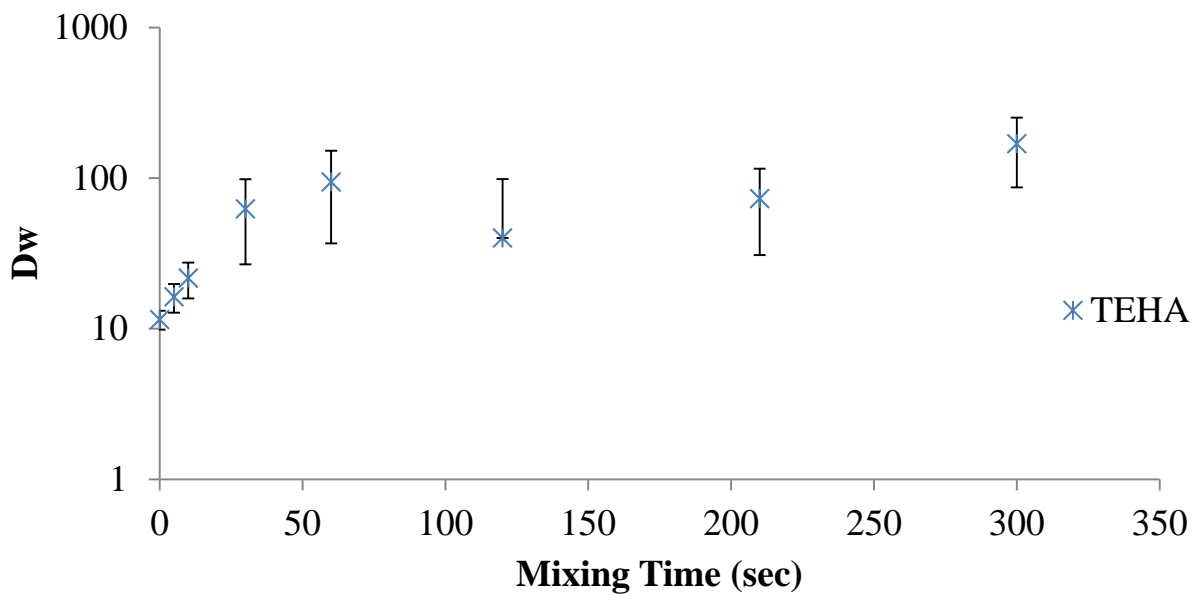
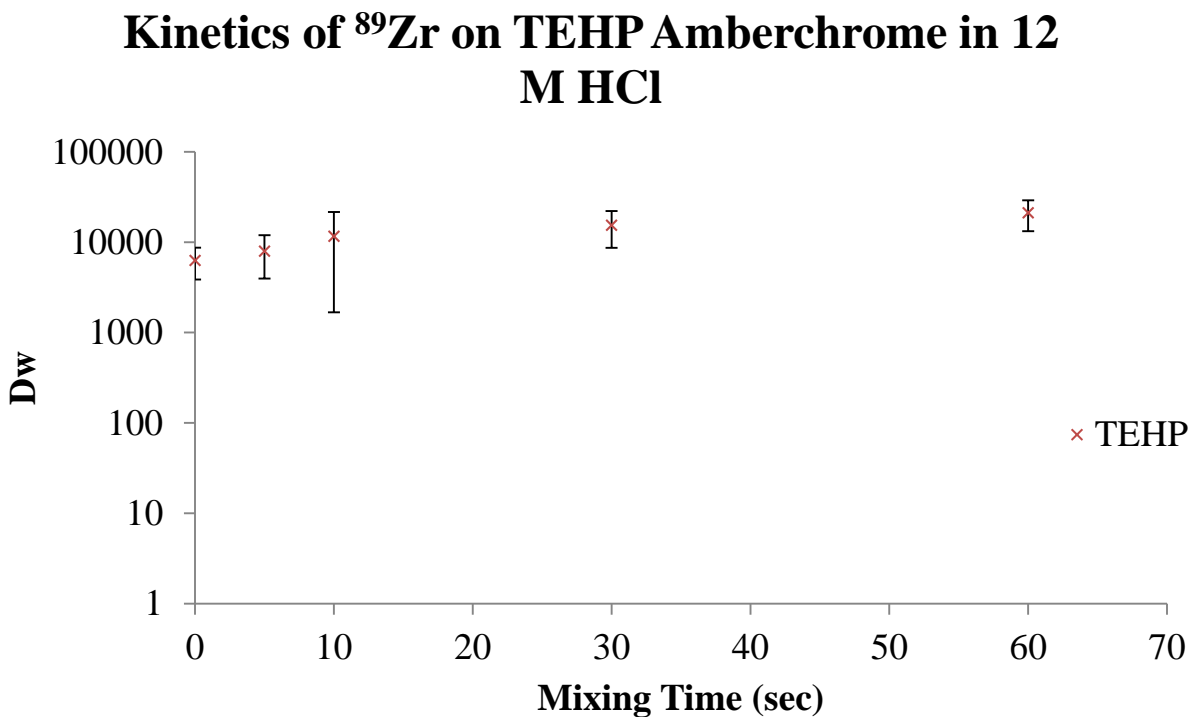


Figure 5.19 Kinetics of  $^{239}\text{Pu}$  on TEHA Amberchrome in 12 M HCl

#### 5.2.2 TEHP

TEHP showed faster kinetics compared to TEHA for all three radionuclides. The  $^{89}\text{Zr}$  extracted into TEHP the fastest with its equilibrium reached within 5 seconds (see Figure 5.20); a trial was completed with no mixing and this resulted in almost complete extraction as well. The  $^{175}\text{Hf}$  was slower as shown in Figure 5.21. It took about 120 seconds to arrive at equilibrium. Again, the kinetics of  $^{239}\text{Pu}$  required the longest equilibrium time, taking up to 30 minutes as seen in Figure 5.22. This is assumed based on the fact that the  $^{239}\text{Pu}$  had not finished extracting in the 5 minute timeframe of the kinetic study and the original mixing time for extraction of  $^{239}\text{Pu}$  was 30 minutes.



**Figure 5.20** Kinetics of  $^{89}\text{Zr}$  on TEHP Amberchrome in 12 M HCl



### Kinetics of $^{175}\text{Hf}$ on TEHP Amberchrome in 12 M HCl

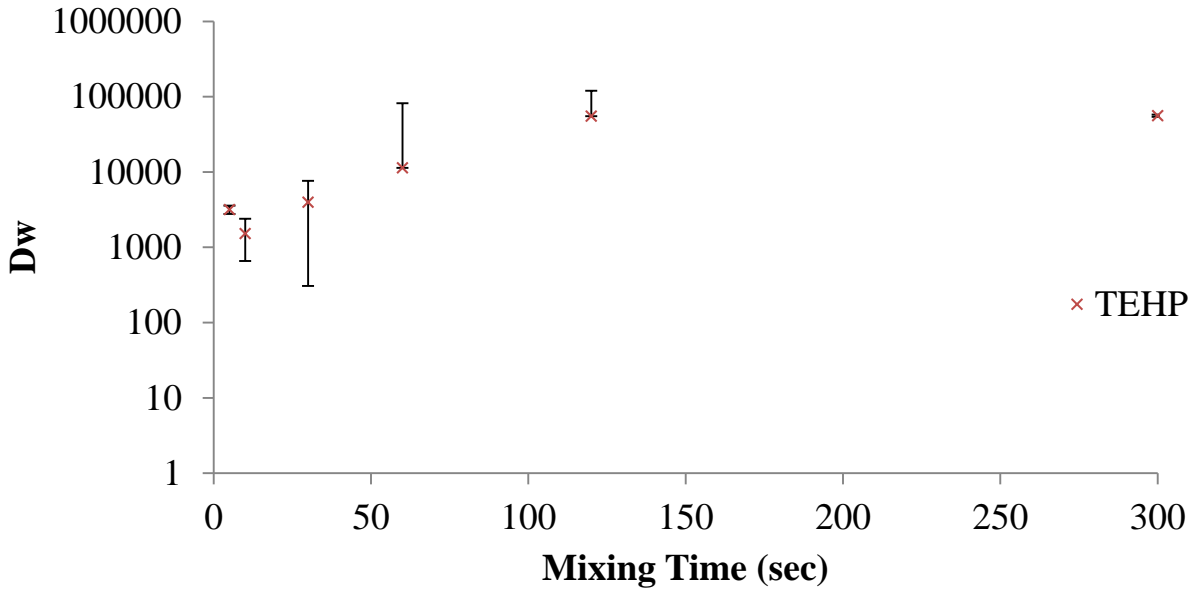


Figure 5.21 Kinetics of  $^{175}\text{Hf}$  on TEHP Amberchrome in 12 M HCl

### Kinetics of $^{239}\text{Pu}$ on TEHP Amberchrome in 12 M HCl

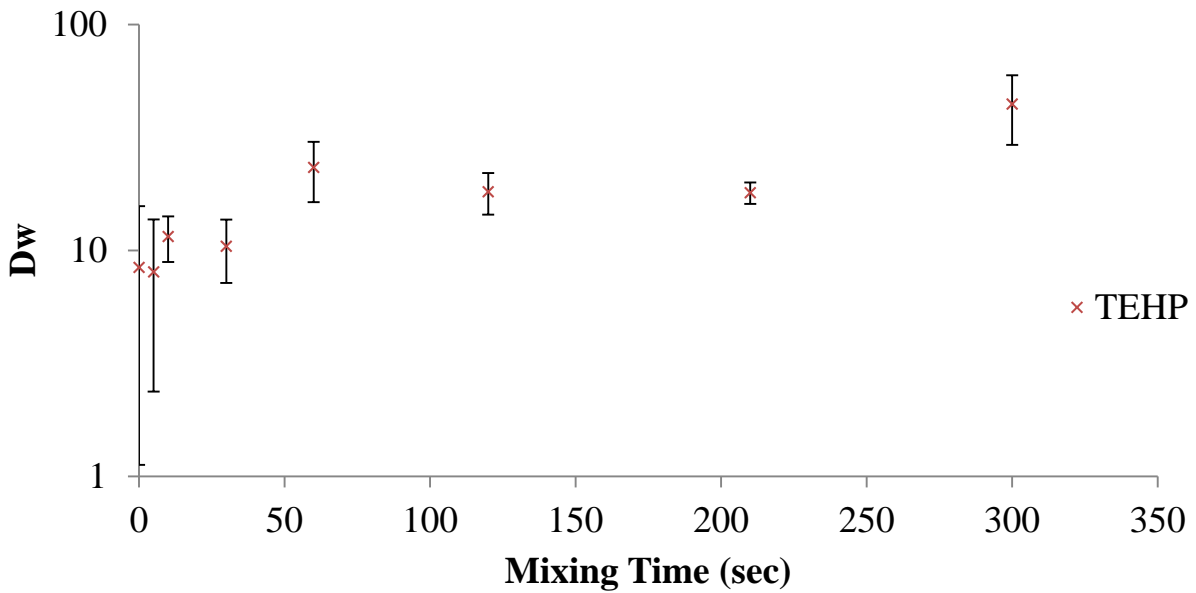


Figure 5.22 Kinetics of  $^{239}\text{Pu}$  on TEHP Amberchrome in 12M HCl

### 5.2.3 Discussion

The TEHA kinetics showed a reasonable result that would predict successful operation of a column and potential for its use in a transactinide experiment with  $^{89}\text{Zr}$  and  $^{175}\text{Hf}$ , with a 60 second and 30 second equilibrium, respectively. However, the  $^{239}\text{Pu}$  kinetics do not lend itself to the successful operation of a rapid column. Again, the possibility of  $^{239}\text{Pu}$ 's different chemistry and steric interferences may be interfering with the relatively rapid uptake compared to  $^{89}\text{Zr}$  and  $^{175}\text{Hf}$ . The TEHP kinetics show a similar trend, with the  $^{175}\text{Hf}$  kinetics being slightly slower at 120 seconds and the  $^{89}\text{Zr}$  being much faster at 5 seconds. The same conclusion for  $^{239}\text{Pu}$  behavior on TEHP can be reached; an interference is preventing the  $^{239}\text{Pu}$  from sorbing to the resin quickly.

The dissimilar kinetics of  $^{89}\text{Zr}$  and  $^{175}\text{Hf}$  on the two resins raises an interesting caveat about the possible chemistries that are occurring. Intriguingly,  $^{89}\text{Zr}$  is slower than  $^{175}\text{Hf}$  on the TEHA yet faster than  $^{175}\text{Hf}$  on the TEHP. With the  $^{89}\text{Zr}$  and  $^{175}\text{Hf}$  bearing almost identical chemical behavior in solution, the variation in the kinetics would point to the slight anion complex size difference that  $^{89}\text{Zr}$  and  $^{175}\text{Hf}$  form. The small divergence in the complex radius can lead to large deviations in extraction behavior on resins due to the requirements of the ligand coordination with the extracted species. This would explain the differences in the kinetics behavior.

## 6 COLUMN STUDIES

Two preliminary studies were performed for TEHA and TEHP each to investigate the column elution behavior of each of the radionuclides studied and to allow for comparison with the batch studies. The columns were set up and prepared as described in the Methods chapter. After the stock solution was added in 11 M HCl, more acid was passed through the column in 1 mL increments. The concentration of hydrochloric acid was decreased by 1 M for each subsequent increment. This continued until the concentration reached 6 M. Looking at the results,  $^{239}\text{Pu}$  had a large percentage (50%) bleed through almost immediately in the first fraction and then the rest (50%) eluted off in the 6 M fraction for both ligands. For both TEHA and TEHP,  $^{175}\text{Hf}$  had a small amount (~5%) of breakthrough in the load and wash fraction with most of it (~80%) eluting off at 7 M hydrochloric acid and a small amount in the 6 M hydrochloric acid. The  $^{89}\text{Zr}$  showed a somewhat similar result, with only a very small percent (1 to 2 %) breaking through in the first fraction, a small amount (~10%) in the 7 M hydrochloric acid, and the rest being eluted off with 6 M hydrochloric acid.

Therefore, two column separation strategies were designed based on these results. For the first, it would be attempted to elute  $^{239}\text{Pu}$  in the first fraction of 2 mL of 11 M hydrochloric acid;  $^{175}\text{Hf}$  would come off the column in 2 mL of 7 M HCl; and  $^{89}\text{Zr}$  would be eluted off in the 6 M HCl. In the second strategy, the  $^{239}\text{Pu}$  elution again would be attempted in the first fraction of 2 mL of 11 M hydrochloric acid;  $^{175}\text{Hf}$  would come off first in 2 mL of 6 M hydrochloric acid; and  $^{89}\text{Zr}$  would elute later in the subsequent fractions of 6 M hydrochloric acid.

### 6.1 Column Elution with 11 M HCl, 7 M HCl, and 6 M HCl

The column featuring the TEHA resin showed the expected elution behavior as seen in Figure 6.1. A 40% of the  $^{239}\text{Pu}$  broke through the column and a small percentage throughout the

elution profile. Once the concentration was switched to 6 M, the remaining 30% of  $^{239}\text{Pu}$  were washed off the column. About 20% of the hafnium breaks through in the first mL of the load fraction; the remainder then completely elutes in the 7 M fractions. Only 2% of the  $^{89}\text{Zr}$  breaks through in the first mL, but ~20% bleeds through the 7 M fraction. The remaining 70% then completely elutes in the 6 M fraction, and there is about a 10% loss of activity.

For the TEHP, a similar column behavior was observed in Figure 6.2. The majority (70%) of the  $^{239}\text{Pu}$  was eluted off in the 11 M hydrochloric acid fraction. Then, a small amount was eluted with 7 M and 6 M fractions. Ten percent of the hafnium also broke through in the 11 M fraction but the rest was essentially eluted off in the 7 M fraction with only 3% remaining in the 6 M. Zr-89 showed almost the same behavior as in the TEHA column with only 2% of the  $^{89}\text{Zr}$  breaking through in the first mL and 20% again eluting through the 7 M fraction. Then the remaining 75% completely eluted in the 6 M fraction, and there was about a 3% loss of activity.

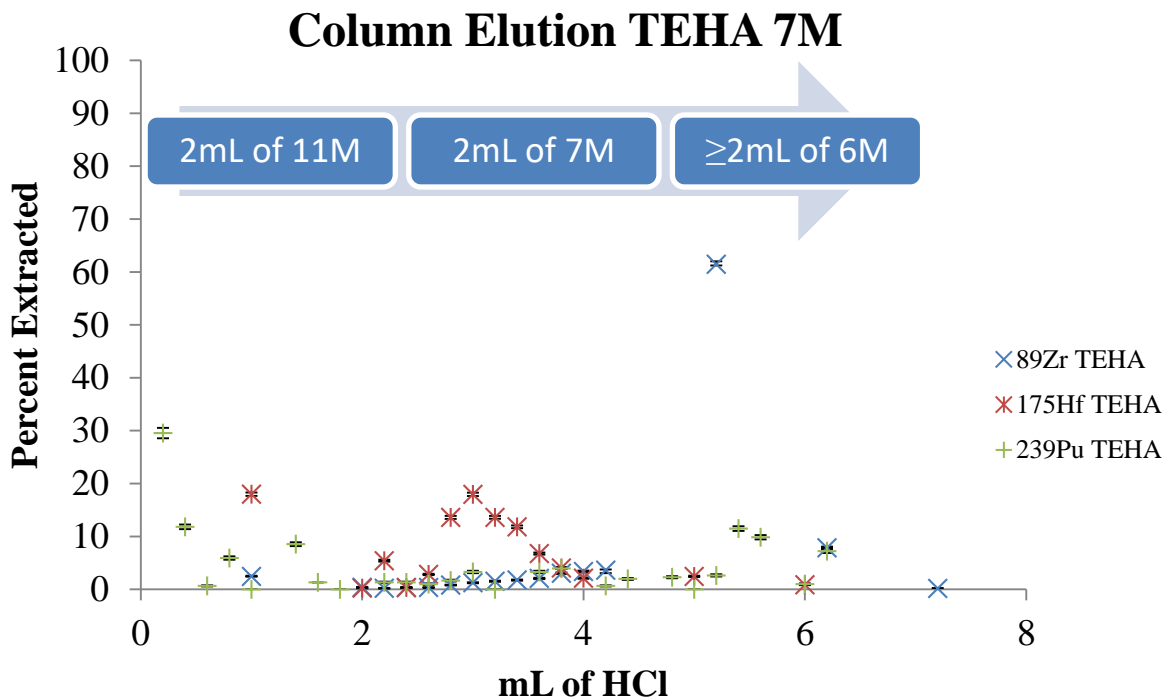


**Figure 6.1** Column elution of  $^{89}\text{Zr}$ ,  $^{175}\text{Hf}$ , and  $^{239}\text{Pu}$  on a 40% TEHA Amberchrome resin, eluting by 2 mL of 11 M HCl, followed by 2 mL of 7 M HCl, and then by 2 mL of 6 M HCl.

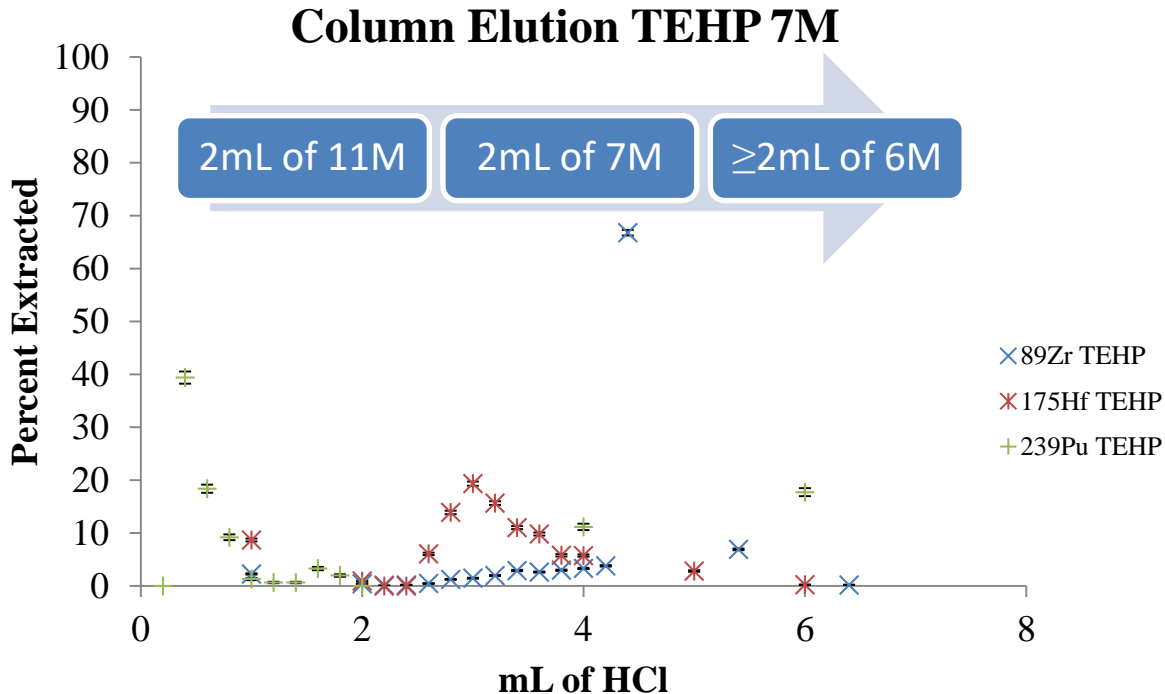


**Figure 6.2** Column elution of  $^{89}\text{Zr}$ ,  $^{175}\text{Hf}$ , and  $^{239}\text{Pu}$  on a 40% TEHP Amberchrome resin, eluting by 2 mL of 11 M HCl, followed by 2 mL of 7 M HCl, and then by 2 mL of 6 M HCl.

## 6.2 Column Elution with 11M HCl and 6M HCl

The results from the TEHA column elution with the 2mL of 11 M hydrochloric acid and  $\geq 2$  mL elution of 6 M is shown in Figure 6.3. Forty-one percent of the  $^{239}\text{Pu}$  eluted off in the first 2 mL of 11 M hydrochloric acid with a peak in the first 0.6 mL and then slowly off in the next 2 mL of 6 M hydrochloric acid. About 10% of the  $^{175}\text{Hf}$  came off in the initial 11 M of hydrochloric acid with the rest coming off around the 2.6 mL elution. The  $^{89}\text{Zr}$  behaved identically to the  $^{175}\text{Hf}$  and showed no separation between the two.

For the TEHP (Figure 6.4), 85% of the  $^{239}\text{Pu}$  eluted off in the first 2 mL of 11 M hydrochloric acid with a peak in the first 0.6 mL and then the remainder was again slowly eluted off in the next 2 mL of 6 M hydrochloric acid. Four percent of the  $^{175}\text{Hf}$  came off in the initial 11 M of hydrochloric acid with the rest coming off after approximately the 0.6 mL of 6 M of hydrochloric acid had been passed through the column. The  $^{89}\text{Zr}$  behaved again identically to the  $^{175}\text{Hf}$  and almost no separation was achieved between the two elements.

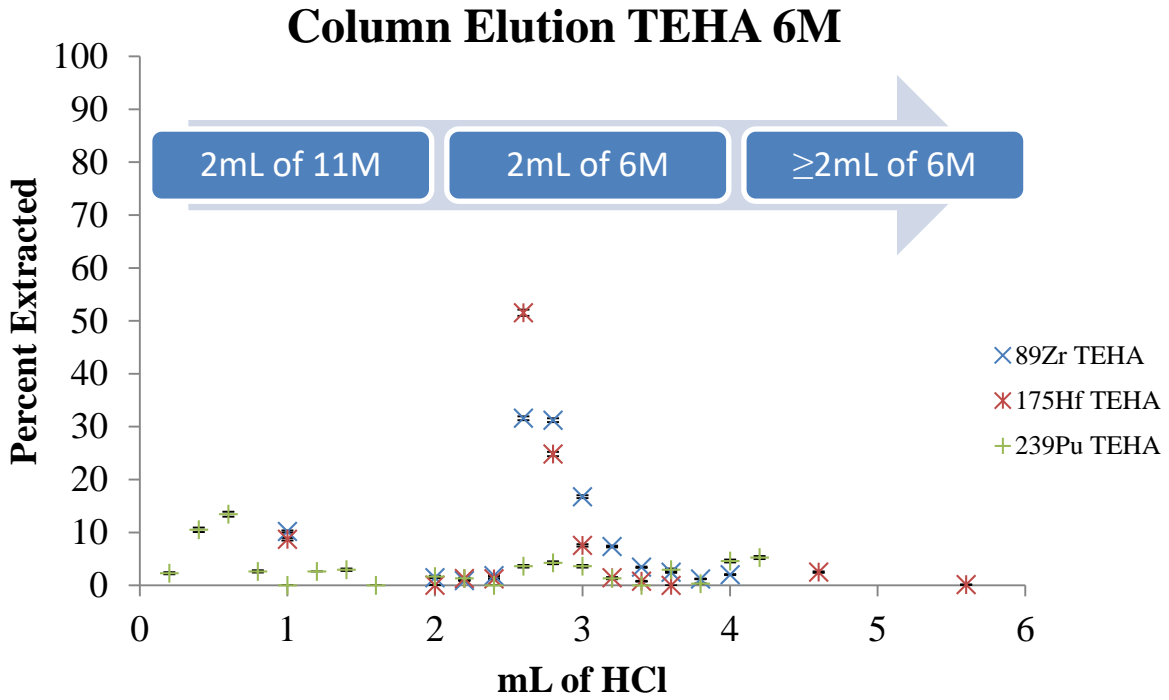


**Figure 6.3** Column elution of  $^{89}\text{Zr}$ ,  $^{175}\text{Hf}$ , and  $^{239}\text{Pu}$  on a 40% TEHA Amberchrome resin, eluting by 2 mL of 11 M HCl and then by 2 mL of 6 M HCl.

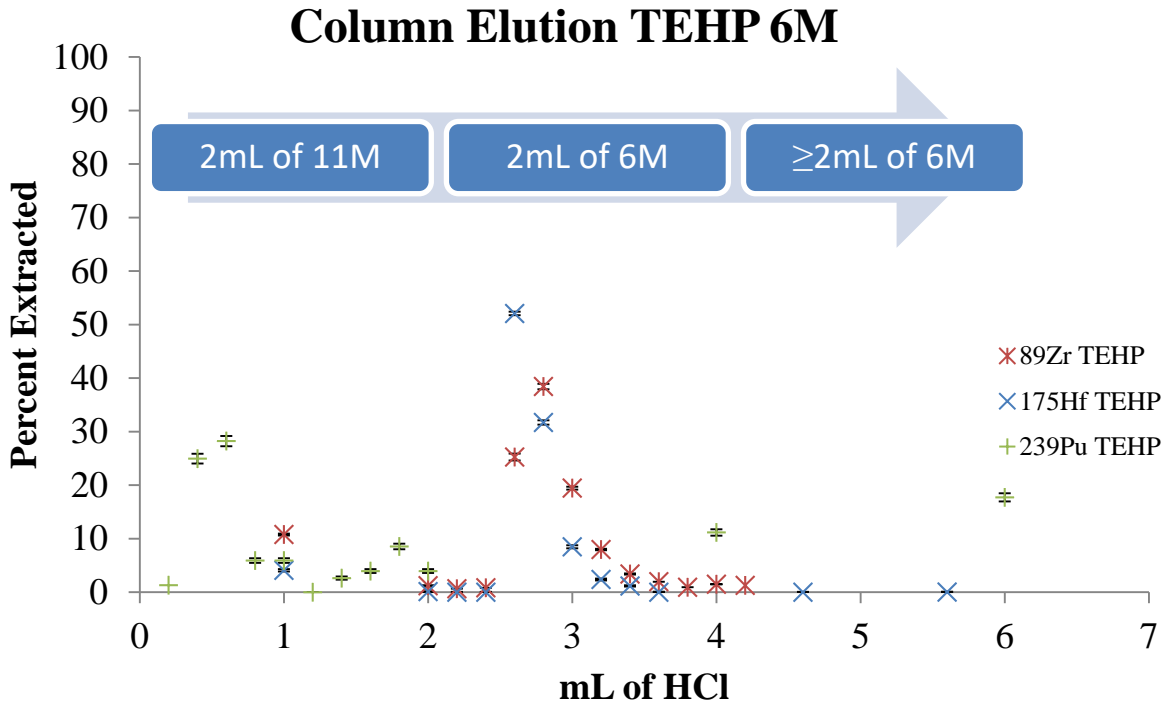


**Figure 6.4** Column elution of  $^{89}\text{Zr}$  and  $^{239}\text{Pu}$  on a 40% TEHP Amberchrome resin, eluting by 2 mL of 11 M HCl and then by 2 mL of 6 M HCl.

### 6.3 Discussion

Overall, the column separations performed poorly for separations between the three elements. Firstly, there was breakthrough in the first mL for all three radionuclides, with the  $^{239}\text{Pu}$  being the most prominent. The long equilibrium times for the radionuclides means that the elements' interaction with the resin was not long enough to become fully adhered on the column, and thus they broke through with the load fraction. Since  $^{239}\text{Pu}$  had the longest equilibrium times, a large fraction predictably breaks through. However, some of the  $^{239}\text{Pu}$  was retained on the resin and could only be eluted off in the 6 M HCl fraction.

The long kinetics on both resins could be exploited into a possible separation of  $^{239}\text{Pu}$  from  $^{89}\text{Zr}$  and  $^{175}\text{Hf}$ , but the column would have to be repeated many times to get a satisfactory purity. A solution to this problem would be to lengthen the column, so that the  $^{239}\text{Pu}$  has more time to reach equilibrium with the resin. However, the length of the column for these conditions was the maximum possible for the laboratory setup, as the column would stop flowing at 4 cm. A vacuum box would be required to operate the column at longer lengths but was unavailable for use at the time.

It was possible to get a separation of  $^{89}\text{Zr}$  and  $^{175}\text{Hf}$  on both the TEHA and TEHP columns using the 11 M HCl, 7 M HCl, and 6 M HCl procedure. Although 20% of the  $^{89}\text{Zr}$  bleeds into the  $^{175}\text{Hf}$  fraction, almost no  $^{175}\text{Hf}$  was present in the  $^{89}\text{Zr}$  fraction. To achieve even better performance, the column length would have to be lengthened and the use of a vacuum box would be required.

For the 11 M HCl and 6 M HCl procedure, almost no separation could be achieved between the  $^{89}\text{Zr}$  and  $^{175}\text{Hf}$ . This happened despite the small but measurable separation factor



between  $^{89}\text{Zr}$  and  $^{175}\text{Hf}$  that was determined in the batch studies. To exploit this small separation factor, the column would have to be lengthened so that the elements would separate from each other thoroughly. At the current column length this could not be achieved.

## 7 CONCLUSIONS

### 7.1 Solvent Extraction

The solvent extraction studies carried out to evaluate the potential of TEHA and TEHP to be used in a rutherfordium experiment were semi-successful. It would however not be possible to compare the behavior of rutherfordium with  $^{239}\text{Pu}$  due to its long kinetics with TEHA and TEHP. However, with  $^{89}\text{Zr}$  and  $^{175}\text{Hf}$ , it is possible to compare the data to a rutherfordium experiment, especially with the TEHA. A large separation factor between  $^{89}\text{Zr}$  and  $^{175}\text{Hf}$  with kinetics faster than a minute allows for the

For the TEHP,  $^{89}\text{Zr}$  and  $^{175}\text{Hf}$  show a similar trend of extraction with smaller separation factors between the two but a higher percent extracted into the organic phase when compared to TEHA. The kinetics for  $^{89}\text{Zr}$  are much faster at five seconds but  $^{175}\text{Hf}$  takes up to two minutes to reach equilibrium. The hafnium kinetics would require that more rutherfordium atoms be collected for comparison of hafnium's and rutherfordium's chemistry.

If not comparing the data for an online rutherfordium experiment, it is possible to separate all three elements in both TEHA and TEHP, given enough mixing time for the solvent extraction. All elements have a  $>10$  separation factor from each other at a certain hydrochloric acid concentration, which is an excellent factor for solvent extractions. For a few data points, the separation factor even exceeded values of 1000. Those values may allow for this separation to be investigated further for use in industrial applications.

The speciation data gathered shows good agreement with what previously was reported in the literature. From the experimental results, zirconium and hafnium both extract at a 2:1 ratio in TEHA, which lends evidence that both form hexachloro complex anions as the extracted species ( $\text{MCl}_6^{2-}$ ). For TEHP, the data shows that zirconium and hafnium both extract at a 1:1 ratio in

TEHP, with plutonium extracting at a 0.8:1. One reason that there may be a difference in this ratio is because the plutonium species in HCl is  $\text{PuO}_2\text{Cl}_4^{2-}$ .

One potential drawback to using high concentrations of HCl in an online chemistry system is the corrosion of the steel parts. Currently, the available liquid chemistry setups cannot handle high concentration of HCl because of this limitation. To remedy this drawback, the use of Teflon based materials would allow automated online use at an accelerator but the high cost of those materials prevents the manufacture of such a system.

## 7.2 Batch Studies and Column Studies

Batch studies for TEHA and TEHP illustrate much of the same results found for the solvent extractions but the possibility of steric hindrances interfering remains an issue with the extraction of all three nuclides with the exception of  $^{89}\text{Zr}$  on TEHP. These steric interferences are seen more greatly with TEHA than with TEHP due to TEHA requiring 2 ligands to extract each nuclide of interest. These interferences continue to influence the performance of kinetics with the exception of the  $^{89}\text{Zr}$  on TEHP. The size of the hexachloro complex for  $^{89}\text{Zr}$  on TEHP must be a complimentary fit into the pore size.

Column studies have shown that for both TEHA and TEHP the use of a column for separating these three elements is not feasible, much less even so when using a column for an automated online study for transactinide chemistry. The kinetics of these elements are too slow in interacting with the resin to be able to have a clear separation from each other. It may be possible to separate these elements with a longer column, however, a vacuum box system will be required to accomplish this process. The columns prepared may possibly be useful for the separation of  $^{89}\text{Zr}$  from other elements as its breakthrough in the load fraction is very minimal.

However, these elements could not be  $^{175}\text{Hf}$  and  $^{239}\text{Pu}$ , as the  $^{239}\text{Pu}$  elutes in every fraction and the  $^{89}\text{Zr}$  bleeds into the  $^{175}\text{Hf}$  fraction.

The poor performance of  $^{239}\text{Pu}$  on the resin could possibly indicate  $^{239}\text{Pu}$  forming the polymer chain and interfering with the poor extraction and slow kinetics. However, since the same stock was used for the all experiments, the  $^{239}\text{Pu}$  still eventually extracts almost completely in the solvent extractions. If the  $^{239}\text{Pu}$  polymer is present, there should be no eventual extraction as this polymer formation is irreversible. Therefore, the likelihood that  $^{239}\text{Pu}$  forming a polymer to inhibit its extraction seems small. Rather, the larger  $^{239}\text{Pu}$  ion forming a larger anion complex than the  $^{89}\text{Zr}$  and  $^{175}\text{Hf}$  complexes making it more difficult to fit into the pores of the resin and coordinate with the TEHA and TEHP ligands seems a more likely conclusion.

### 7.3 Future Work

Some of the work that needs to be further elaborated on is an in depth study of the resin characteristics and properties. If these are further investigated, then  $k'$  values could be calculated for the radionuclides on each of the resins. The use of  $k'$  values is superior to the use of  $D_w$  values as they provide a measure of column performance that is independent of the column parameters. Another way to improve performance would to lengthen the column to separate the peaks further from each other.

It is desirable to also study the  $^{239}\text{Pu}$  kinetics further. The longest mixing time used in this work only went up to 30 minutes. It is possible that the  $^{239}\text{Pu}$  could extract even more, but this was not attempted to because the purpose of these experiments is to test the suitability of the solvent extraction and resin in a super heavy element study.

Only three elements in one acid matrix were evaluated for extraction in TEHA and TEHP. While other preliminary studies failed to see extraction in nitric and sulfuric matrices

with zirconium, it is possible that plutonium may behave differently in those acids. It is also possible that other elements may be able to be extracted by TEHA and TEHP as well. The first preliminary solvent extraction study carried out for this research with TEHA used  $^{95}\text{Zr}$  as the tracer, and  $^{95}\text{Nb}$  (a decay product of  $^{95}\text{Zr}$ ) was observed being extracted in the organic phase starting at 4-6 M HCl. Such studies may be beneficial for extractions with other elements.

## REFERENCES

1. Rutherford, E., Atomic Projectiles and Their Collisions with Light Atoms. *Science* **1919**, 50 (1299), 467-73.
2. Bothe, B. H. a. W., *The  $\gamma$ -rays excited in boron and beryllium*. 1932; Vol. 76.
3. Joliot, I. C. a. F., The Emission of High energy Photons from Hydrogenous Substances Irradiated with Very Penetrating Alpha Rays. *Cr Acad Sci Li C* **1932**, 194 (273).
4. Chadwick, J., The existence of a neutron. *P R Soc Lond a-Conta* **1932**, 136 (830), 692-708.
5. Joliot, I. C. a. F., Effect of Absorption of Gamma Rays of Very High Frequency by Projection of Light Nuclei. *Comptes Rendus* **1932**, 194 (708).
6. Perrier, C.; Segre, E., Radioactive isotopes of element 43. *Nature* **1937**, 140, 193-194.
7. Fermi, E.; Amaldi, E.; D'Agostino, O.; Rasetti, F.; Segre, E., Artificial radioactivity produced by neutron bombardment. *P R Soc Lond a-Conta* **1934**, 146 (A857), 0483-0500.
8. Hahn, O.; Strassmann, F., About the evidence and the behavior in uranium radiation using neutron occuring earth alkaloid metals. *Naturwissenschaften* **1939**, 27, 11-15.
9. Meitner, L.; Frisch, O. R., Products of the fission of the uranium nucleus. *Nature* **1939**, 143, 471-472.
10. Seaborg, G. T.; Mcmillan, E. M.; Kennedy, J. W.; Wahl, A. C., Radioactive Element-94 from Deuterons on Uranium. *Phys Rev* **1946**, 69 (7-8), 366-367.
11. Seaborg, G. T., The chemical and radioactive properties of the heavy elements. *Chem. Eng. News* **1945**, 23, 2190-3.
12. Thompson, S. G.; Ghiorso, A.; Seaborg, G. T., Element 97. *Phys Rev* **1950**, 77 (6), 838-839.
13. Thompson, S. G.; Street, K.; Ghiorso, A.; Seaborg, G. T., Element 98. *Phys Rev* **1950**, 78 (3), 298-299.
14. Ghiorso, A.; Thompson, S. G.; Higgins, G. H.; Seaborg, G. T.; Studier, M. H.; Fields, P. R.; Fried, S. M.; Diamond, H.; Mech, J. F.; Pyle, G. L.; Huizenga, J. R.; Hirsch, A.; Manning, W. M.; Browne, C. I.; Smith, H. L.; Spence, R. W., New Elements Einsteinium and Fermium, Atomic Numbers 99 and 100. *Phys Rev* **1955**, 99 (3), 1048-1049.
15. Choppin, G. R., Liljenzin, J.O., Rydberg, J., *Radiochemistry and Nuclear Chemistry*. Butterworth-Heinemann: Woburn, 2002.
16. Schadel, M., Chemistry of superheavy elements. *Angew Chem Int Edit* **2006**, 45 (3), 368-401.
17. Myers, W. D.; Swiateck.Wj, Nuclear Masses and Deformations. *Nucl Phys* **1966**, 81 (1), 1-&.
18. Oganessian, Y. T.; Utyonkov, V. K.; Dmitriev, S. N.; Lobanov, Y. V.; Itkis, M. G.; Polyakov, A. N.; Tsyganov, Y. S.; Mezentsev, A. N.; Yeregin, A. V.; Voinov, A. A.; Sokol, E. A.; Gulbekian, G. G.; Bogomolov, S. L.; Iliev, S.; Subbotin, V. G.; Sukhov, A. M.; Buklanov, G. V.; Shishkin, S. V.; Chepygin, V. I.; Vostokin, G. K.; Aksenov, N. V.; Hussonnois, M.; Subotic, K.; Zagrebaev, V. I.; Moody, K. J.; Patin, J. B.; Wild, J. F.; Stoyer, M. A.; Stoyer, N. J.; Shaughnessy, D. A.; Kenneally, J. M.; Wilk, P. A.; Loughheed, R. W.; Gaggeler, H. W.; Schumann, D.; Bruchertseifer, H.; Eichler, R., Synthesis of elements 115 and 113 in the reaction Am-243+Ca-48. *Phys Rev C* **2005**, 72 (3).
19. Oganessian, Y. S.; Utyonkov, V. K.; Lobanov, Y. V.; Abdullin, F. S.; Polyakov, A. N.; Shirokovsky, I. V.; Tsyganov, Y. S.; Gulbekian, G. G.; Bogomolov, S. L.; Gikal, B. N.;

- Mezentsev, A. N.; Iliev, S.; Subbotin, V. G.; Sukhov, A. M.; Voinov, A. A.; Buklanov, G. V.; Subotic, K.; Zagrebaev, V. I.; Itkis, M. G.; Patin, J. B.; Moody, K. J.; Wild, J. F.; Stoyer, M. A.; Stoyer, N. J.; Shaughnessy, D. A.; Kenneally, J. M.; Loughheed, R. W., Measurements of cross sections for the fusion-evaporation reactions Pu-244(Ca-48,xn)(292-x)114 and Cm-245(Ca-48,xn)(293-x)116. *Phys Rev C* **2004**, *69* (5).
20. Oganessian, Y. T.; Utyonkov, V. K.; Lobanov, Y. V.; Abdullin, F. S.; Polyakov, A. N.; Sagaidak, R. N.; Shirokovsky, I. V.; Tsyganov, Y. S.; Voinov, A. A.; Gulbekian, G. G.; Bogomolov, S. L.; Gikal, B. N.; Mezentsev, A. N.; Iliev, S.; Subbotin, V. G.; Sukhov, A. M.; Subotic, K.; Zagrebaev, V. I.; Vostokin, G. K.; Itkis, M. G.; Moody, K. J.; Patin, J. B.; Shaughnessy, D. A.; Stoyer, M. A.; Stoyer, N. J.; Wilk, P. A.; Kenneally, J. M.; Landrum, J. H.; Wild, J. F.; Loughheed, R. W., Synthesis of the isotopes of elements 118 and 116 in the Cf-249 and Cm-245+Ca-48 fusion reactions. *Phys Rev C* **2006**, *74* (4).
21. Dayah, M., Casagrande., Periodic Table of the Elements.
22. Flerov, G. N.; Oganessian, Y. T.; Lobanov, Y. V.; Kuznetsov, V. I.; Druin, V. A.; Perehygin, V. P.; Gavrilov, K. A.; Tretiakova, S. P.; Plotko, V. M., Synthesis and Physical Identification of the Isotope of Element 104 with Mass Number 260. *Phys Lett* **1964**, *13* (1), 73-75.
23. Ghiorso, A.; Nurmia, M.; Harris, J.; Eskola, K.; Eskola, P., Positive Identification of 2 Alpha-Particle-Emitting Isotopes of Element 104. *Phys Rev Lett* **1969**, *22* (24), 1317-&.
24. Flerov, G. N.; Oganessian, Y. T.; Lobanov, Y. V.; Lazarev, Y. A.; Tret'yako, S. P.; Kolesov, I. V.; Plotko, V. M., Synthesis of Element 105. *Sov at Energy-Ussr* **1970**, *29* (4), 967-&.
25. Ghiorso, A.; Nurmia, M.; Eskola, K.; Harris, J.; Eskola, P., New Element Hahnium, Atomic Number 105. *Phys Rev Lett* **1970**, *24* (26), 1498-&.
26. Ghiorso, A.; Nitschke, J. M.; Alonso, J. R.; Alonso, C. T.; Nurmia, M.; Seaborg, G. T.; Hulet, E. K.; Loughheed, R. W., Element 106. *Phys Rev Lett* **1974**, *33* (25), 1490-1493.
27. Munzenberg, G.; Hofmann, S.; Hessberger, F. P.; Reisdorf, W.; Schmidt, K. H.; Schneider, J. H. R.; Armbruster, P.; Sahm, C. C.; Thuma, B., Identification of Element 107 by Alpha-Correlation Chains. *Z Phys a-Hadron Nucl* **1981**, *300* (1), 107-108.
28. Munzenberg, G.; Armbruster, P.; Folger, H.; Hessberger, F. P.; Hofmann, S.; Keller, J.; Poppensieker, K.; Reisdorf, W.; Schmidt, K. H.; Schott, H. J.; Leino, M. E.; Hingmann, R., The Identification of Element-108. *Z Phys a-Hadron Nucl* **1984**, *317* (2), 235-236.
29. Munzenberg, G.; Armbruster, P.; Hessberger, F. P.; Hofmann, S.; Poppensieker, K.; Reisdorf, W.; Schneider, J. H. R.; Schneider, W. F. W.; Schmidt, K. H.; Sahm, C. C.; Vermeulen, D., Observation of One Correlated Alpha-Decay in the Reaction Fe-58 on Bi-209-]267109. *Z Phys a-Hadron Nucl* **1982**, *309* (1), 89-90.
30. Hofmann, S.; Ninov, V.; Hessberger, F. P.; Armbruster, P.; Folger, H.; Munzenberg, G.; Schott, H. J.; Popeko, A. G.; Yeregin, A. V.; Andreyev, A. N.; Saro, S.; Janik, R.; Leino, M., Production and Decay of (269)110. *Z Phys a-Hadron Nucl* **1995**, *350* (4), 277-280.
31. Hofmann, S.; Ninov, V.; Hessberger, F. P.; Armbruster, P.; Folger, H.; Munzenberg, G.; Schott, H. J.; Popeko, A. G.; Yeregin, A. V.; Andreyev, A. N.; Saro, S.; Janik, R.; Leino, M., The New Element-111. *Z Phys a-Hadron Nucl* **1995**, *350* (4), 281-282.
32. Oganessian, Y. T.; Utyonkov, V. K.; Lobanov, Y. V.; Abdullin, F. S.; Polyakov, A. N.; Shirokovsky, I. V.; Tsyganov, Y. S.; Gulbekian, G. G.; Bogomolov, S. L.; Gikal, B. N.; Mezentsev, A. N.; Iliev, S.; Subbotin, V. G.; Sukhov, A. M.; Buklanov, G. V.; Subotic, K.; Itkis, M. G.; Moody, K. J.; Wild, J. F.; Stoyer, N. J.; Stoyer, M. A.; Loughheed, R. W., Synthesis of superheavy nuclei in the Ca-48+Pu-244 reaction. *Phys Rev Lett* **1999**, *83* (16), 3154-3157.

33. Morita, K.; Morimoto, K.; Kaji, D.; Akiyama, T.; Goto, S.; Haba, H.; Ideguchi, E.; Kanungo, R.; Katori, K.; Koura, H.; Kudo, H.; Ohnishi, T.; Ozawa, A.; Suda, T.; Sueki, K.; Xu, H. S.; Yamaguchi, T.; Yoneda, A.; Yoshida, A.; Zhao, Y. L., Experiment on the synthesis of element 113 in the reaction Bi-209(Zn-70,n)(278)113. *J Phys Soc Jpn* **2004**, *73* (10), 2593-2596.
34. Schadel, M., The chemistry of superheavy elements. *Acta Phys Pol B* **2003**, *34* (3), 1701-1728.
35. Hofmann, S., New elements - approaching Z=114. *Rep Prog Phys* **1998**, *61* (6), 639-689.
36. Seaborg, G. T.; Loveland, W. D., *The elements beyond uranium*. Wiley: New York, 1990; p xiii, 359 p.
37. Pyykko, P., Relativistic Effects in Structural Chemistry. *Chem Rev* **1988**, *88* (3), 563-594.
38. Oganessian, Y. T., Synthesis and properties of even-even nuclei with Z=114-116 produced in Ca-48 induced reactions. *Acta Phys Hung Ns-H* **2004**, *19* (1-2), 39-52.
39. Loveland, W., Synthesis of transactinide nuclei using radioactive beams. *Phys Rev C* **2007**, *76* (1).
40. Dvorak, J.; Bruchle, W.; Chelnokov, M.; Dressler, R.; Dullmann Ch, E.; Eberhardt, K.; Gorshkov, V.; Jager, E.; Krucken, R.; Kuznetsov, A.; Nagame, Y.; Nebel, F.; Novackova, Z.; Qin, Z.; Schadel, M.; Schausten, B.; Schimpf, E.; Semchenkov, A.; Thorle, P.; Turler, A.; Wegrzecki, M.; Wierczinski, B.; Yakushev, A.; Yereimin, A., Doubly magic nucleus (108)(270)Hs162. *Phys Rev Lett* **2006**, *97* (24), 242501.
41. Rydberg, J., *Solvent extraction principles and practice*. 2nd ed.; M. Dekker: New York, 2004; p ix, 750 p.
42. Goto, T.; Smutz, M., Separation factors for solvent extraction processes: The system of 1 M di-(2-ethyl-hexyl) phosphoric acid (in amsc 125-82)-Pr-Nd salts as an example. *Journal of Inorganic and Nuclear Chemistry* **1965**, *27* (6), 1369-1379.
43. Countercurrent vs. Cross current Solvent Extraction. In *Robatel Inc.*, Pittsfield MA.
44. Vasudeva, P., Third Phase formation in the extraction of thorium nitrate by trialkyl phosphates. *IOP Conference Series L Materials Science and engineering* **2010**, *9*.
45. Horwitz, E. P.; McAlister, D. R.; Dietz, M. L., Extraction chromatography versus solvent extraction: How similar are they? *Separ Sci Technol* **2006**, *41* (10), 2163-2182.
46. Horwitz, E., Extraction Chromatography of actinides and Selected Fission Products: Principles and Achievement of Selectivity.
47. Horwitz, E. P.; Bloomqui, Ca, Preparation, Performance and Factors Affecting Band Spreading of High Efficiency Extraction Chromatographic Columns for Actinide Separations. *J Inorg Nucl Chem* **1972**, *34* (12), 3851-&.
48. Horwitz, E. P.; Bloomqui, Ca, High Speed High Efficiency Separation of Transplutonium Elements by Extraction Chromatography. *J Inorg Nucl Chem* **1973**, *35* (1), 271-284.
49. Guillaumont, R.; Adloff, J. P.; Peneloux, A., Kinetic and Thermodynamic Aspects of Tracer-Scale and Single Atom Chemistry. *Radiochim Acta* **1989**, *46* (4), 169-176.
50. Guillaumont, R.; Adloff, J. P.; Peneloux, A.; Delamoye, P., Sub-Tracer Scale Behavior of Radionuclides - Application to Actinide Chemistry. *Radiochim Acta* **1991**, *54* (1), 1-15.
51. Borg, R. J.; Dienes, G. J., On the Validity of Single Atom Chemistry. *J Inorg Nucl Chem* **1981**, *43* (6), 1129-1133.
52. Ghiorso, A., Recoil Spectrometer for the Detection of Single Atoms. *J Radioan Nucl Ch Ar* **1988**, *124* (2), 407-413.
53. Subotic, K.; Oganessian, Y. T.; Utyonkov, V. K.; Lobanov, Y. V.; Abdullin, F. S.; Polyakov, A. N.; Tsyganov, Y. S.; Ivanov, O. V., Evaporation residue collection efficiencies and



position spectra of the Dubna gas-filled recoil separator. *Nucl Instrum Meth A* **2002**, 481 (1-3), 71-80.

54. Persson, H.; Skarnemark, G.; Skalberg, M.; Alstad, J.; Liljenzin, J. O.; Bauer, G.; Haberberger, F.; Kaffrell, N.; Rogowski, J.; Trautmann, N., Sisak-3 - an Improved System for Rapid Radiochemical Separations by Solvent-Extraction. *Radiochim Acta* **1989**, 48 (3-4), 177-180.

55. Schadel, M.; Bruchle, W.; Haefner, B., Fast Radiochemical Separations with an Automated Rapid Chemistry Apparatus. *Nucl Instrum Meth A* **1988**, 264 (2-3), 308-318.

56. Schadel, M.; Bruchle, W.; Jager, E.; Schimpf, E.; Kratz, J. V.; Scherer, U. W.; Zimmermann, H. P., Arca-Ii - a New Apparatus for Fast, Repetitive Hplc Separations. *Radiochim Acta* **1989**, 48 (3-4), 171-176.

57. Noren, B., Hydrolysis of Zr-4+ and Hf-4+. *Acta Chem Scand* **1973**, 27 (4), 1369-1384.

58. El-Ammouri, E. G. Hafnium solvent extraction from chloride solutions using organophosphorus reagents (Cyanex 923, 925). Thesis (M Eng ), 1994.

59. Pershina, V.; Trubert, D.; Le Naour, C.; Kratz Jens, V., Theoretical predictions of hydrolysis and complex formation of group-4 elements Zr, Hf and Rf in HF and HCl solutions. In *Radiochim Acta*, 2002; Vol. 90, p 869.

60. Silva, R.; Harris, J.; Nurmia, M.; Eskola, K.; Ghiorso, A., Chemical Separation of Rutherfordium. *Inorg Nucl Chem Lett* **1970**, 6 (12), 871-&.

61. Hulet, E. K.; Lougheed, R. W.; Wild, J. F.; Landrum, J. H.; Nitschke, J. M.; Ghiorso, A., Chloride Complexation of Element-104. *J Inorg Nucl Chem* **1980**, 42 (1), 79-82.

62. Rajan, K. S., Gupta, J., Separation of zirconium and hafnium by means of anion-exchange resins. I. Qualitative studies. *Journal of Scientific and Industrial Research* **1955**, 14B, 453-6.

63. Pfrepper, G.; Pfrepper, R.; Krauss, D.; Yakushev, A. B.; Timokhin, S. N.; Zvara, I., Ion exchange equilibria and stoichiometry of complexes of element 104 and hafnium in hydrofluoric acid solutions. *Radiochim Acta* **1998**, 80 (1), 7-12.

64. Trubert, D.; Guzman, F. M.; Le Naour, C.; Brillard, L.; Hussonnois, M.; Constantinescu, O., Behaviour of Zr, Hf, Nb, Ta and Pa on macroporous anion exchanger in chloride-fluoride media. *Anal Chim Acta* **1998**, 374 (2-3), 149-158.

65. Strub, E.; Kratz, J. V.; Kronenberg, A.; Nahler, A.; Thorle, P.; Zauner, S.; Bruchle, W.; Jager, E.; Schadel, M.; Schausten, B.; Schimpf, E.; Li, Z. W.; Kirbach, U.; Schumann, D.; Jost, D.; Turler, A.; Asai, M.; Nagame, Y.; Sakama, M.; Tsukada, K.; Gaggeler, H. W.; Glatz, J. P., Fluoride complexation of rutherfordium (Rf, element 104). *Radiochim Acta* **2000**, 88 (5), 265-271.

66. Ishii, Y.; Toyoshima, A.; Tsukada, K.; Asai, M.; Toume, H.; Nishinaka, I.; Nagame, Y.; Miyashita, S.; Mori, T.; Sukanuma, H.; Haba, H.; Sakamaki, M.; Goto, S.; Kudo, H.; Akiyama, K.; Oura, Y.; Nakahara, H.; Tashiro, Y.; Shmohara, A.; Schadel, M.; Bruchle, W.; Pershina, V.; Kratz, J. V., Fluoride complexation of element 104, rutherfordium (Rf), investigated by cation-exchange chromatography. *Chem Lett* **2008**, 37 (3), 288-289.

67. Toyoshima, A.; Haba, H.; Tsukada, K.; Asai, M.; Akiyama, K.; Goto, S.; Ishii, Y.; Nishinaka, I.; Sato, T. K.; Nagame, Y.; Sato, W.; Tani, Y.; Hasegawa, H.; Matsuo, K.; Saika, D.; Kitamoto, Y.; Shinohara, A.; Ito, M.; Saito, J.; Kudo, H.; Yokoyama, A.; Sakama, M.; Sueki, K.; Oura, Y.; Nakahara, H.; Schadel, M.; Bruchle, W.; Kratz, J. V., Hexafluoro complex of rutherfordium in mixed HF/HNO<sub>3</sub> solutions. *Radiochim Acta* **2008**, 96 (3), 125-134.

68. Kronenberg, A.; Eberhardt, K.; Kratz, J. V.; Mohapatra, P. K.; Nahler, A.; Thorle, P.; Bruchle, W.; Schadel, M.; Turler, A., On-line anion exchange of rutherfordium in HF/HNO<sub>3</sub> and HF solutions. *Radiochim Acta* **2004**, *92* (7), 379-386.
69. Huffman, E. H.; Iddings, G. M.; Lilly, R. C., Anion Exchange of Zirconium, Hafnium, Niobium and Tantalum in Hydrochloric Acid Solutions. *J Am Chem Soc* **1951**, *73* (9), 4474-4475.
70. Huffman, E. H.; Lilly, R. C., Anion Exchange of Complex Ions of Hafnium and Zirconium in Hcl-Hf Mixtures. *J Am Chem Soc* **1951**, *73* (6), 2902-2905.
71. Szegłowski, Z.; Guseva, L. I.; Lien, D. T.; Domanov, V. P.; Kubica, B.; Tikhomirowa, G. S.; Constantinescu, O.; Constantinescu, M.; Yakushev, A. B., Online ion exchange separation of short-lived Zr, Hf, Mo, Ta and W isotopes as homologs of transactinide elements. *J Radioanal Nucl Ch* **1998**, *228* (1-2), 145-149.
72. Li, Z. J.; Toyoshima, A.; Asai, M.; Tsukada, K.; Sato, T. K.; Sato, N.; Kikuchi, T.; Nagame, Y.; Schadel, M.; Pershina, V.; Liang, X. H.; Kasamatsu, Y.; Komori, Y.; Ooe, K.; Shinohara, A.; Goto, S.; Murayama, H.; Murakami, M.; Kudo, H.; Haba, H.; Takeda, Y.; Nishikawa, M.; Yokoyama, A.; Ikarashi, S.; Sueki, K.; Akiyama, K.; Kratz, J. V., Sulfate complexation of element 104, Rf, in H<sub>2</sub>SO<sub>4</sub>/HNO<sub>3</sub> mixed solution. *Radiochim Acta* **2012**, *100* (3), 157-164.
73. Banda, R.; Lee, H. Y.; Lee, M. S., Separation of Zr and Hf from strong hydrochloric acid solution by solvent extraction with TEHA. *J Radioanal Nucl Ch* **2013**, *295* (2), 1537-1543.
74. Gaudh, J. S.; Shinde, V. M., Liquid-Liquid-Extraction of Vanadium(V) and Niobium(V) with Tris(2-Ethylhexyl)Phosphate - Mutual Separation of Vanadium(V), Niobium(V), and Tantalum(V), and Analysis of Steel Samples. *Separ Sci Technol* **1995**, *30* (12), 2573-2584.
75. Marcus, Y.; Kertes, A. S., *Ion exchange and solvent extraction of metal complexes*. Wiley-Interscience: London, New York etc., 1969; p ix, 1037 p.
76. Czerwinski, K. R. Studies of fundamental properties of rutherfordium (Element 104) using organic complexing agents. ; Lawrence Berkeley National Lab. (LBNL), Berkeley, CA (United States), 1992.

## CURRICULUM VITAE

### Jeff Rolfes

Email: [jeffrolfes@gmail.com](mailto:jeffrolfes@gmail.com)

### Education

- Ph.D. University of Nevada Las Vegas Radiochemistry Spring 2018**  
Dissertation: Solvent Extraction and Extraction Chromatography of Homologs and Pseudohomologs of Rutherfordium using TEHA and TEHP  
Graduate Advisor: Dr. Ralf Sudowe
- B.S. Newman University, Wichita, KS Chemistry May 2010**
- B.A. Newman University, Wichita, KS Biology & History May 2010**

### Work Experience

**DTRA Postdoctoral Program Manager (Contractor through Penn State)** Oct. 2017-present  
*Fort Belvoir, VA*

- Analyzed and identified DTRA technical needs in nuclear forensics
- Assisted in planning, coordinating, integrating, implementing, and evaluating research and development programs
- Developed and presented information in a colloquium to support informed decision-making

**ACS Nuclear Summer School Teaching Assistant 2010** Summer 2010  
*San Jose State University, San Jose, CA*

- Prepared and supervised 16 experiments in a nuclear chemistry lab
- Assisted in lecturing and graded student lab assignments

### Research Experience

**Research Assistant** Fall 2011-Sept. 2017  
*University of Nevada at Las Vegas, Las Vegas, NV*

- Tested solvent extractions using of novel ligands of zirconium, hafnium, thorium, neptunium, and plutonium for homolog studies on rutherfordium
- Developed new extraction chromatographic resin for the separation of zirconium, hafnium, thorium, neptunium, plutonium, americium, and curium

**Graduate Fellowship Practicum** Summer 2013 & 2016  
*Lawrence Livermore National Laboratory, Livermore, CA*

- Continued thesis work in collaboration with Livermore scientists
- Used isotopes produced at the Center for Accelerator Mass Spectrometry as tracers in separations

**Graduate Intern in Environmental Sample Analysis IAEA Safeguards** Summer 2012  
*Lawrence Livermore National Laboratory, Livermore, CA*

- Purified U and Pu from bulk environmental samples, and measured U and Pu isotope ratios by MC-ICP-MS
- Conducted research to analyze U collection efficiency on different swipes and other materials

### Related Experience

## ACS Nuclear Summer School Student 2009

Summer 2009

San Jose State University, San Jose, CA

- Studied introductory nuclear chemistry and worked in a radiation laboratory
- Attended the 2009 Actinides Conference in San Francisco, CA

## Presentations

*Oral Presentation:* "Development of a Chemical System for Rutherfordium using TEHA and TEHP," Rolfes, Jeff; Despotopulos, John; Sudowe, Ralf. American Chemical Society Meeting; Philadelphia, PA. August 22 2016

*Oral Presentation:* "Development of a Chemical System for Rutherfordium using TEHA and TEHP," Rolfes, Jeff; Despotopulos, John; Sudowe, Ralf. Academic Laboratory Collaboration Meeting, SCUREF review meeting; Los Alamos, NM. August 5 2016

*Oral Presentation:* "Development of a Chemical System for Rutherfordium using TEHA and TEHP," Rolfes, Jeff; Despotopulos, John; Sudowe, Ralf. American Chemical Society Meeting; San Diego, CA. March 17 2016.

*Oral Presentation:* "Development of a Chemical System for Rutherfordium," Rolfes, Jeff; Despotopulos, John; Sudowe, Ralf. 5<sup>th</sup> International Conference on the Chemistry and Physics of the Transactinide Elements, Urabandai, Japan. May 27 2015

*Oral Presentation:* "Development of a Chemical System for Rutherfordium," Rolfes, Jeff; Despotopulos, John; Sudowe, Ralf. Methods and Application of Radiochemistry X, Kailua-Kona, HI. April 14 2015

*Oral Presentation:* "Development of a Chemical System for Rutherfordium," Rolfes, Jeff; Despotopulos, John; Sudowe, Ralf. American Chemical Society Meeting, San Francisco CA, August 11 2014

*Oral Presentation:* "Development of a Chemical System for Rutherfordium," Rolfes, Jeff; Despotopulos, John; Sudowe, Ralf. Academic Laboratory Collaboration Meeting, SCUREF review meeting; Argonne National Lab, Lemont, IL August 5 2014

*Poster Presentation:* "Development of a Chemical System for Rutherfordium," Rolfes, Jeff; Despotopulos, John; Sudowe, Ralf. LLNL Summer Student Symposium, Livermore, CA. August 8 2013

## Skills

- Radioanalytical chemistry & radiochemistry
- Chemistry of the actinide and transactinide elements
- Nuclear properties of the actinide and transactinide elements.
- Handling of radioactive material
- Alpha, beta and gamma Spectroscopy
- Analytical chemistry (UV-Vis, FT-IR, MC-ICP-MS, GC-MS, ICP-AES, HPLC)
- Manual and automated separation and chromatography techniques (liquid-liquid extraction, ion exchange and extraction chromatography)
- Nuclear forensics

## Honors and Awards

- Nuclear Forensics Graduate Fellow, Department of Homeland Security
- Cardinal Newman Scholar, Newman University
- Graduated *summa cum laude*, Newman University
- Dean's list (10 semesters), Newman University
- AP Scholar with Distinction

- Eagle Scout
- Two time Science Olympiad National Medalist in Tower Building

**CITIZENSHIP:** United States of America

**CLEARANCE LEVEL:** Interim Secret - DoD

## **References**

**Ralf Sudowe**

Email: [Ralf.Sudowe@colostate.edu](mailto:Ralf.Sudowe@colostate.edu)

**Gary Cerefice**

Email: [Cerefigs@nv.doe.gov](mailto:Cerefigs@nv.doe.gov)

**Roger Henderson**

Email: [henderson55@llnl.gov](mailto:henderson55@llnl.gov)

**Ken Czerwinski**

Email: [czerwin2@unlv.nevada.edu](mailto:czerwin2@unlv.nevada.edu)